ABSTRACT

Title of Document: INCREASING STABILITY OF LITHIUM-ION BATTERIES WITH ORDERED GRAPHENE-SILICON NEGATIVE ELECTRODES.

Asif Ahmed, Jan Babiuch-Hall, Taarika Babu, Gary Chen, Desiree Devries, Karen Dunford, Madara Jayatilake, Emily Li, Scott Wingate, and Joseph Yan

Directed By: Dr. Chunseng Wang
Chemical and Biomolecular Engineering

Currently, lackluster battery capability is restricting the widespread integration of Smart Grids, limiting the long-term feasibility of alternative, green energy conversion technologies. Silicon nanoparticles have great conductivity for applications in rechargeable batteries, but have degradation issues due to changes in volume during lithiation/delithiation cycles. To combat this, we use electrochemical deposition to uniformly space silicon particles on graphene sheets to create a more stable structure. We found the process of electrochemical deposition degraded the graphene binding in the electrode material, severely reducing charge capacity. But, the usage of mechanically mixing silicon particles with grapheme yielded batteries better than those that are commercially available.

INCREASING STABILITY OF LITHIUM-ION BATTERIES WITH ORDERED GRAPHENE-SILICON NEGATIVE ELECTRODES

By

Team IEDOB

Asif Ahmed
Jan Babiuch-Hall
Taarika Babu
Gary Chen
Desiree Devries
Karen Dunford
Madara Jayatilake
Emily Li
Scott Wingate
Joseph Yan

Thesis submitted in partial fulfillment of the requirements of the
University of Maryland, College Park
Gemstone Program
2013

Advisory Committee:
Professor Chunsheng Wang, Mentor
Professor Ayyakkannu Manivannan
Mr. Xinyin Chen
Mr. Liangbing Hu
Mr. Alexander Kozen

Contents

List of Figures

Chapter 1

Introduction

The reduction of carbon emissions to combat global climate change presents many challenges in terms of the technological advances needed to facilitate such a change. Specifically, the development of renewable energy sources in addition to the emphasis on deprecating legacy technologies and systems that depend on the use of non-renewable fossil fuel sources are critical to protecting the environment and attempting to reverse the detrimental effects that have come with modernization. This is a tall order that requires fundamental changes in social policy and existing infrastructure as well as in the technologies used on a daily basis. The advancement of lithium-ion batteries is one of the most promising avenues. The use of rechargeable lithium-ion batteries is widely considered to be most effective in renewable energy storage and electric vehicles. It is also very important for powering portable electronics.[11] These technologies would greatly benefit from the high energy density, stability, and portability of improved lithium-ion batteries.

In pursuit of improving the quality of our environment and providing a more reliable source of energy, the last few decades have brought rapid development of a variety of alternative, green energy sources. Photovoltaic, geothermal, and wind technologies, to name a few, have seen many advances and improvements in efficiency and

are becoming commonplace around the world. However, the successful implementation and long-term widespread adoption of these technologies are contingent on more efficient methods of energy storage. For example, solar energy that is inefficiently stored during peak sunlight hours may not support peak energy demand times. The application of an efficient rechargeable battery will support the development of all technologies dependent on energy storage.

With the end goal of allowing consumers to be more energy-aware for economic and environmental purposes, Smart Grid technology is beginning to be researched and developed in the United States. A Smart Grid power network is the result of modernizing existing electrical grids to empower consumers by providing them with more information regarding their energy usage in near real-time. The various components that make up the network can be seen in figure 1.1. The power distribution is made to be more energy-efficient due to the grids ability to dynamically change energy distribution levels in an automated fashion based upon set parameters regarding energy consumption behavior. In Smart Grid systems, the capability to efficiently store and release large amounts of energy on-demand allows for the storage system to be modularized so that energy storage is localized to where it will be needed. This resulting modularization and localization not only improves the stability and reliability of the power grid, but also greatly reduces energy loss due to transmission over long high-voltage lines.[12]

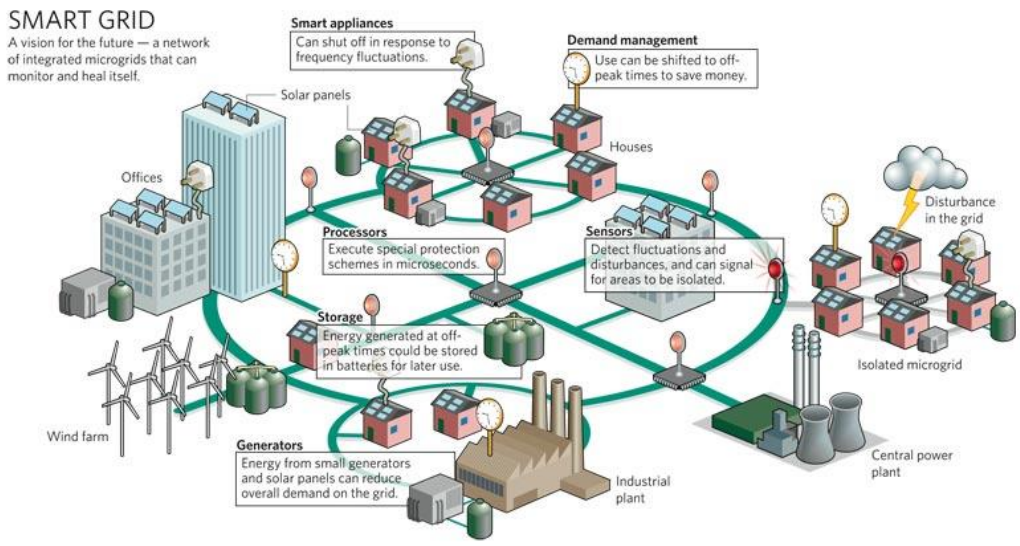

Figure 1.1: Smart Grids depend on reliable forms of rechargeable energy storage to store energy generated during off-peak times for later use during peak times and ensure maximum energy and cost efficiency of the Grid under the principle of demand management. Image found on http://horizonenergy.blogspot.com. Reproduced with pending permission from the Consumer Energy Report. Copyright http://www.consumerenergyreport.com/smart-grid

The advantages of such energy storage include, but are certainly not limited to: more efficient transmission of electricity, increased integration of large-scale renewable energy systems, and quicker restoration of electricity after power disturbances. The efficiency of traditional central power plant generation is at most 55% without including transport losses, and distributed storage has the potential to cut down this figure by reducing load from peak energy usage demands and allowing the integration of less-mature renewable energy sources into the larger overall system.[13]

While the theoretical benefits of adoption are many, adopting Smart Grid systems would require a fundamental reconstruction of the existing power infrastructure in the United States, including the technological challenge of creating an information network on top of a dynamic power distribution network as well as that of storing power in such a system. Smart Grid applications require stationary batteries that can

store large amounts of energy and produce enough power to support sudden spikes in electricity demand. Currently, energy storage in the Smart Grid is not limited to one specific type of battery; due to the development of reliable power conversion systems that can convert direct current battery power to the alternating current power supplied to consumers, a wide variety of battery technologies can be used in tandem to store energy. Lithium-ion batteries in particular may find themselves ubiquitous in portable energy conversion integrated into Smart Grid technologies because of their comparatively high energy density compared to other legacy battery technologies, and their light weight, as seen in figure 1.2.

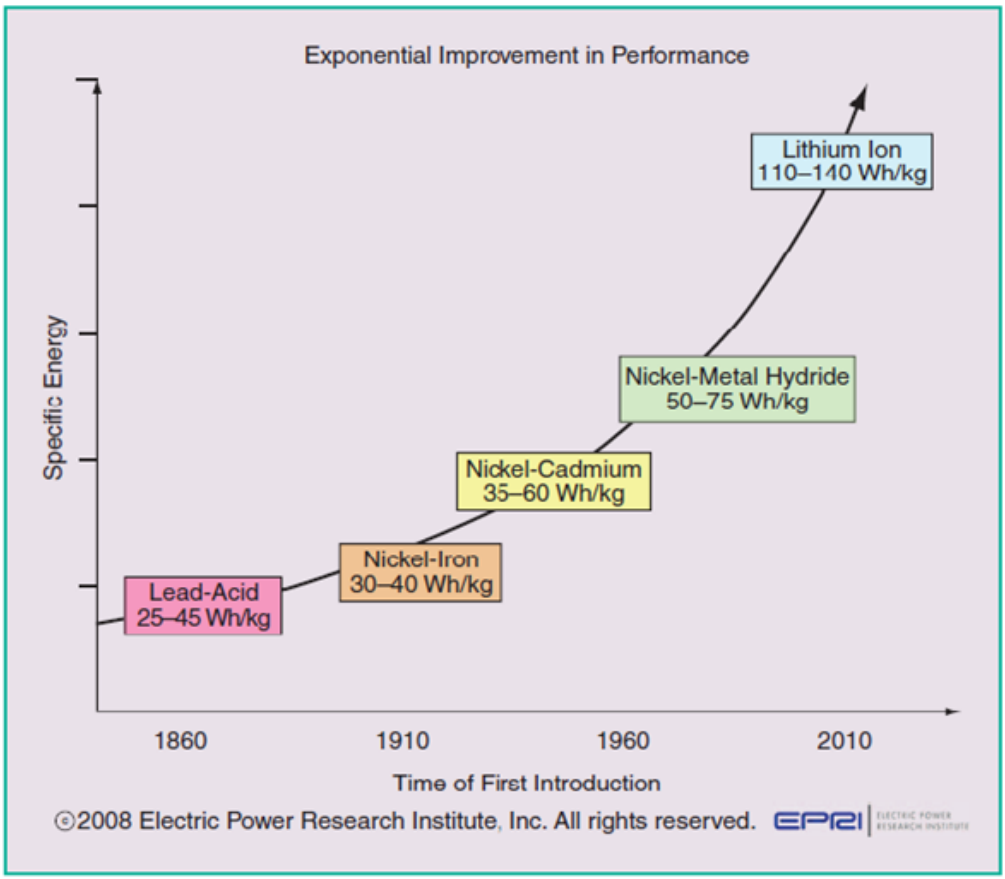

Figure 1.2: Battery performance has been exponentially increasing since 1860.[1]

To many, the convenience provided by the portability of lithium-ion batteries is its

most characteristic property. This is particularly true in the case of vehicles that are used in exploration-dependent research in remote areas, such as in the deep oceans or on other planets. This is also true of the electric vehicle. Currently, the Tesla Roadster, an all-electric sports car, fits 6,831 lithium-ion cells in its chassis in order to store enough energy to travel about 250 miles in one charge, the equivalent of about nine gallons of gasoline. Given that this battery pack occupies a volume comparable to that of the trunk of a similar gas-powered vehicle and weighs 450 kg, it is easy to see the need to develop batteries capable of storing the same or greater amount of energy in a much smaller space.[14]

Lithium-ion batteries have already undergone many technological developments and transformations that have made them an ideal energy source for electric vehicle applications. Improvements in the amount of energy that can be moved into the battery without overheating have allowed engineers to refine regenerative braking features on electric vehicles, increasing fuel efficiency by allowing energy from the motion of the wheels to be harnessed and stored into the battery system rather than being wasted in the brake pads. Additionally, the development of larger lithium cells and the subsequent resulting lower vehicle weight has been cited as a significant plus; in particular, city transit vehicles require a great deal of starting and stopping, so weight is a major contributor to higher fuel consumption. The larger cells have replaced the need for the aggregation of thousands of smaller cells in order to meet the energy demands of a full-sized bus, offering lower system integration costs and better reliability.[15] These recent improvements give a glimpse into the ways that more advanced battery technologies can be further taken advantage of in electric vehicles.

Battery performance serves as a bottleneck to processing power in a wide variety of potential portable electronics applications, including defense, ocean exploration, space exploration, and consumer products. Portable electronics require that batteries be charged and discharged many times, meaning that these batteries should have a

high cycle life. Additionally, portable applications require batteries that can carry significant amounts of charge while staying compact and lightweight. The capability to quickly charge the battery to maximum capacity is very desirable in all of the above applications as well.

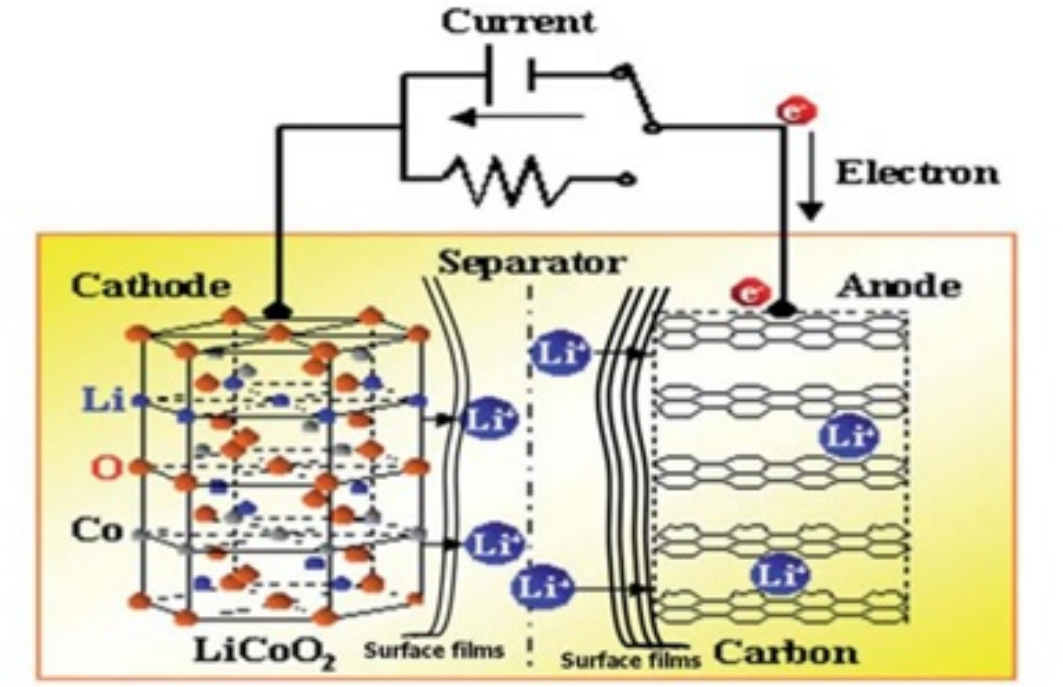

Figure 1.3: Schematic of how lithium-ion batteries work.

The primary material used for negative electrodes in industry is graphite. For standard testing, lithium metal is typically used. However, it has many problems with cycling because of the dendrite formation which short circuits the battery. Furthermore, typically used in industry, are carbon-sourced materials (i.e. graphite) due to their low cost and availability, while its drawbacks are its low capacity of 372 mAh/g when compared with lithium metal (3,862 mAh/g). Branching from this source, researchers have been working with graphene and carbon nanotubes (CNT) that have increased capacity but are facing with the obstacle of cost and processing. Alloy composites and silicon electrodes show great promise in terms of capacities but

their greatest drawbacks are with volume change that inhibits cycling stability.

Many developments have been made in recent years in regards to positive electrode materials for lithium-ion batteries. The most promising and current materials used are lithium-metal oxides such as $LiCoO_2$ and $LiMn_2O_4$. Even more, in recent trends olivines, which have a moderate capacity and stable cycling ability, such as $LiFePO_4$ have been used in commercial applications. Currently, researchers are working on combining transition metal oxides together to form a stable positive electrode, using layered oxides such as nickel and cobalt. The advantages to using a layered lithium oxide structure is that they have stability and a high-voltage range, however, this is mitigated by the fact that cobalt is toxic, which demands strict regulations on disposal; manufacturing processes become more difficult as a result. Lastly, another compound used in positive electrode research is vanadium oxide, which has a large capacity and great kinetic properties but its drawback is that due to lithium insertion/extraction vanadium oxide becomes amorphous and thus limits its cycling ability.

The main characteristics needed for an electrolyte for a lithium-ion battery are to withstand high voltages and temperatures while allowing transfer lithium ions in a stable manner. The three main types of electrolytes used in industry are liquid, polymer, and solid-state. The main liquid electrolytes used in industry are mostly inorganic salts such as $LiBC_4O_8$ and $LiPF_6$. Polymer electrolytes contain a mixture of ceramic nanoparticles that allow high conductivity and resistance to high voltages. Even more, polymer electrolytes have the ability to deter lithium dendrite formation, which can be used in conjunction with lithium metal electrodes. Lastly, in solid-state electrolytes show a promising future because they eliminate the need for separators in batteries. However, researchers are still working with solid-state electrolytes because of their special deposition conditions which cannot be utilized in commercial processes.

To better quantify the performance of a lithium-ion battery, a number of terms must first be understood. The specific capacity of a battery is defined by the amount of charge it can hold per unit mass of the battery. Lithium-ion batteries with high specific capacities can provide a considerable amount of charge over a long period of time, making them ideal for portable electronic applications. The specific energy density of a battery refers to the energy a battery can produce per unit mass of the battery. Specifically, a battery with a higher energy density stores more charge in the same amount of volume as a battery with a lower energy density. Batteries must demonstrate this characteristic in order to provide sufficient power on demand. The cycle life of a battery is defined as the number of charge/discharge cycles a battery can endure before it loses 20% of its initial capacity.

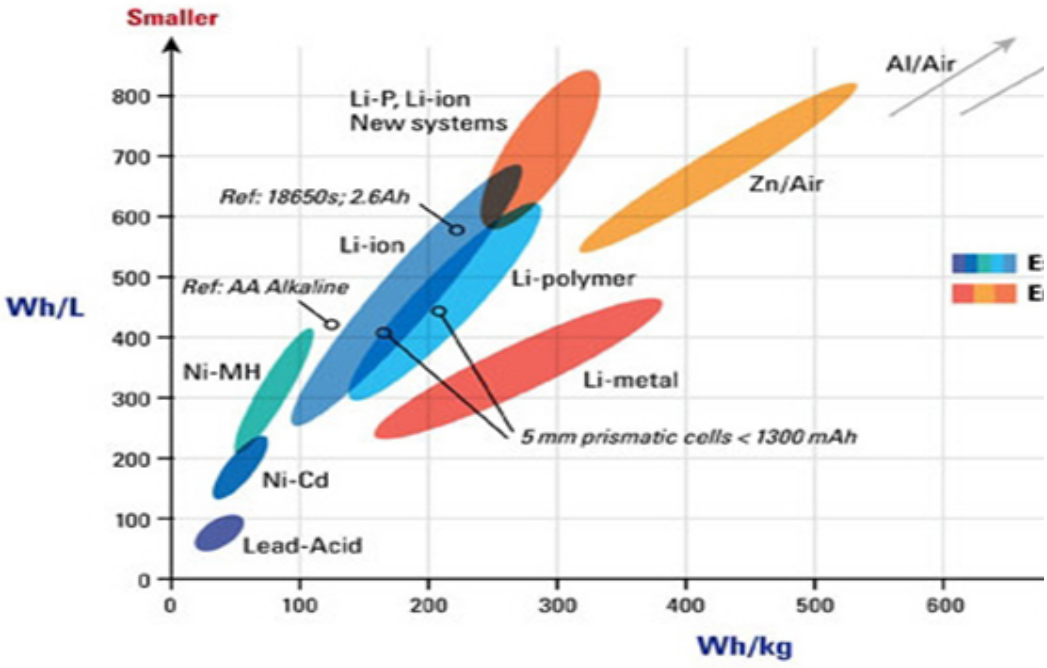

Figure 1.4: Specific volumes of different batteries. Reproduced with pending permission from reference.[2]

Figure 1.4 depicts the relative energy densities of various rechargeable batteries in weight on the x-axis and volume on the y-axis. Lithium-ion batteries are shown

on the graph in blue. Lithium-ion batteries have significant potential for high energy density relative to their weight and volume as compared to other standard rechargeable batteries currently used in portable consumer electronics such as Ni-Cd, AA Alkaline, Ni-MH, and Lead-Acid batteries.

Commercially available lithium-ion batteries with graphite electrodes have a capacity of approximately 370 mAh/g. Changing the electrode material of a battery from graphite to silicon can theoretically increase the capacity up to 4200 mAh/g, more than a tenfold improvement. However, a major problem with the silicon electrode is its relatively short cycle life.[16] Industry-standard batteries containing graphite electrodes have cycle lives of around 400 to 1200 cycles.[17] Currently, silicon electrodes can only go through about 20 to 30 lithiation/delithiation cycles before losing over 20% of their capacity and thus losing much of their utility, especially in applications where consistent capacity is required.[11]

The issue with silicon electrodes stems from nanomechanical processes that occur during lithiation/delithiation cycles; as the battery is charged, the silicon grows in size by approximately 400%.[18] During discharging, as lithium-ions are removed, cracks are introduced in the silicon structure and it crumbles, causing parts of the electrode to electrically disconnect from the current collector. Fractured pieces of silicon insulated from the current collector create irreversible capacity loss as electrons cannot flow from them through the charging circuit. Subsequently, the electrode rapidly loses capacity after only a small number of charge cycles. Different methods to improve the cycle life have been researched, but none have significantly curbed the accompanying degradation in the capacity of the battery.[18]

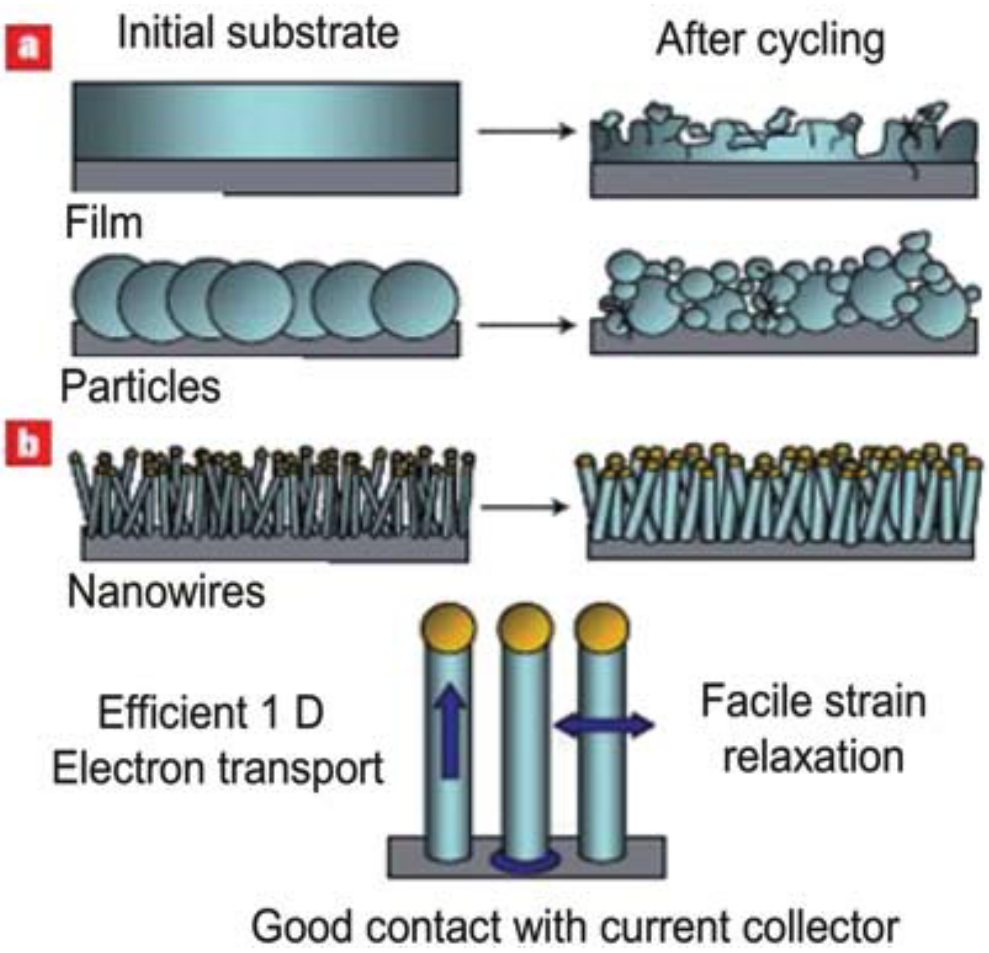

Figure 1.5: Silicon electrode pulverization with various particle geometries. Reproduced with pending permission from reference.[3]

Figure 1.5 shows a silicon electrode before and after cycling. During lithiation, the silicon electrode expands as lithium ions bond to the silicon particles. When the cell discharges, the lithium ions leave the silicon electrode, which leaves gaps between the silicon electrode and the current collector. As a result, the silicon electrode loses significant capacity with each lithiation/delithiation cycle because electrons cannot flow as easily through the silicon electrode to the current collector.

Our project aims to eliminate this drawback by creating a novel electrode material for rechargeable lithium-ion batteries that consists of silicon nanoparticles electrochemically deposited onto a graphene base. The graphene provides a strong

framework for silicon to hold it together, maintain electrical connection during lithiation/delithiation cycles, and prevent their fragmentation. The structure of graphene allows silicon molecules to expand and discharge without losing electrical contact with the current collector, achieved partly due to the excellent electrical conductivity of graphene, which connects silicon fragments to the current collector of the battery.[19] We plan to use this unique electrode structure to answer the following question: Will a more homogeneous electrode composed of electrochemically deposited silicon particles onto graphene result in better performance than a mechanically mixed graphite-silicon composite electrode in terms of capacity and cycle life?

We hypothesize that, through the electrochemical deposition of silicon onto graphene, the combination of less aggregated silicon particles and layered graphene reinforcement will reduce fragmentation, increase contact with the electrical connector, and thus increase the capacity and cycle life of lithium-ion batteries. In this paper, we first discuss the other methods we referenced in preparing our graphene-silicon composite electrodes. Then we will discuss our methods and testing of the electrodes. Finally, we discuss the results of our experiment in comparison to our control group, and implications from our research for the future. Through this research, we plan to advance current knowledge on graphene-silicon composite electrode batteries and their applications that may be further adapted for eventual use in commercial and industry settings.

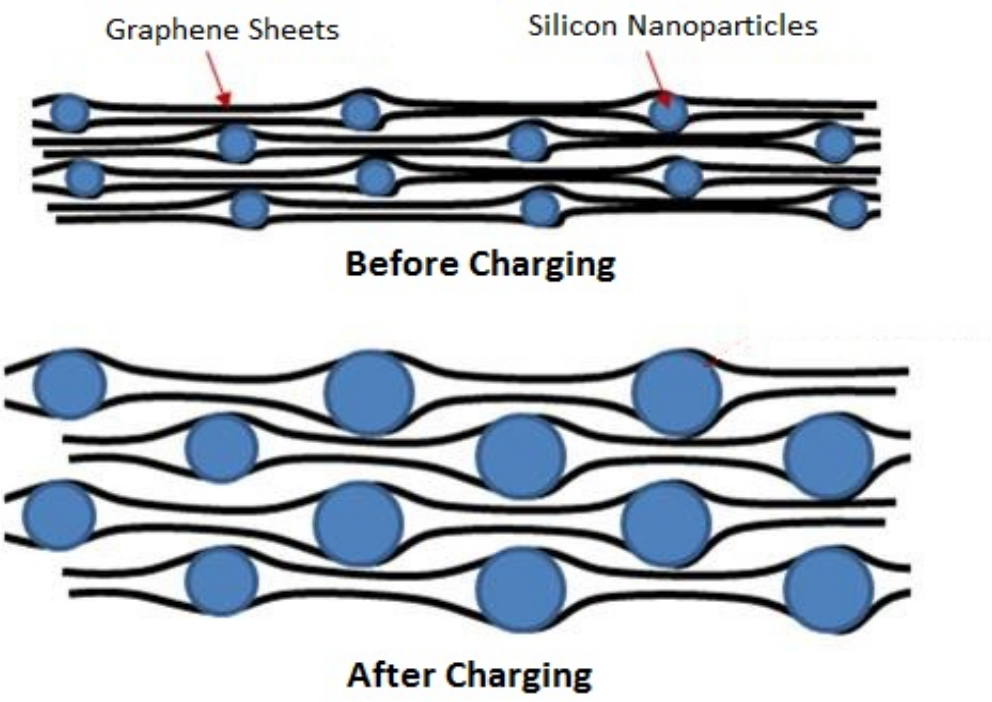

Figure 1.6: A visual representation of the desired electrode composite structure.

Chapter 2

Literature Review

2.1 Silicon

Silicon is one of the most abundant elements on this planet. As such, it has a variety of uses in daily life. This ubiquitous element is currently being investigated as a viable material for lithium-ion batteries. Silicon is a popular experimental electrode material for secondary lithium-ion batteries because of its high theoretical energy density and storage capacity of lithium ions. It has many advantages that allow it to be a good electrode material, including a small discharge potential, and a large theoretical capacity. However, silicon and silicon compound electrodes are rarely used because of their degradation due to changes in volume during lithiation/delithiation cycles, which limits their cycle life. Even though it has a high capacity, its low cycle life leads to a short-term use. One way to improve the performance of the battery is by reducing the size of the silicon to a nanoparticle level.

To improve the electrode capabilities, silicon nanostructures were assembled as early as 1988. Furukawa and Miyasato created ultrafine silicon particles in crystallized structures while looking for three-dimensional quantum confinement effects in silicon-based materials. They created the silicon nanoparticles in a crystal structure through

a sputtering technique. The electrical properties were tested by evaporating aluminum on the surface of the nanoparticles on fused quartz substrates. In testing, Furukawa and Miyasato discovered that the silicon nanoparticles exhibited energy gaps higher than what was theorized through the quantum well model. They extrapolated that even a small deviation in the silicon particle size causes a reduction in the energy gap from that predicted by a uniform size. This is the foundation for proving that silicon nanoparticles have great conductivity for applications in rechargeable batteries.[20] Another nanostructure in use is the silicon nanowire. Silicon nanowires can cycle without as much degradation as unstructured silicon because smaller wires do not continue to fracture, giving them higher cycle lives. Having dispersed, smaller wires allows for more homogeneous expansion, reducing stress. However, producing silicon nanowires is prohibitively expensive and energy intensive, not suitable for commercial mass production.[21]

Due to its high theoretical energy density, silicon was quickly adapted to improving secondary lithium-ion batteries as early as 1993. Walton et al. were some of the first to study the effects of intercalating lithium ions into a silicon electrode to increase the capacity of lithium-ion batteries. The silicon electrode was composed of floating zone p-type silicon wafers. The Gettering method in the experiment was found to resolve the issue of lithium-ion drifting previously experienced by silicon-lithium electrode manufacturers. Now lithium-ion batteries were able to travel through the battery without experiencing significant mobility-reducing imperfections within the electrode.[22]

In 1995, Xue et al. expanded upon the potential for silicon in rechargeable lithium-ion batteries by experimenting with methods to change the ratio of silicon, carbon, and oxygen in a pyrolyzed epoxy-silane electrode to increase the capacity of nonaqueous lithium electrochemical cells. Xue et al. decided to experiment with mixtures of silicon-containing and non-silicon-containing polymers so that the ratio of silicon

to carbon in the electrode could be adjusted. The silane percentage, the amount of silicon in the cells, was measured using a thermal gravimetric analyzer (TGA).The carbon content of these cells was measured by first applying a chemical leaching technique using hydrofluoric acid, then calculating the weight difference before, and after the HF acid treatment. Xue et al. then intercalated lithium ions using constant current methods applied to non-aqueous electrochemical cells. They found that the carbon-silicon-oxygen glasses experienced high levels of irreversible capacity and high charging voltages.[4]

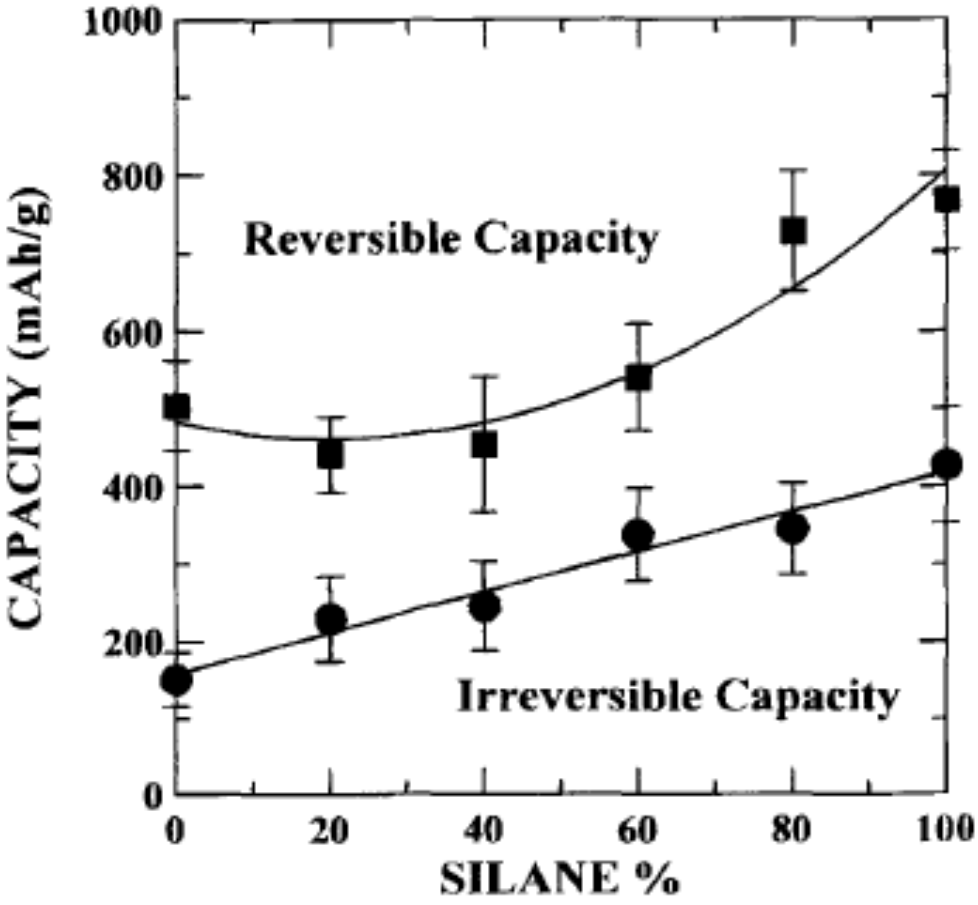

Figure 2.1: Trends in both reversible and irreversible capacities increase with silicon content. Reproduced with pending permission from reference.[4]

Figure 2.1 is a graph of reversible and irreversible capacity of all six data sets from

the study performed by Xue et. al. In their study, they were determined to find the ratio of silicon, carbon, and oxygen in nonaqueous lithium-ion cells that would result in the highest capacity. Each paired data set represents an electrode containing a different percentage of silane. According to this graph, Xue et. al discovered that though the carbon-silicon-oxygen glasses had high reversible capacities, they also experienced high irreversible capacities.

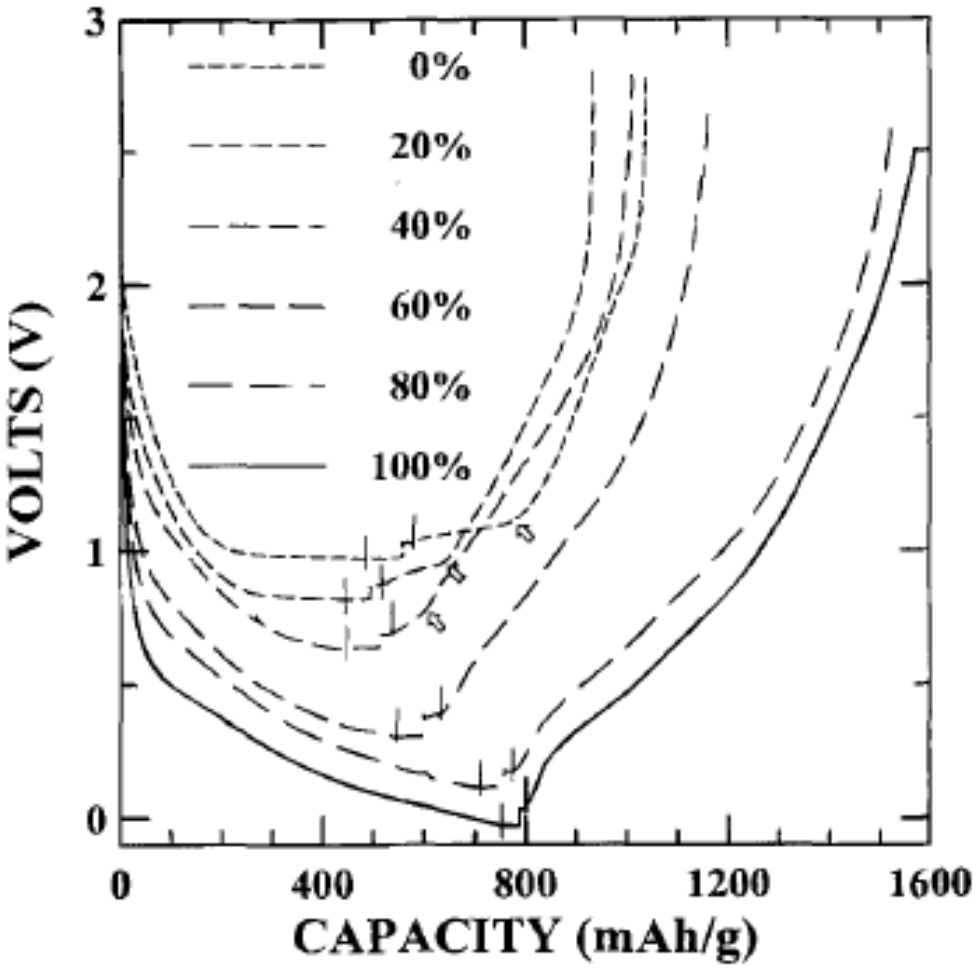

Figure 2.2: Charging and discharging curves of 6 samples display high charging voltages. Reproduced with pending permission from reference.[4]

Figure 2.2 is a lithiation/delithiation profile of all six data sets from the study performed by Xue et. al under a constant current of 18.6 mA/g. According to this

graph, there is a high charging voltage in these carbon-silicon-oxygen glasses that must be remedied if they are to become commercially relevant.

In 1997, Wilson et al. also tested the electrical characteristics of other forms of silicon polymers in rechargeable lithium-ion batteries as a function of their stoichiometry and structural properties. They tested 50 different silicon-containing polymers, including polysilanes, polysiloxanes, and pitch silane blends formed using alternating precursors of pitch, pitch blends or polysiloxanes and reducing them at lower temperatures using pyrolysis. These electrodes were tested for reversible and irreversible capacity, and average lithiation/delithiation voltages as a function of their stoichiometry. They found that silicon performed as hoped, significantly increasing the capacity of the lithium-ion electrode materials, while retaining the high reversibility of carbon. Wilson et. al also conjectured that their electrodes prepared using CVD represented nanodispersed materials and that nanodispersed materials could be the next promising research area for lithium-ion battery technologies because these materials also showed high reversible capacities.[23]

Silicon nanostructures were also being implemented in lithium-ion batteries, starting in 1994. Wilson and Dahn prepared an unordered compound pregraphitic carbon and silicon nanoparticle electrode for rechargeable lithium-ion batteries and found that silicon nanoparticles increase the specific capacity from around 300 mAh/g to nearly 500 mAh/g. This electrode was also able to significantly maintain its capacity over lithiation/delithiation cycles, which set a precedent for using silicon nanoparticles in the electrodes of secondary lithium-ion batteries.[5]

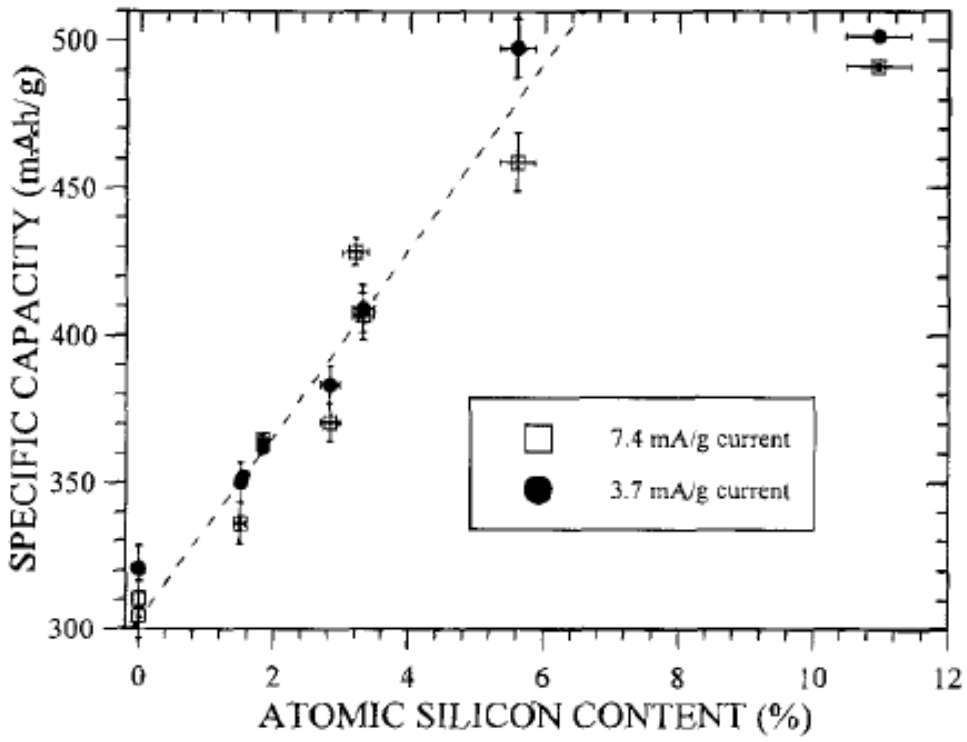

Figure 2.3: Specific capacity is linearly correlated to the percentage of silicon content in the battery electrode. Reproduced with pending permission from reference.[5]

The use of silicon nanostructures reduces some of the strain during the expansion/contraction period, increasing the cycle life. However, just decreasing the size of the nanoparticle does not ensure that the silicon will not degrade. Due to its high surface energy, the nanoparticles will eventually aggregate, rendering them useless in the electrochemical process. Similar to the case of larger particles, an agglomeration of many nanoparticles will localize the expansion and cause fracturing.[?] Another method is to try to obtain uniform spacing of particles. Particle-particle interactions also play a role in further destruction of the element. Evenly spacing out the particles reduces the chance that they will interact with one another. One of the most promising avenues for reducing breakage of silicon is the use of carbon sheets to retain the negative electrodes shape. The tensile strength of the carbon sheets helps the negative electrode retain its shape after lithiation and delithiation. The conductivity of

the material also improves the electronic properties of the silicon.

2.2 Graphene

For decades, graphene was considered a purely theoretical construct, and 2D materials were argued to be thermodynamically unstable by Landau and Peirels. It was not until 2004 when Novoselov and Geim published the groundbreaking paper, Electric field effect in atomically thin carbon films, that a real single layered graphene structure was created and tested on. In their 2004 paper, Novoselov and Geim tested the electrical properties of graphene and discovered some of its remarkable properties; for one, the electrons behave like massless Dirac fermions, meaning they act as if they have lost their rest mass and move at relativistic speeds. Graphene is also a zero-gap semiconductor where the band and valence gap separation is negligible, the material carries both electrons and holes. These allow for unique properties, for example when applying a potential across the material, the band gaps can be tuned, imitating other materials.[24][25]

2.2.1 Chemical Vapor Deposition

As graphene garnered great attention in the scientific world, attention turned to the problem of how to make large sheets of graphene efficiently. The original method involved using scotch tape to remove layers of graphene off of graphite sources.[24] As low cost and effective as this was, it was not a viable process to create large amounts of material at a time. Chemical vapor deposition techniques were developed and proved to be effective creating clean, monolayers of graphene on various surfaces.[26][27] One drawback of many of the methods was the difficulty of transferring the graphene from the silicon-carbon substrate to a metal substrate. More techniques were developed, including CVD onto nickel but suffered from grain limitations on the size and purity

of graphene sheets.[26]

For many uses, deposition onto copper is the best solution. In the paper by Li et. al., Large-Area Synthesis of High-Quality and Uniform Graphene Films on Copper Foils, Li touches on these concerns and introduces a method of using CVD to deposit onto copper. The use of Ar, H_2, and CH_4 gas in a tube furnace, flowed over the copper sample allowed at 1000° in an isothermal and isobaric environment created clean graphene sheets of varying thickness. The growth of graphene is also a self-limiting process where the number of sheets grown stops after $\approx$ 10 minutes of annealing with the CH_4 flow.[27]

To verify that the material is created successfully, Raman spectroscopy is used to analyze the order and disorder of a sample through inelastic scattering of phonons and incident laser light. By referring to literature, we can determine the quality and thickness of our graphene samples.

2.2.2 Mechanical Mixing

Unlike CVD, which yields a large single layer of graphene, published mechanical mixing methods yield multi-layered graphene. Here, we discuss five methods that yield different graphene purities, cracks, and interlayer distances.

In one method by Saner et al., the graphene is synthesized from graphite oxide using a modified Hummers method (see Graphite Oxide (GO) in the Literature Review section) that substitutes $KMnO_4$ with $K_2Cr_2O_7$, which minimizes the risk of explosion due to the highly exothermic nature of the reaction with H_2SO_4 later. The resulting graphite oxide is exfoliated via ultrasonic vibration, and expanded by heating in a tube furnace in an argon atmosphere. After another ultrasonic water bath, the expanded graphite oxide is exfoliated and reduced via reflux in hydroquinone and distilled water under a nitrogen atmosphere for one day. These graphene-based sheets are separated by filtration, washed with methanol and water, and dried in a

vacuum oven overnight.[28] This method would be inefficient for making the graphene needed for this experiment, as we do not need or want a large interlayer spacing for the graphene sheets.

In another method by Wan et al., graphite oxide made from a modified Hummers method is thermally reduced in a tube furnace under argon atmosphere at a fixed heating rate of 10°C/min. Between 300°C, 600°C, and 800°C, 300°C produced the highest specific surface area, fewer layers, more curled sheets, and were best at lithium storage.[29] However, due to instrument size, tube furnace reduction yields small amounts of product compared to microwave reduction discussed later in this section.

In yet another method by Pu et al., a supercritical CO_2 exfoliation of graphite results in 30-40% weight graphene sheets.[30] However, this percent weight is too low for comparison to CVD graphene and especially to CVD graphene-silicon composite.

Ultimately studied for modification and optimization, a microwave method developed by Zhu et al. involves synthesizing graphite oxide from a modified Hummers method and microwaving it in ambient conditions at 700 W. This method is simple, versatile, and yields a high enough percent weight graphene for comparison with CVD graphene.[31]

A similar method by Chen et al. is a rapid microwave reduction using a reducing agent such as hydrazine or NH_4OH.[32] However, this method begins to reduce the graphite oxide to graphene in a mixing step before the microwave reduction. This causes a problem for our study on graphene-silicon composites, where adding silicon nanoparticles to the graphite oxide mixture prior to adding a reducing agent may yield poorly distributed silicon nanoparticles throughout the graphene sheets. Thus, the previously mentioned microwave-only reduction method was used to make mechanically mixed graphene comparable to CVD graphene and the graphene-silicon composites.

2.3 Graphene-Silicon Composite

Due to the limitations of silicon in an electrode, graphene-silicon composites are an answer to increasing capacity and cycle lives. The high theoretical capacity of silicon can be maintained for many cycles through a graphene base. The graphene base acts as a scaffold to the silicon as it expands during battery cycling. The composites have been made in a variety of ways. The silicon structures include silicon particles, films, and wires.[6][7].[8] To support the silicon structures, the graphene also has been formed into a variety of structures through different methods. By making graphene-silicon composite electrodes batteries are able to have higher capacities and cycle lives. To consistently create the higher capacities and cycle lives, composites that have homogeneous dispersion of silicon is important.

Addressing the aggregation problem with carbon nanoparticles, Zhou et. al synthesized a 3D network of graphene sheets. The silicon nanoparticles are distributed and separated by graphene sheets with carbon nanoparticles that encapsulate the particles as seen in Figure 2.4.[6] Through electrochemical impedance spectra, the graphene structure proved to be effective to increase the cycle life of the graphene-silicon composite. While it is cost-effective and commercially available, the bulk polycrystalline silicon used in the process does not allow the silicon particle size to be controlled.[6]

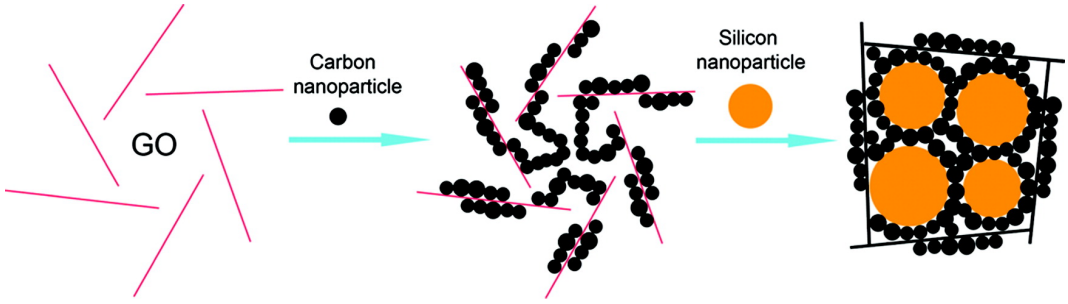

Figure 2.4: Illustration of encapsulated silicon particles in graphene and carbon nanoparticles. Reproduced with pending permission from reference[6] Copyright 2012 J. Mater. Chem.

A method by Luo et al. used an aerosol method to create crumpled graphene structures to surround silicon nanoparticles as seen in Figure 2.5. The crumpled ball morphology prevents strong interparticle van der Waals attraction, which ensures homogeneity. Unlike Zhou et al., they were able to control the silicon nanoparticle size to be between 50 to 100 nm. Through scanning electron microscopy, scanning transmission electron microscopy, electron loss spectroscopy and energy- dispersive X-ray spectroscopy, this structure was verified. The graphene-silicon composite retains 83% of the higher charge capacity after 250 cycles proving its cycle life. While the silicon size is more specified, this method requires further research to control the mass ratio of silicon to graphene.[7]

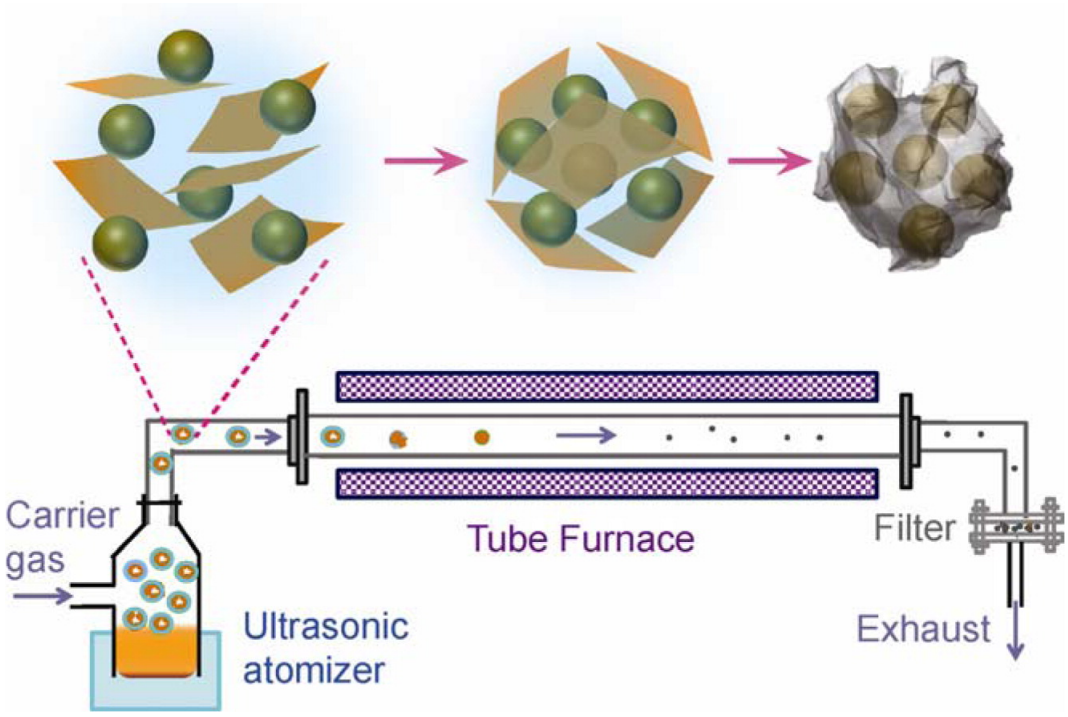

Figure 2.5: Illustration of encapsulated silicon particles in crumpled graphene. Reproduced with pending permission from reference[7] Copyright 2012 J. Phys. Chem. Lett.

A method proposed by Yang et al. was able to address the aggregation problem while controlling the silicon particle size and mass ratio as seen in Figure 2.6.

transmission electron microscopy, Raman, thermogravimetric analysis and X-ray photoelectron spectroscopy prove Phenyl linkers bonded silicon particles homogeneously on top of graphene sheets. The silicon particle size was controlled to 50-200 nm. The weight ratio of silicon to graphene was controlled to 5:2. The batteries were able to have higher reversible capacities for 50 cycles.[8]

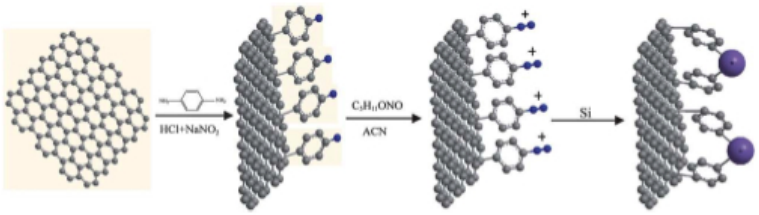

Figure 2.6: Illustration of silicon particles bonded on graphene sheets. Reproduced with pending permission from reference[8] Copyright 2012 J. Mater. Chem.

Recently, the graphene-silicon composite electrode has gained such popularity that California Lithium Battery Inc. and Argonne National Laboratory plan to release a graphene-silicon battery electrode in 2014. The electrode composite that they utilized used chemical vapor deposition to create layers of graphene and silicon proved to be successful.[33]

2.3.1 Microwave Reduced Graphene-Silicon

Graphite Oxide (GO)

GO can be obtained only by oxidation of graphite salts (nitrate or bisulfate) either with strong oxidizing agents (i.e. $KClO_3$, $KMnO_4$, bichromate, ClO_2), or electrochemically. There are three main methods for the preparation of graphite oxide: Brodie (1860), Staudenmaier (1898), and Hummers-Offeman (1958). Each is based on the oxidation of graphite in concentrated strong mineral acid with strong oxidizing agents, but vary in levels of efficiency, GO quality, and safety. Solid GO may then be recovered via drying in a high vacuum at room temp, lyophilization (freeze-

drying), or heating in air to low temperatures (45-50°C) to prevent decomposition of oxygen-containing functional groups of GO.[34]

The Hummers method involves graphite oxidized by $KMnO_4$ in concentrated sulfuric acid. Hummers and Offeman stirred flake graphite and sodium nitrate into sulfuric acid. The purpose of the sodium nitrate is to aid in better dispersal. The flask was put into a ice bath, and agitated vigorously. Then, $KMnO_4$ was slowly and carefully added to the flask. The danger here is that adding the $KMnO_4$ too quickly may result in an explosion, so caution must be taken not to exceed 20°C. On a hot plate, the flask was brought to 35°C, not above 38°C and not below 32°C, so that the reaction may proceed at a safe but reasonably fast rate. By the end of the reaction, aided with added water, the mixture was treated with H_2O_2 until the solution was mostly clear. The mixture was filtered while still warm, leaving a solid yellow-brown filter cake, a significant but somewhat impure yield of graphite oxide.[35]

Brodies method involves graphite oxidized by $KClO_3$ in fuming nitric acid, which is more dangerous, takes longer, and is not as efficient as Hummers-Offeman. Brodie cooled a 500 mL flask containing 165 mL of fuming nitric acid to 0°C in an ice bath. He mixed 10 g of graphite into the flask, and slowly added 110 g of $KClO_3$ while stirring. He then transferred the mixture into 10 L of distilled H_2O, and filtered it immediately. Immediately following that, the mixture was washed with 5% HCl until the sulfates completely disappeared, indicated by the color of the draining liquid becoming clear. The bright yellow-brown filter cake was dried at 50°C in an oven for 16 hrs.[36]

Staudenmaiers method involves graphite powder oxidized by fuming nitric acid, 97% H_2SO_4, and $KClO_3$. It is the same procedure as Brodies method, replacing nitric acid with a H_2SO_4/nitric acid mixture. This substitution is intended to increase the acidity of the reactants. This method yields about the same oxidation level as Brodies method and is more efficient than Brodies method, but is not safe.[37]

Overall, Brodies method yields the lowest contamination and smallest interlayer distance graphite oxide, brightly colored and very stable. Staudenmaiers and Hummers methods yield unstable, more contaminated, and degraded graphite oxide. With Staudenmaiers method specifically, the method takes the longest but yields the lightest-colored GO. Hummers method, however, is by far the fastest method, as well as the safest. It yields a slightly brownish-colored GO, but the speed of the method allows for large amounts of GO to be made very quickly. Therefore, the Hummers method was chosen to be modified for the experiment.

Reduced Graphite Oxide

Once the Hummers-Offeman method was selected for use and modification, the options for reduction to graphene were narrowed down.

- Reducing agent (hydrazine or NH_4OH) + microwave[32]
- Microwave-assisted exfoliation & reduction of GO.[31]
- Thermal reduction in tube furnace under argon atmosphere. With this method, GO is thermally reduced in the tube furnace assembly under argon atmosphere with heating rate of 10°C/min. Between 300°C, 600°C, and 800°C, 300°C produced the highest specific surface area, fewer layers, more curled sheets, and were best at lithium storage.[29]

Ultimately, microwave-assisted exfoliation and reduction was chosen as a method for reduction to graphene. A chemical microwave was more accessible at the time than a tube furnace. This left two microwave methods to choose from. For the purpose of creating a graphene-silicon material, it is best not to use a reducing agent prior to microwaving. It is also favorable to know for sure that the graphite-oxide was not being reduced before the silicon nanoparticles had a chance to disperse. Therefore, the

microwave-assisted reduction without reducing agent was selected for optimization as a reduction method, resulting in MMG and MMG-Si.

2.3.2 Mechanically Mixed Graphene-Silicon

Multiple methods have been employed to create graphene-silicon composite electrodes with varying results. The most common procedure involves sonicating a mixture of graphene oxide sheets and silicon nanoparticles, and then drying/filtering this mixture. Lee et al. used this procedure and controlled the extent of graphitic regions within the electrode by controlling the time and temperature during thermal reduction. Their batteries exhibited stable capacities of over 1500 mAh/g over 200 cycles.

In 2003, a study by Yoshio et al. was conducted to create a carbon-coated silicon electrode. Silicon and graphite were mixed and then used as a starter for thermal vapor deposition. By changing the water composition of the mixture, they were able to obtain up to 40 cycles at 800 mAh/g as seen in figure 2.7. Unfortunately, as the cycles continued, lithium-ion build-up occurred creating structural defects in the electrode, causing capacity loss.

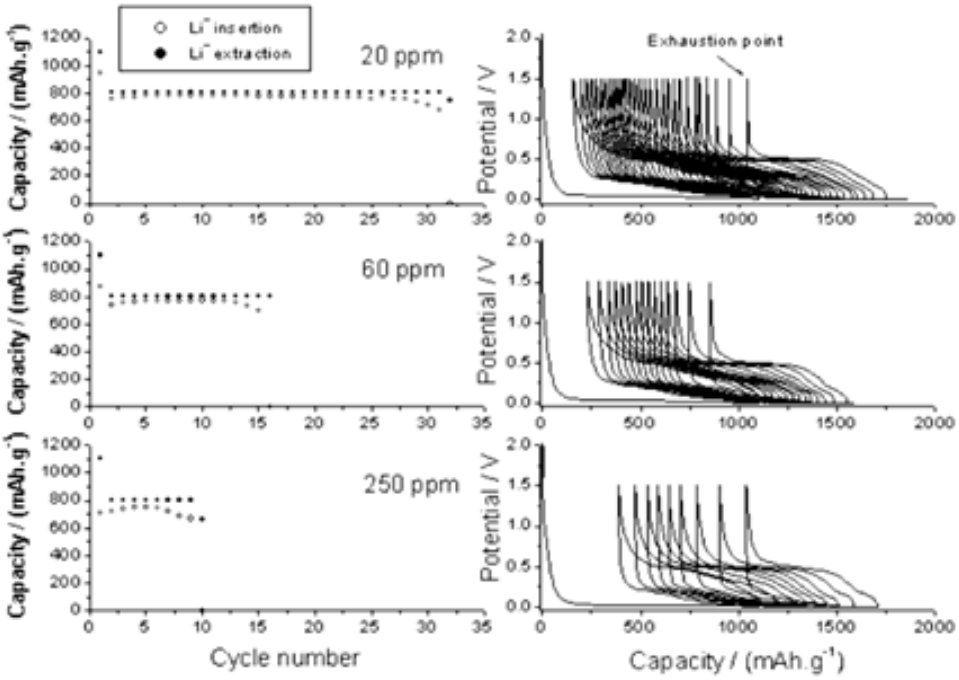

Figure 2.7: Overview of electrode groups of single layer graphene-silicon, multilayer ordered reduced-graphite oxide silicon, mechanically mixed reduced graphite oxide, and mechanically mixed reduced-graphite oxide silicon.[9]

In 2010, a study was conducted by Chou et al. where silicon nanoparticles were mixed in a 1-to-1 weight ratio with graphene. A cross-section of the SEM image of this composite shows the nanoparticles within the graphene matrix as seen in figure **??**. When tested, this battery shows a much improved capacity with a more stable cycle life. Figure **??** compares the graphene-silicon composite electrode with the other possible electrode materials. Short of a theoretical silicon contribution, the composite has the highest capacity over a set number of cycles. The paper showed that the battery maintained a 1168 mAh/g capacity for at least 30 cycles. While this is an improvement on earlier silicon electrodes, the cycle life is still not ideal for commercial applications.

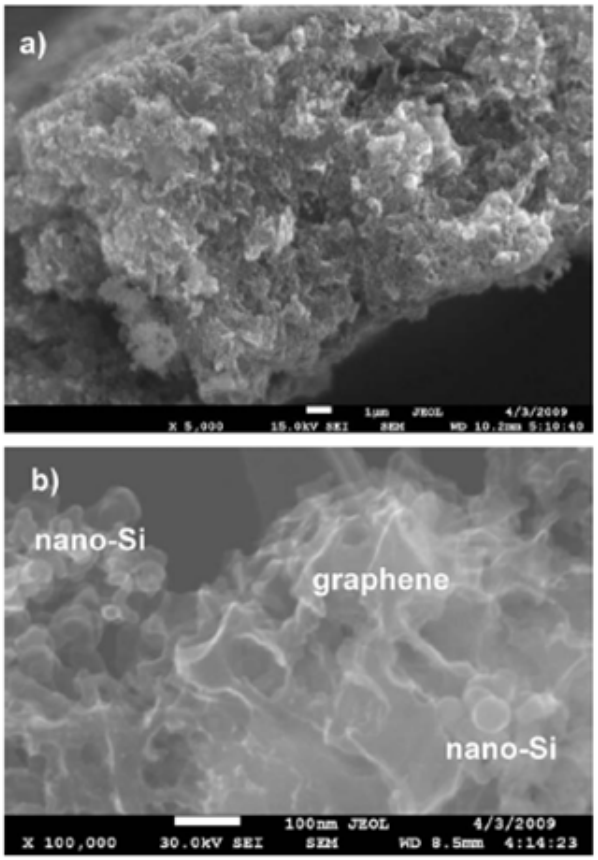

Figure 2.8: Overview of electrode groups of single layer Graphene-Si, multilayer ordered reduced-graphite oxide silicon, mechanically mixed reduced graphite oxide, and mechanically mixed reduced-graphite oxide silicon.[10]

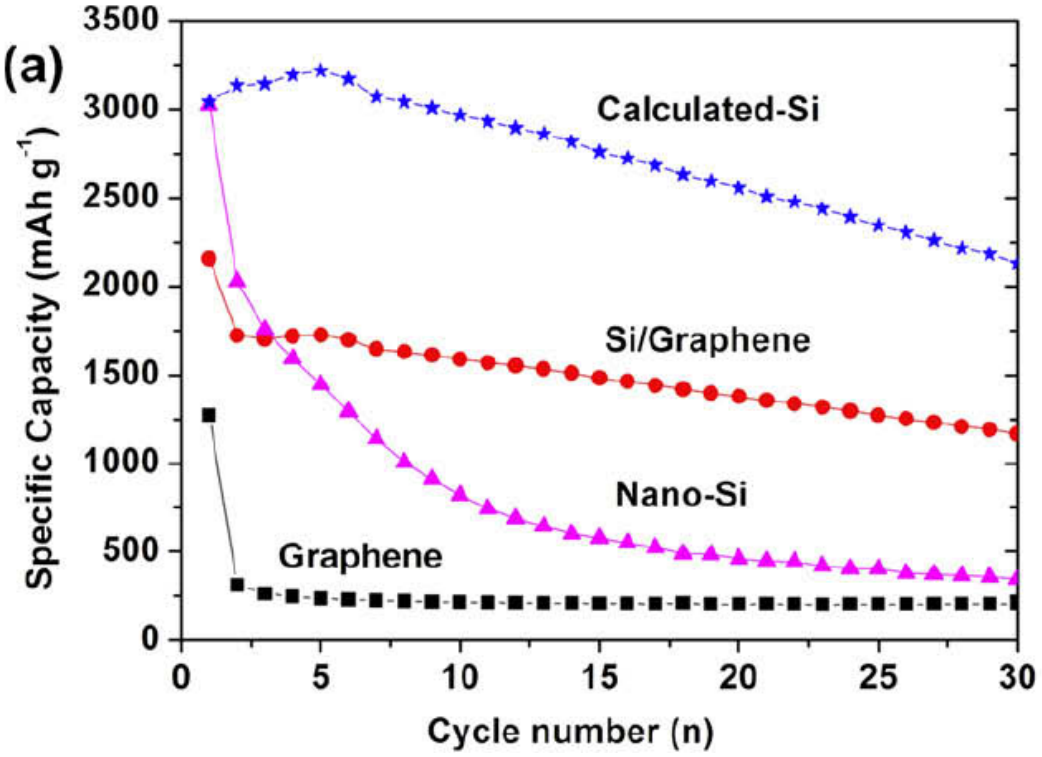

Figure 2.9: Overview of electrode groups of single layer graphene-silicon, multilayer ordered reduced-graphite oxide silicon, mechanically mixed reduced graphite oxide, and mechanically mixed reduced-graphite oxide silicon.[10]

Some variations on this method have been attempted. For example, Zhou et al. created solutions of graphene oxide and silicon nanoparticles as usual, but then freeze-dried and thermally reduced it to form the electrode material. This freeze drying process avoided the higher temperatures associated with a normal process that can cause the silicon to agglomerate. However, batteries constructed with this material showed stable capacity of 1153 mAh/g over 100 cycles. The research presented in this paper will attempt to create batteries with cycle lives better than the ones currently found in literature.

In a 2012 study by Zhou et al., a graphene-silicon mixture was obtained using electrostatic attraction. In this experiment, both graphene and silicon were oxidized to make negatively charged GO and silicon-oxide. They were then self-assembled

using a positive binder, PDDA, and reduced. This allowed for a well-dispersed and encapsulated silicon nanoparticle. The capacity obtained from this composite was 1205 mAh/g over 150 cycles. It was stated that this improved cycle life could be attributed to a good buffering of the volume expansion, by the graphene, as well as an increased lithium-ion diffusion.

As can be seen in these five papers, particle size greatly affects the cycle life of the battery. A graphene electrode has a stable capacity of about 250 mAh/g. A nanosilicon electrode has a trend of continuously decreasing capacity after each cycle. When graphene and nanosilicon particles are combined into an electrode, the electrode has a higher stable capacity than either material on its own. By tweaking the structural properties of these particles, their electrical properties are changed as well, allowing for the possibility of a stable, significantly increased cycle life.

2.3.3 Electrochemical Deposition

Electrochemical deposition has been known for many decades to be an effective tool for depositing metals on the nanoscale onto various surfaces. Electrochemical deposition is the process by which an electrical current provided by an external source is run through an electrochemical cell. The donation of electrons from the induced current causes the reduction of a metal solute species onto an electrically conductive surface. However, the successful implementation of electrochemical deposition is much more complex; the correct combination of solvent, electrolyte, and voltage/current parameters must be carefully considered. A number of studies in recent years have shown the techniques utility in depositing silicon onto graphite to produce various silicon/carbon structures for lithium-ion batteries.

Several classifications of solvent exist for the deposition of silicon onto a metal substrate. Aqueous solvents cannot be used to deposit silicon due to the large negative potentials required for the positive electrode. The organic solvent propylene

carbonate (PC) was used with trichlorosilane, $SiHCl_3$, as the silicon source for the electrochemical deposition of silicon onto various metal substrates.[38][39]

Schmuck et al discussed the viability of electrochemical deposition of silicon thin-films. An organic and ionic liquid electrolyte solution was used to deposit silicon onto a copper current collector. Electrochemical deposition was performed using a self-made three-electrode Swagelok® cell. Copper foil, lithium piston, and lithium foil was used as the working, reference and counter electrodes respectively. The paper compared the effectiveness of the organic solvent propylene carbonate (PC) and the ionic liquid solvent N-butyl-N-methylpyrrolidinium bis (triflourmethanesulfonyl) imide (Pyr_14TFSI). Both solutions were made using 1 M $SiCl_4$ as the silicon source, with 1 M LiTFSi as the conducting salt. The electrochemically deposited electrode structures of these two solvents were then compared to a silicon composite material sample formed by mixing nanosized silicon powder and a small amount of carbon black with Na-CMC binder. This slurry was coated by the electroplating method onto copper foil. This silicon composite electrode was used as the control group to which the electrochemically deposited silicon electrodes would be compared.[40]

CV scans were performed on the both the organic and ionic liquid-based electrochemical system. It was confirmed that $SiCl_4$ was reduced at approximately 1000 mV versus Li/Li+. A potentiostatic method was used to deposit silicon at room temperature at 1.0 V versus Li/Li+ for a time of 3,600 seconds. Scanning Electron Microscopy (SEM) imaging determined that both methods produce silicon particles that were comparable in size and in the range of 100-500 nm. Charge capacity versus cycle life plots indicated that there was a significant drop-off in capacity for the two electrochemically deposited electrodes. This occurred by the second cycle. The silicon composite on copper current collector electrodes performed without seeing any significant drop in capacity after 5 cycles. This is likely due to the lax connection of deposited silicon particles to the copper substrate surface. The lithiation/delithiation

process is likely to break apart the deposited silicon from the surface.[40]

Though the deposited silicon electrodes were less successful than the silicon composite electrode, the study proved that the electrochemical deposition of silicon onto a copper current collector is not only possible, but is an effective alternative to producing thin-film silicon structures with nanosized particles. It was also determined that the substrate surface played a surprising role in the deposition process. It appeared that deposition was more successful when the copper substrate had a roughened surface. It is believed that these regions on the substrate incur the highest current densities, corresponding to a larger amount of deposited silicon per unit area.[40]

In another study by Chen et al., it was determined that the electrochemical deposition technique could deposit silicon onto complex substrates to fabricate unique silicon electrode materials. Silicon as an electrode material is extremely promising. Its high theoretical capacity and low lithiation/delithiation voltage makes it an ideal candidate for lithium-ion batteries. Due to the inherent pulverization of the silicon structure during the lithiation/delithiation process, unique and alternative silicon-based electrode structures for lithium-ion batteries are being investigated.[41]

The reduction of silicon tetrachloride ($SiCl_4$) was found to be:

$$SiCl_4 + 4e- \rightarrow Si + 4Cl - (workingelectrode)$$

$$4Cl- \rightarrow 2Cl_2 + 4e - (counterelectrode)$$

In this paper, silicon is electrochemically deposited onto a nickel current collector composed of nanowire-like rods of tobacco mosaic virus coated with nickel. This produces a complex and conductive substrate with a large surface area. A number of electroanalytical techniques were used to determine the deposition potential of $SiCl_4$ in the cell. A linear sweep was conducted with platinum foil and platinum wire was used as the counter electrode and the quasi-reference electrode respectively.

The TMV1/Ni current collector was used as the working electrode. The organic solvent PC was used with 0.1 M tetrabutylammonium chloride (TBACl) with 0.5 M $SiCl_4$. Linear polarization was performed on the cell, which indicated a cathodic peak at approximately -2.33 V. Chronoamperometry and chronopotentiometry techniques were performed on the same cell, which reconfirmed the reduction potential of SiCl4 at around -2.3V for the electrochemical system. Current density was set to a constant -1 $mAcm^{-2}$ current density while the chronoamperometry was set to a constant -2.4 V versus Pt QRE.[41]

It was determined through SEM imaging that the electrochemically deposited silicon was slightly transparent. SEM imaging of silicon layers prepared by physical vapor deposition were not transparent, however; this indicates that silicon prepared by electrochemical deposition is less dense and more porous. It was determined that the nickel current collector within each individual electrochemically deposited silicon nanowire resulted in a high aspect ratio electrode with a capacity of 2300 $mAhg^{-1}$, which is significantly higher than pure graphite based electrodes (372 $mAhg^{-1}$). The electrode also demonstrated improved capacity retention of 1200 $mAhg^{-1}$ at 173 cycles. The total amount of deposited silicon was controlled by the total amount of electrical charge consumed.[41]

As discussed earlier, researchers are specifically focusing on doping or modifying the electrode of the lithium-ion battery to increase its electrochemical performance and stability. One proposed idea is to create lithium-siliconfilms (LSF) for the electrodes using a multi-step electrochemical deposition process. The researchers of this method, Wang, et al., believe that creating a nanoporous lithium-silicon film as the electrode will allow the electrode to better accommodate the varying volume change of the silicon during lithiation-delithiation than other methods. The volume change of silicon is one such issue that the following experiments presented in this paper, will investigate.[42]

The proposed method used a two-step electrochemical deposition process under constant current conditions on a copper substrate under Argon. The first solution comprised of $SiCl_4$ and TBACl in PC and the second solution was $SiCl_4$ and $LiClO_4$ in PC. The electrochemical deposition process was done using the standard three-electrode setup, where the copper film is the working electrode, Pt wire (Pt Q.R.E) as the reference electrode, and a polished graphite plate as the counter electrode. First, the electrochemical deposition of silicon onto the copper substrate was conducted using solution 1 at a constant current of (-3.82 $mAcm^{-2}$, -6.37 mA cm^{-2} for 600 s), separate trials were conducted with each current. Secondly, the co-electrochemical deposition of lithium on to the silicon-infused copper substrate was done by solution 2 at a current of -1.27 $mAcm^{-}2$ for 10800 and 7200 seconds, whereas again separate trials for each time constraint. The three samples with varied current and time constraints (LSF-1, LSF-2, LSF-3) were then characterized by SEM, Energy- dispersive X- ray Spectroscopy (EDX), and Inductively Coupled Mass Spectroscopy (ICP-MS).[42]

From the results of the characterization the Si/Li ratio of the LSF-1, LSF-2, and LSF-3 are 0.31, 0.62, 0.45 respectively. The presence of lithium in the LSF allows electronic conductivity to occur faster and more efficiently and counteracts the solid electrolyte interface (SEI) that causes the irreversibility of the cell. The three types of LSF were electrochemically tested with a potential range of 0.01-1.40 V versus Li/Li+. The LSFs produced varied charge capacities because of the deposition time allowing for a different structure t -2, which compared to the initial capacity of 240.6 μAh cm^{-2}, retained a 74.4% of its initial charge capacity. The coulombic efficiencies of LSF-1,2,3 are 121.7%, 77.2%, and 97.1%.

This method is promising and upon further refinement of procedure can significantly affect the lithium-ion industry. Furthermore, this method is unique since it allows the user to vary the Si/Li ratio via electrochemical deposition times so that the coulombic efficiency can be optimized.[42]

One recent trend in lithium-ion battery development is to couple the current technology with another material to enhance the electrochemical performance (i.e. power density, energy density, and cycle life) as well as to increase the safety of the product as well. Silicon is one such material that is being investigated for composite material purposes. Momma et al. describes a unique method of producing a silicon carbon composite material to increase specific capacity and other electrochemical properties. An electrochemical deposition method was used with organic solvent to produce a novel silicon oxy carbide (SiOC) composite material.[43]

Electrochemical deposition was performed onto a copper substrate with an organic electrolyte solution of $SiCl_4$, tetrabutyl ammonium perchlorate (TBAP), and PC under Argon to deposit a uniform layer of silicon on the copper substrate. This deposition was conducted under a 3-electrode system consisting of copper as the working electrode, Pt as the counter electrode, and a Li/Li+ reference electrode using a constant cathodic current of 0.70 $mAcm^{-2}$. Next, the deposited copper film was inserted into an electrolyte solution of $LiClO_4$/PC to be reduced into a SiOC composite. The reduction process occurred at a constant-current-constant-voltage mode at 250 μAcm^{-2} and 0.01 V versus Li/Li+ for 5200s.[43]

Following the production of the composite, characterization of the material was done using Scanning Electron Microscopy (SEM), Energy- dispersive X- ray Spectroscopy (EDX), Transmission Electron Microscopy (TEM), Glow Discharge Optical Emission Spectroscopy (GDOES), and X- ray Photoelectron Spectroscopy (XPS). The XPS report stated a uniform composite of SiOC was formed and the TEM depicted a semi-uniform amorphous product with an average thickness of 3.3 μm on the copper substrate. The electrochemical testing (lithiation-delithiation curves) of the composite was done with a charge potential of 0.3 V versus Li/Li+ and discharged at 0.6 V versus Li/Li+. There was an initial drop in capacity but by the 300th cycle the curves began to stabilize at $630mAhg^{-1}$. The cell was able to cycle to a minimum

of 2000 cycles with a slow degradation of charge capacity.[43]

To explain the initial drop of capacity, it was suggested that the reduction of $SiCl_4$ was not properly completed thus not forming a uniform electrical pathway for electrons to conduct. It is believed that only when the cell was being cycled that the current from the testing completed the reduction of silicon to make it an silicon-oxygen composite in carbon. Once this reaction was completely done, the cell began to stabilize and allowed a strong pathway in the silicon matrix to be formed for electrons to pass, thus, the capacity began to level off and slowly degrade over time.[43]

Chapter 3

Methodology

3.1 Experimental Procedure

Each type of graphene-silicon composite electrode has a unique purpose and method of construction. The electrodes can be divided into three different groups: fundamental, experimental and control. The division of groups can be followed in figure 3.1 (CVD= Chemical vapor deposition, E-dep= electrochemical deposition, re-GO= reduced graphite oxide, MM= mechanically mixed). The fundamental batteries were designed to understand electrochemical deposition before designing our experimental group. Chemical vapor deposition of graphene onto a copper substrate creates a single layer useful for observing the deposition process. The single layer of graphene enables us to have a better understanding of silicon deposition onto graphene before using a multilayer graphene. The electrochemical deposition of silicon onto multilayer reduced graphite oxide is then our experimental testing group. The experimental group is then compared to our control groups of mechanically mixed reduced graphite oxide and mechanically mixed reduced graphite oxide with silicon nanoparticles. Our experiment electrode is to test to see if ordered electrochemical deposition of silicon onto reduced graphite oxide has higher cycle life than the ordered reduced graphite

alone or mixed with silicon.

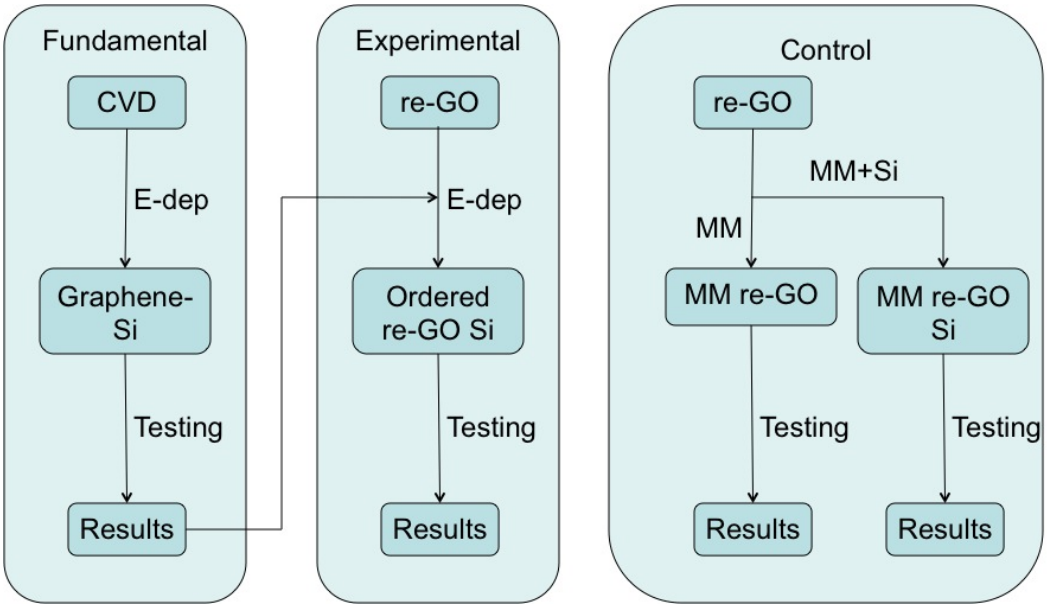

Figure 3.1: Breakdown of electrode groups of single layer Graphene-Si, multilayer ordered reduced-graphite oxide silicon, mechanically mixed reduced graphite oxide, and mechanically mixed reduced-graphite oxide silicon.

We review the methodologies for making CVD graphene, graphite oxide (GO) synthesis, reduced graphite oxide (MMG), electrochemical deposition of silicon onto CVD graphene and electrochemical deposition of silicon onto MMG graphene. To create the graphene for mechanically mixing graphite oxide was synthesized and then reduced.

The fundamental chemical vapor deposition batteries were used to determine voltage, current and timing parameters for electrochemical deposition. These parameters were then applied to the experimental group. Chemical vapor deposition of graphene creates a single layer scaffold for silicon. The single layer of graphene-silicon composite allows for easier characterization of the electrode, through nanoscale imaging, which can then be used to predict the effect of electrochemical deposition of silicon nanoparticles on a multilayer graphene substrate, the experimental testing group. Control groups of mechanically mixed graphene and mechanically mixed graphene with sil-

icon are compared in order to characterize the increase in capacity associated with the addition of silicon. Then the experimental mechanically mixed graphene with electrochemically deposited silicon is compared to the mechanically mixed graphene silicon to show that the increase in cycle life is due to the electrochemical deposition process.

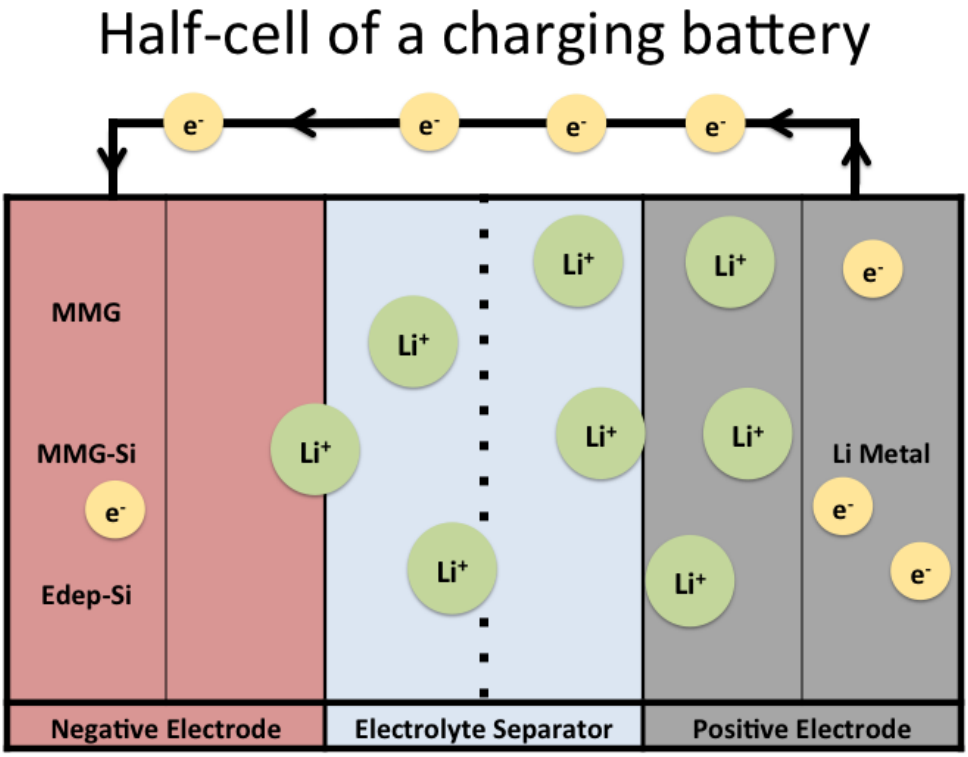

Figure 3.2: A schematic of a half-cell battery for testing as it is being charged. The negative electrode is MMG, MMG-Si or an Edep-Si sample. The positive electrode is a standard lithium metal.

3.2 Chemical Vapor Deposition *Fundamental*

Graphene was primarily grown on high purity copper sheets of disks in a tube furnace. A typical growth process is:

1. Load the copper foil on a boat into the furnace with the foil bent so the arch is in the air allowing gases to flow both over and under

2. Secure the tubes on either end of the furnace and flush for 10 minutes. With the annealing flow rates: 1212sccm for Ar, 164.16sccm for H_2 and 25.38sccm for CH_4

3. Turn off the CH_4 and increase the temperature of the furnace to 1000°C over 1 hour

4. Allow the temperature to stabilize for 30 minutes

5. Turn on the CH_4 again and anneal for 3-10 minutes depending on desired graphene coverage

6. Turn off the furnace and CH_4 for cool down.

The furnace used in this experiment is the Blue M 1200oC Small Tube Furnace. Model 55122A. It is used in conjunction with Moldatherm® Tube adaptors and Process tubes. The Blue M's timing and temperature were set by a custom controller designed by Dr. Fuhrers lab.

3.3 Microwave Reduced Graphene *Experimental*

3.3.1 Graphite Oxide (GO) Synthesis

A slightly modified Hummers method was used. At room temperature, 10 g Johnson Matthey graphite powder (regular graphite powder) and 5g $NaNO_3$ into 230 mL concentrated sulfuric acid was stirred. The mixture was put into 0°C ice bath and continued stirring. While stirring, 30 g $KMnO_4$ was slowly added. The temperature was not allowed to exceed 20°C. The mixture was brought to 35°C, and maintained for 30 min. Slowly 460mL room temperature H_2O was stirred into the paste. The

temperature should have risen fairly quickly. The paste was allowed to reach 98°C and maintained at 98°C for 15 min. Then the paste was diluted to 1.4 L with warm H_2O and treated with 30% H_2O_2 (the mixture fizzed with small bubbles). The mixture was filtered while still warm, changing filters as needed. The liquid that comes through should have been mostly clear and golden. Then the brown filter cake was washed 3 times using a total of 1.4 L of warm H_2O. The brown filter cake was dried in vacuum overnight. The resulting powder was distinctly brown. This was the GO powder reduced in a chemical microwave to make MMG and MMG-Si.

3.3.2 Mechanically Mixed Graphene

Into each of the microwave canisters, 200 mg GO, 1 mL NH_4OH, and 50mL DI H_2O was added. The mixture was microwave reduced using XF100 rotor, power 900 W, no ramp, held at 15 minutes, fanned at maximum speed, and stirred at maximum speed.

3.3.3 Mechanically Mixed Graphene-Silicon

There were three different graphene/silicon samples. All contained 200 mg GO and 50 mL DI H_2O. 20-nm diameter silicon nanoparticles were added to each sample to make the samples 20% silicon by weight. Confirmed by TGA. (Figure 3.3) Microwave reduction done using XF100 rotor, power 900W, no ramp, fan at maximum speed, and stir at maximum speed.

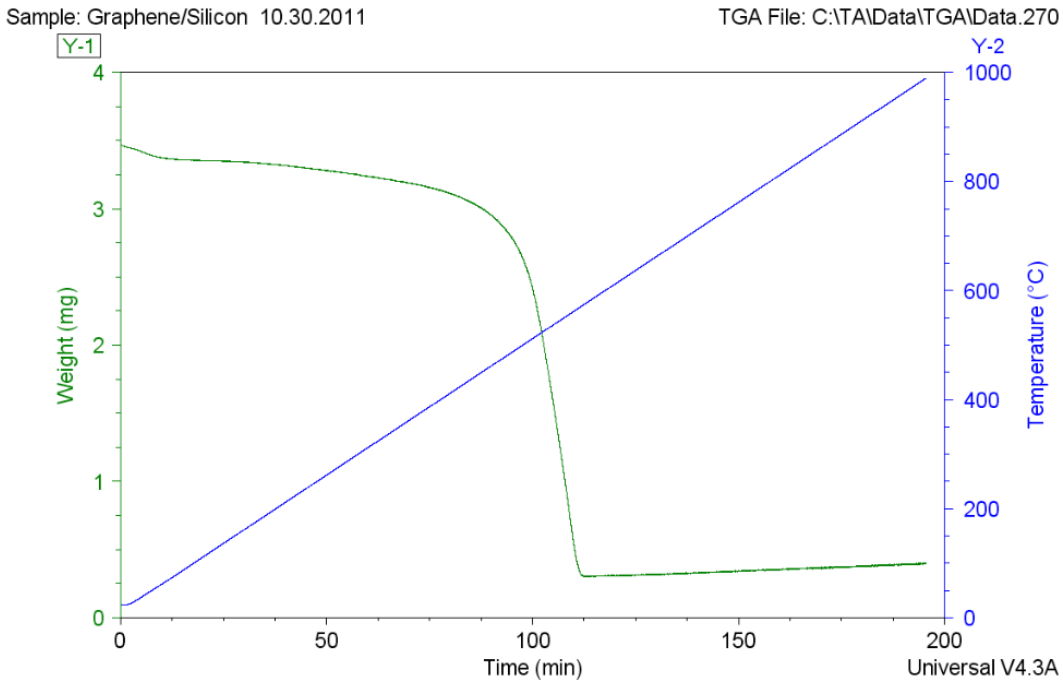

Figure 3.3: TGA analysis showing the presence of silicon.

3.4 Electrochemical Deposition *Experimental*

Electrochemical deposition was performed on two graphene substrates produced through two different methods. The first of these two disks is formed using chemical vapor deposition, while the second is formed using the mechanical mixing method. Both of these methods are described above. The following procedure was performed on both types of graphene substrates. The graphene was placed onto the copper base through its respective method. A circular disk was cut from this graphene-copper sheet using a half inch diameter circular cutter. In early attempts, a hammer was used to cut the disk from the sheet but it was quickly realized that the percussive strikes would cause the graphene layer to separate from the copper sheet. Subsequently, the cutter was placed onto the sheet and was pressed firmly in order to cut the disk from the sheet without significant agitation. After being removed from the sheet and the weight recorded, the disk is transferred into the glove box.

A three-electrode cell was used to perform the electrochemical deposition under a nonreactive argon atmosphere inside the glove box. The graphene-copper substrate served as the working electrode, while platinum foil was used as both the counter and reference electrode. A diagram of this setup is provided in figure 3.4.

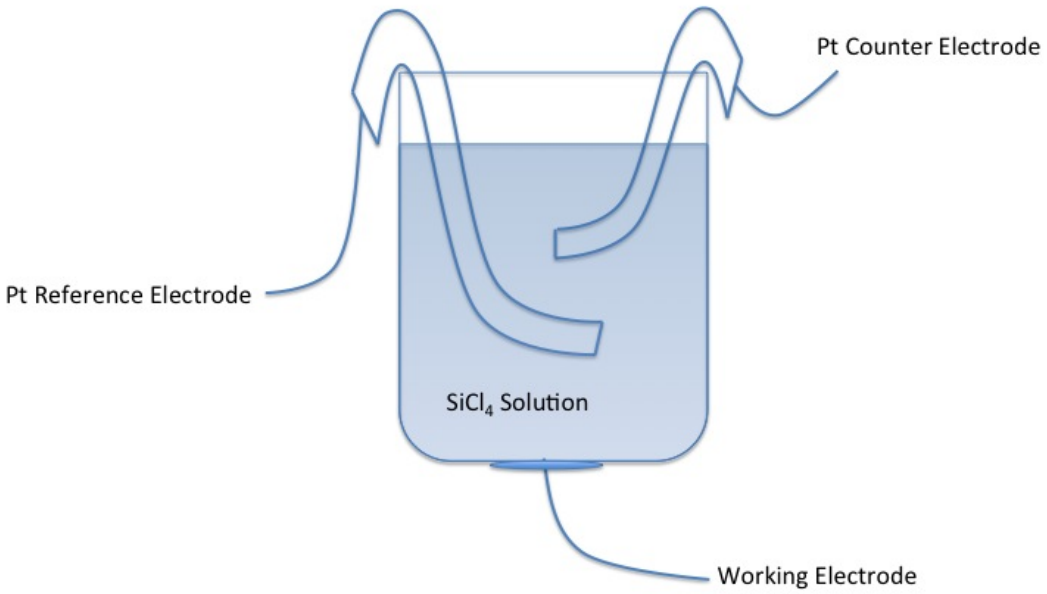

Figure 3.4: Illustration of electrochemical deposition setup.

Two pieces of platinum foil, the necessary wiring, alligator clips and current collector were placed into the glove box. The deposition will occur in a glass bottle that was cut in half. A hole about 0.5 inch in diameter was cut into the bottle cap. Outside of the glove box, on one side, a stainless steel washer was taped with double-sided copper tape such that the entire surface is covered with copper. The copper side of the graphene-copper substrate was placed in the center of the stainless steel disk, which is placed into the bottle-cap with the graphene-copper disk facing up. A silicon ring was placed on top of this, with the graphene-copper disk in the

center of the ring. This ensured a tight seal. The cap was screwed back onto the glass half-bottle and placed into an oven overnight at 100°C to remove moisture and oxygen from the component. The half-bottle and cap system was then placed into the glove box and set up for electrochemical deposition.

The current collector is an external device that is contacted to the stainless steel disk on the bottom side of the bottle cap. The current collector was taped with electrical tape to the bottle to ensure stable contact between the current collector and stainless steel disk. The platinum foil strips should be sanded down to remove any residue. They were attached to the edges of the half bottle with alligator clips that lead to an electrical box at the edge of the glove box. The electrochemical deposition cell was checked to ensure that connections are secure and leakage opportunity is nonexistent.

The electrolyte solution was made using the aprotic solvent propylene carbonate (99.98% anhydrous Sigma Aldrich), tetrabutylammonium chloride (dehydrated) as electrolyte, and silicon tetrachloride (99.7% Fluka) as the silicon source.

Before running the electrochemical test, the cell was again checked for secure connections. The Gamry Reference 3000 is an external device that was then connected to the electrical box of the glove box from the outside. The working, counter, and reference electrodes were connected to their respective components on the electrical box of the glove box. A more detailed description is given in Appendix B which provides a section of the Gamry Reference 3000 user manual. Please review Appendix B to review the precise parameters utilized in the Gamry Reference 3000 for each test run.

This is the general setup for the electrochemical deposition cell. Different electrochemical techniques can be applied to the cell using different manipulations of cell current and voltage. It should also be noted that all metal pieces used in the electrochemical deposition, i.e. the stainless steel disk, electrode connections, platinum foil,

etc. should be sanded down prior to each test run. This is to avoid oxidation deposits on the surface of these metals, which may produce charge sinks and create inaccuracies in measurements. Additionally, high deposition voltages (> -4.5V) should be avoided. Such high voltages have resulted in separation of graphene from the copper substrate. Copper exposure can cause the cell to short circuit when performing electrochemical tests.

3.5 Characterization of Materials

Once each electrode material has been prepared following its own methodology, the resulting material is analyzed to determine if the process was successful. Several different methods of microscopy were considered for characterization: Raman spectroscopy, X-ray diffraction (XRD), atomic force microscopy (AFM), and scanning electron microscopy (SEM).

Graphene created through chemical vapor deposition was analyzed through Raman spectroscopy. Raman spectroscopy is a method used to analyze the atomic makeup of a sample through the analysis of inelastic scattering of phonons and incident laser light. For graphene, it has a distinct signature which helps indicate the quality of the sample as well as the number of layers created.

Figure 3.5 highlights all major peaks of graphene Raman spectroscopy. In determining the quality of graphene sheets, the D, D', and D+G peaks are caused by imperfections in the graphene. In particular, the D peak is caused by disorder in the sp^2 orbitals. The G peak is caused by the doubly degenerate E_{2g} mode. While the 2D band is the result of second order zone-boundary phonons.[44]

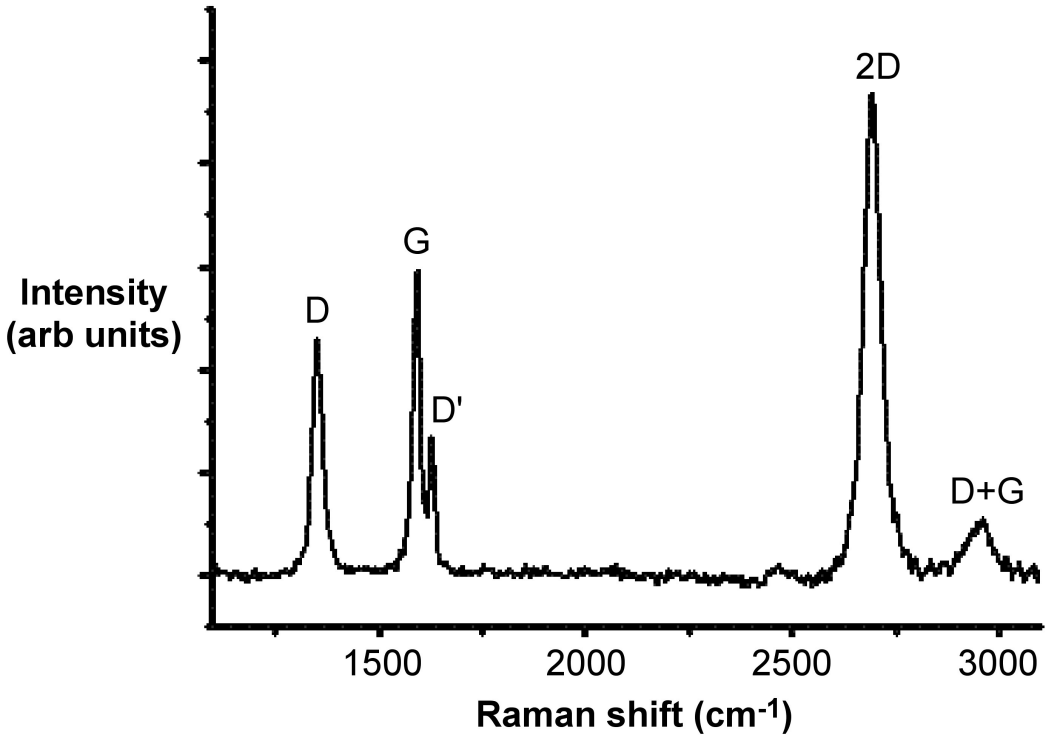

Figure 3.5: Example Raman spectrum using 514.5nm diode laser of N-doped graphene.

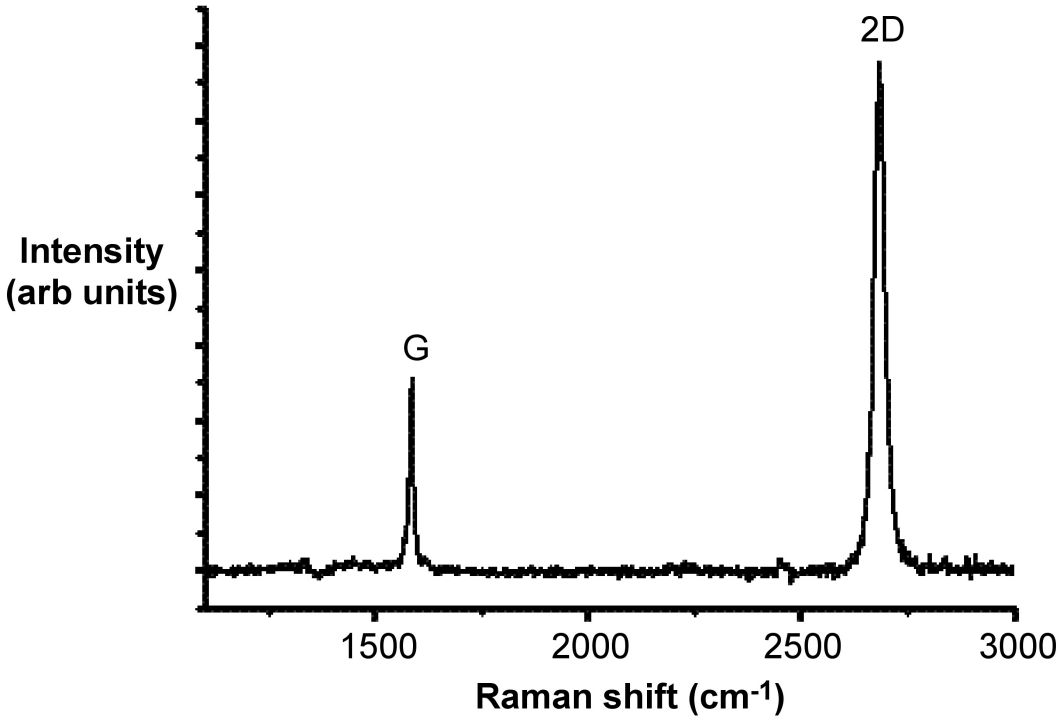

Figure 3.6: Raman spectrum of a pristine monolayer of a graphene sheet.

A pristine graphene sheet would not have any peaks caused by imperfections, as shown in figure 3.6. Only the G and 2D peaks are visible and a comparison of the two will give an approximation on the number of layers.

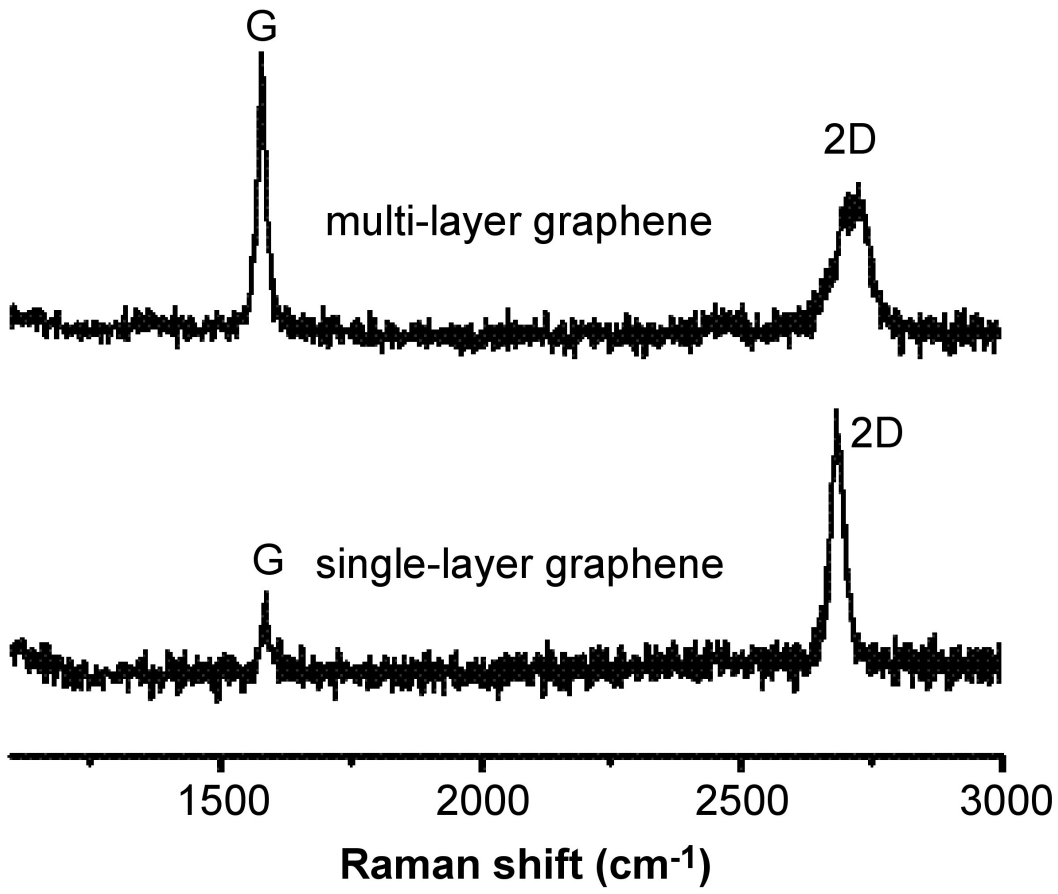

Figure 3.7: Raman spectrum of mono and multi layered graphene sheets.

Monolayer graphene will have a 2D peak that is approximately twice the size of the G peak, while multilayered graphene exhibit larger G peaks. The exact number of layers cannot be reliably inferred from the multilayer Raman graphs outside of 3 layers.[44 45 46 47]

XRD measures the diffraction of an X-ray beam as it is reflected off of some material. The material's crystal structure can be inferred by observing the diffraction pattern of X-rays reflected off of it. We used XRD before and after the process

of creating MMG and MMG-Si to prove that the process created true graphene. Small amounts of the graphite and graphene materials were imaged and the resulting diffraction patterns were compared. Graphite oxide displays two distinct intensity peaks at two theta values of 12 and 43 which disappear when it is converted to graphene. Adding silicon introduces peaks at two theta values of 29, 46, and 54.

AFM uses a cantilever with a nanometer-scale tip to scan over the surface of a sample. This probe interacts with the molecules of a sample and experiences extremely small electrostatic forces based on the topography of the surface. These forces can be determined by measuring the deflection of the cantilever using a laser bounced off the back of the cantilever. Ultimately, the samples topography is calculated from the forces felt by the cantilever tip. This method, while useful for imaging smooth materials at the atomic level, was unable to provide us with clear images of our electrode material. We suspect that the surface of our electrodes was irregular on a scale too large for the AFM to accommodate.

We finally turned to SEM to accurately image the electrode materials. SEM uses a beam of electrons to scan over the surface, which interact with the electrons in the sample. Then the SEM observes the products of these interactions, such as backscattered electrons, secondary electrons, and characteristic X-rays. Using these signals, the topography of the sample can be derived. After creating our graphene-silicon composites, a small portion of the material was sent for SEM in order to determine its geometry.

3.6 Electrochemical Performance Measurement

To characterize the performance of each type of electrode material, a constructed cell corresponding to each material was charged and discharged for many cycles in a half cell configuration. A half cell consists of the electrode material bonded to

a current collector, the separator with liquid electrolyte, and lithium metal as the positive electrode on another current collector. This configuration is referred to as a half cell because the voltage difference between the electrode and lithium metal is less than that of the normal voltage difference between an electrode and a commercial positive electrode (such as lithium cobalt oxide.) Despite this difference, a half cell can determine the electrochemical performance of the electrode material without requiring the use of more expensive positive electrode materials.

The first step in the cell construction process involves creating a stable electrode from the powdery electrode material, which is generated from the preceding processes. This involves mixing the electrode material with a binder, and then coating a thin copper substrate with the mixture and letting it dry. The binder carboxymethyl cellulose (CMC) was chosen due to its hydrophilicity, which allows easy mixing with the electrode powder in an aqueous environment. The electrode material was combined with an 8% CMC, 92% water solution in proportion to create an electrode with 12% CMC by weight after the water has evaporated. This electrode powder, CMC, water mixture was placed in a zirconium ball mill and mixed for one hour to ensure homogeneity. After mixing, the material was spread 60 μm thick on a copper substrate and allowed to dry under vacuum.

The second step of cell construction must be conducted in a glove box under an atmosphere of argon in order to prevent the oxidization of the half cell components. A half inch diameter circle of the stabilized electrode material is punched out and weighed to determine the electrode mass. It is then placed on top of a stainless steel separator inside the bottom half of the cell casing. On top of this, a separator is placed with one mL of liquid electrolyte. Subsequently, a half inch in diameter circle of lithium metal is punched out and placed on top with another stainless steel separator and spring to keep the components in compression. Finally the other half of the cell casing is applied and the entire stack is crimped shut.

At this stage, the completed half cells can be removed from the glove box and placed in an Arbin BT-2000 battery testing station for cycling analysis. The lithiation/delithiation current is determined by assuming an approximate charge capacity and using the measured electrode mass to calculate the current that would give a 1 C charge rate as specified by the equation:

$$\text{Capacity} = \frac{(current * chargerate)}{mass} \tag{3.1}$$

The charge capacity is approximated using the theoretical limit for the capacity of the electrode material in question. The electrode mass is determined by subtracting an average of three blank copper disk masses from the electrode mass measured when constructing the cell. When cycling a graphitic electrode, the cell is discharged to 0.02 V and charged to 2 V before restarting the cycle. But when cycling a graphene-silicon composite, the cell is only charged to the stability limit of the silicon at 1.5 V.

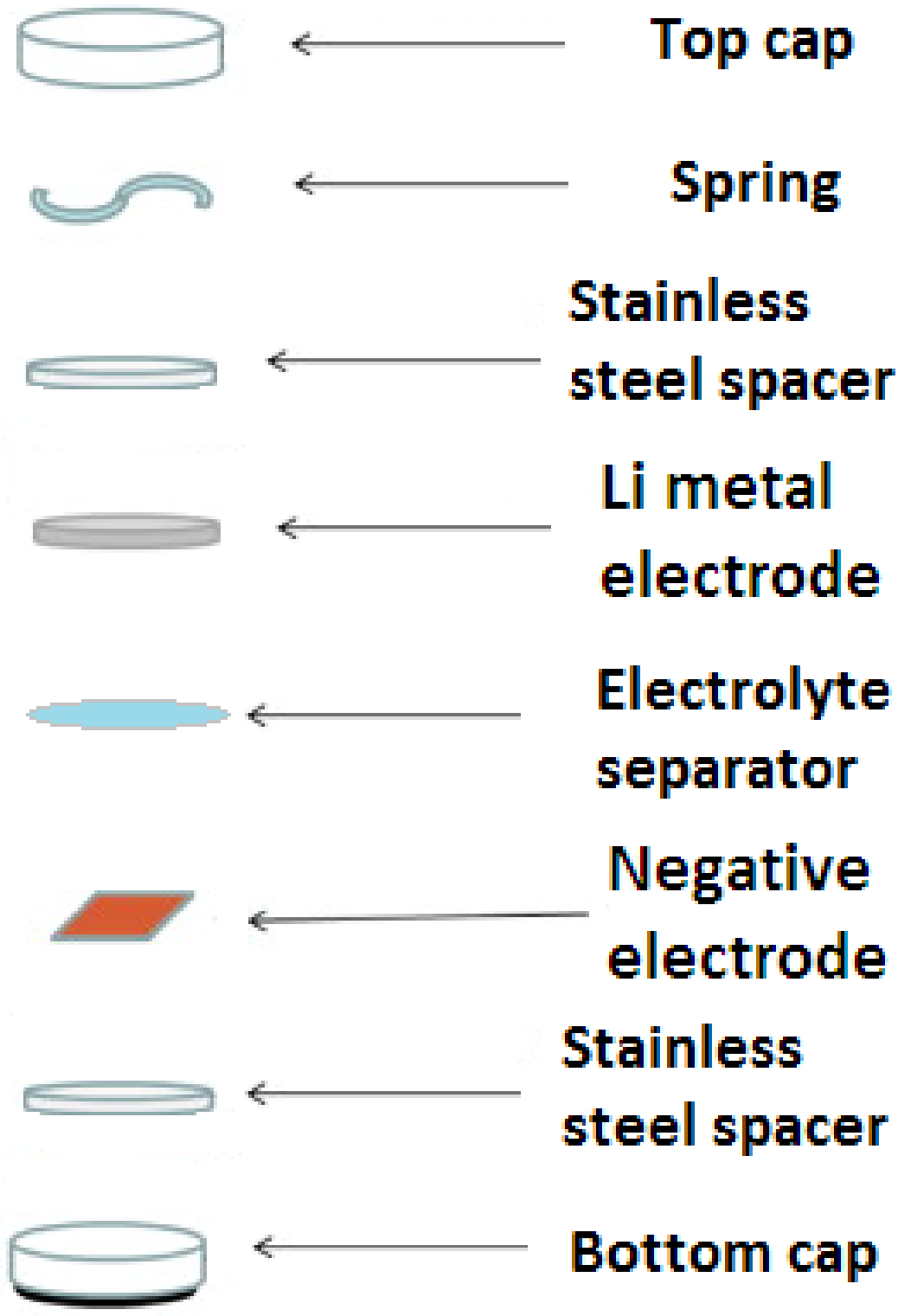

Figure 3.8: A breakdown of a coin cell battery shows each component.

Chapter 4

Data Analysis

4.1 Chemical Vapor Deposition

To verify that a pure sheet of CVD graphene was deposited, Raman spectroscopy was used to determine the purity and spread of the graphene sheet.

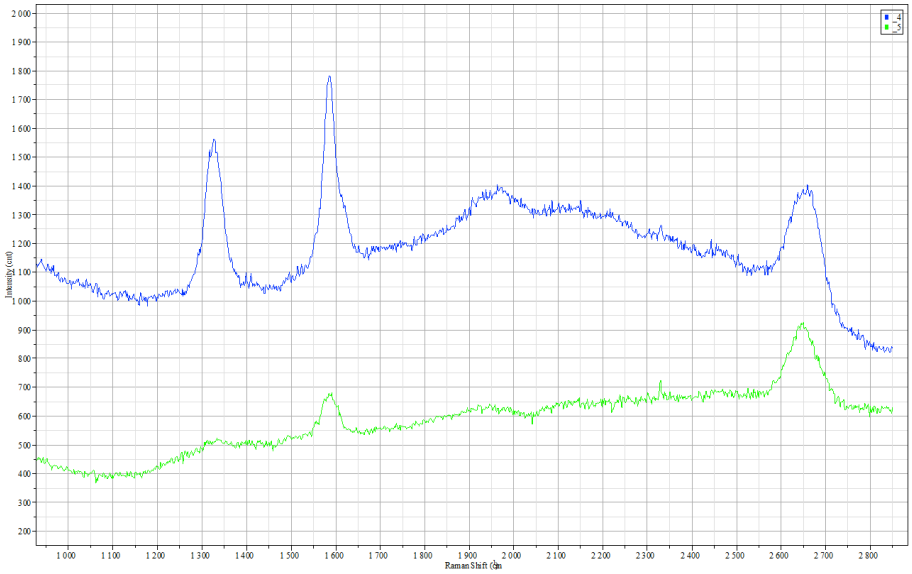

Figure 4.1: Raman spectroscopy of copper and CVD graphene on copper shows clean single/double layer graphene.

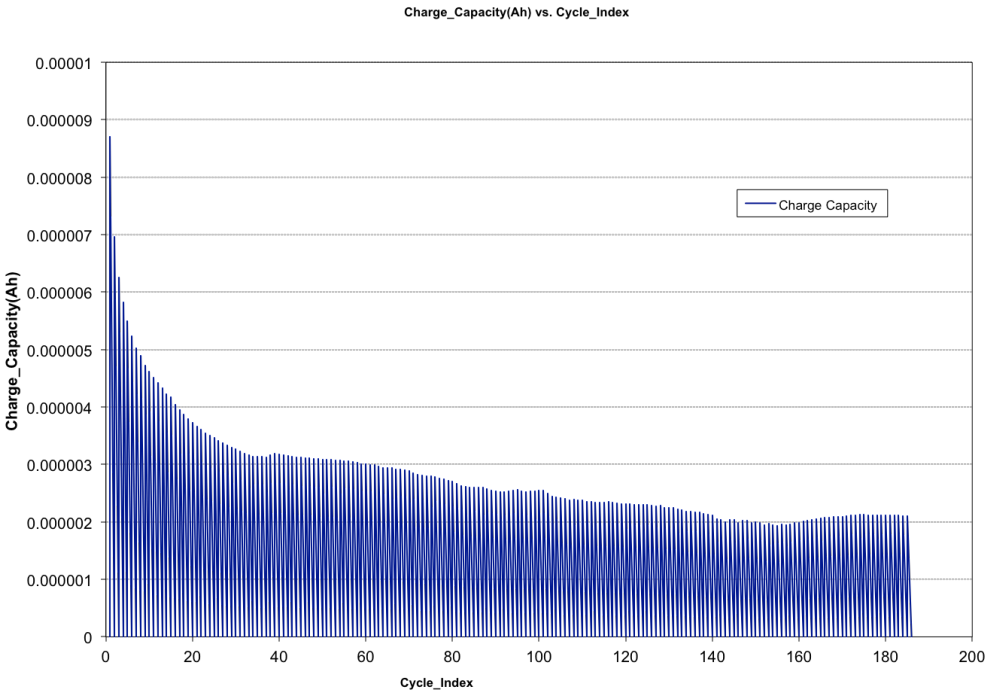

Figure 4.2: Charge capacity over charge cycles for electrochemically deposited silicon on CVD graphene.

The CVD-Si cell cycling data has a high initial peak that could be due to the electrochemically deposited silicon particles.

The CVD graphene electrode with silicon deposition was made into a cell battery. The purpose was to determine the effectiveness of depositing silicon onto a graphene surface by using electrochemical deposition.

A CVD graphene electrode without silicon was made to act as a control. The CVD procedure used to create both CVD sheets were identical.

4.2 Microwave Reduced Graphene

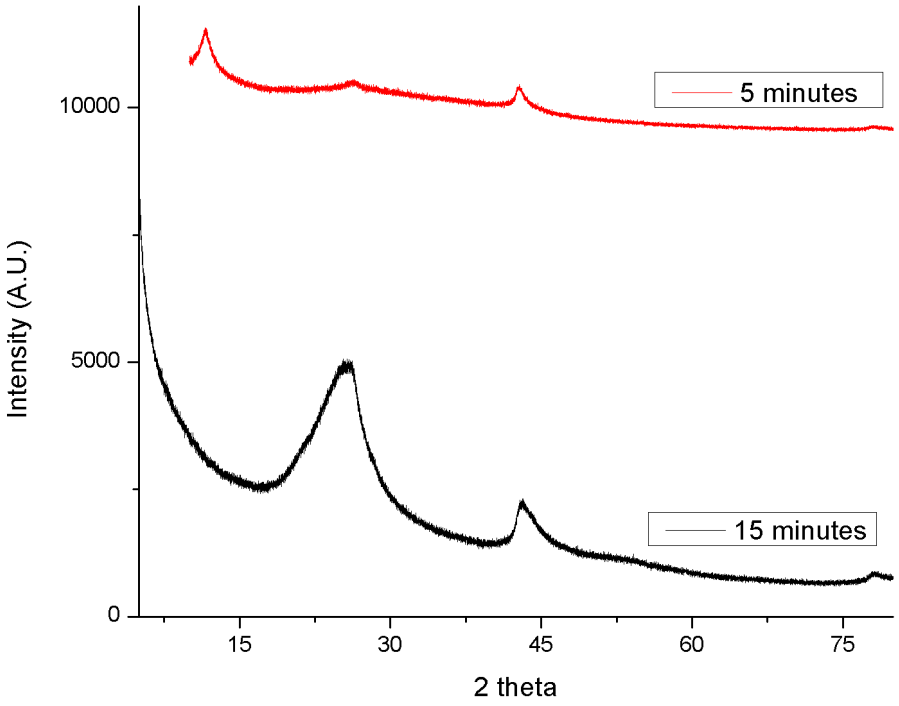

Figure 4.3: XRD analysis of reduction times; 5 and 15 minutes.

Reduction of graphite oxide requires at most 15 minutes of 900 W microwave reduction to fully become graphene. Graphite-oxide peaks are around 12° while full graphene peaks are seen around 25°.

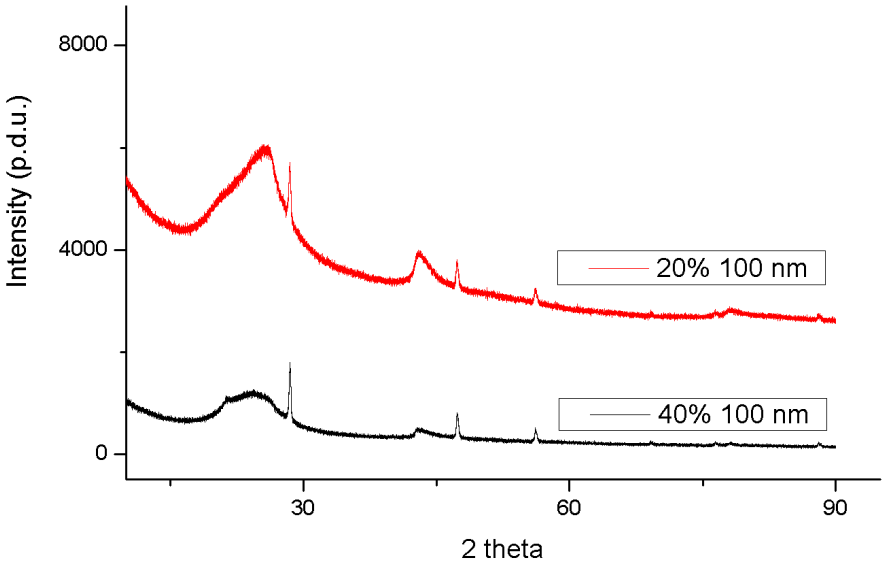

Figure 4.4: XRD analysis of graphene-silicon mixtures with varied amounts of silicon as a percentage of graphene weight and silicon particle size.

A change in the particle size from 1 μm to 100 nm shows an absence of the silicon peak seen in the other samples. One micron sized particles disrupt the reduction of graphite-oxide showing a peak at 12 corresponding to residual graphite-oxide.

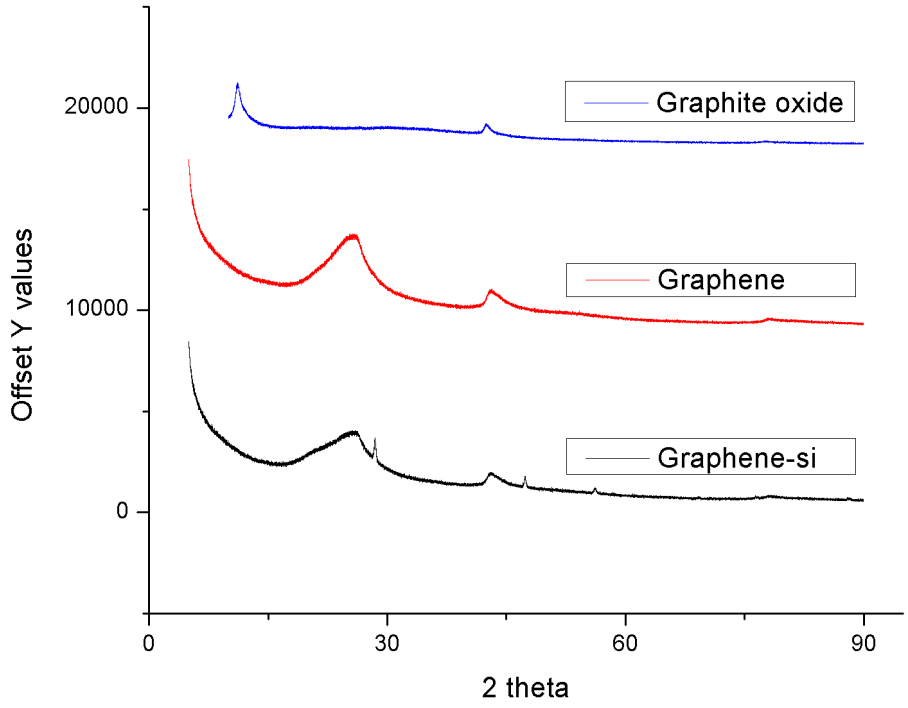

Figure 4.5: Analysis of various stages of graphene-silicon.

The blue line at the top is a sample from after the first step of making graphene. At this point it should still be graphite oxide. The blue peaks are unique to graphite oxide, confirming successfully made graphite oxide.

The graphite oxide was reduced into two graphene materials: the red is graphene, and the black is graphene with silicon nanoparticles. Since neither line has the graphite oxide peak, showing that all of the graphite oxide was successfully reduced. Furthermore, both lines contain a broad graphene peak around 28°, and the small graphene peak around 45°, indicating the samples are in fact graphene materials. The black line shows silicon peaks that indicate the silicon nanoparticles.

4.3 Mechanically Mixed Graphene-Silicon

The mechanically mixed graphene-silicon electrode material was created using the same mechanically mixed graphene that was analyzed using X-ray diffraction. After being mixed with silicon nanoparticles, the resulting material was imaged using scanning electron microscopy to verify that the procedure produced the proper graphene-silicon composite structure.

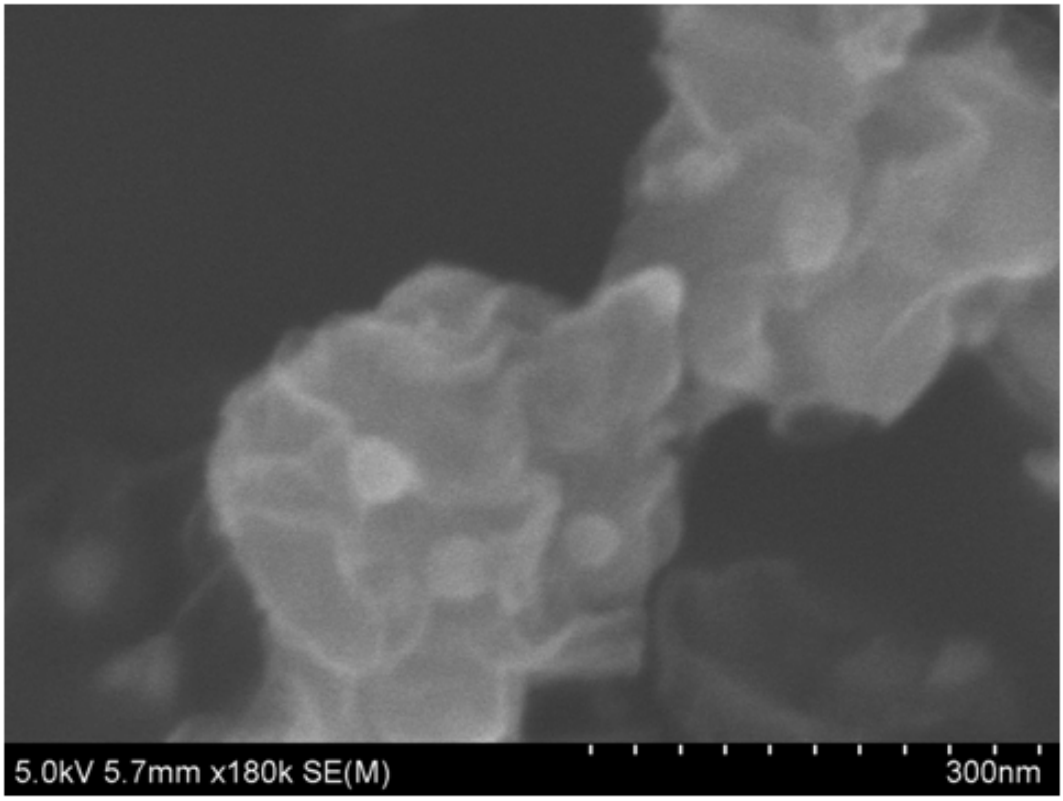

Figure 4.6: SEM image of MMG-Si electrode material.

Figure 4.6 shows the presence of silicon nanoparticles of the proper size mixed with the graphene sheets.

4.4 Mechanically Mixed Graphene with Electrochemically Deposited Silicon

A number of electrochemical techniques were utilized in order to determine the reduction potential of silicon tetrachloride. A chronopotentiogram is given in Figure 4.7 in which the current was stepped from -0.0019 A to -6.4x10^{-4}. This plot shows that the electrochemical deposition cell voltage responded linearly to the current change. The lack of a distinct potential peak implies that reduction did not occur in this cell. In a repeated chronopotentiogram with the same step current shown in figure A.7 for another electrochemical deposition cell, we can see that the voltage varied at step current in a nonlinear fashion. The small fluctuations of potential around the step current change are likely due to internal resistances of the cell. However, we see a distinct peak just before 4000 seconds dropping to -2.7 V. This potential drop is very likely due to the reduction of silicon from silicon tetrachloride in the deposition solution.

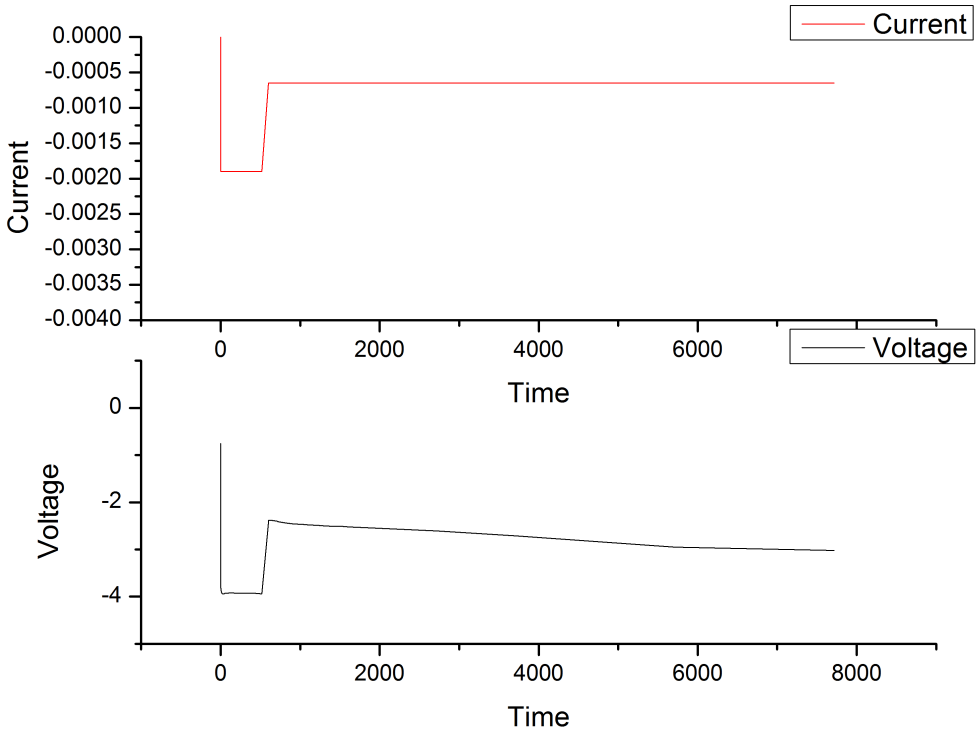

Figure 4.7: Chronopotentiogram 1.

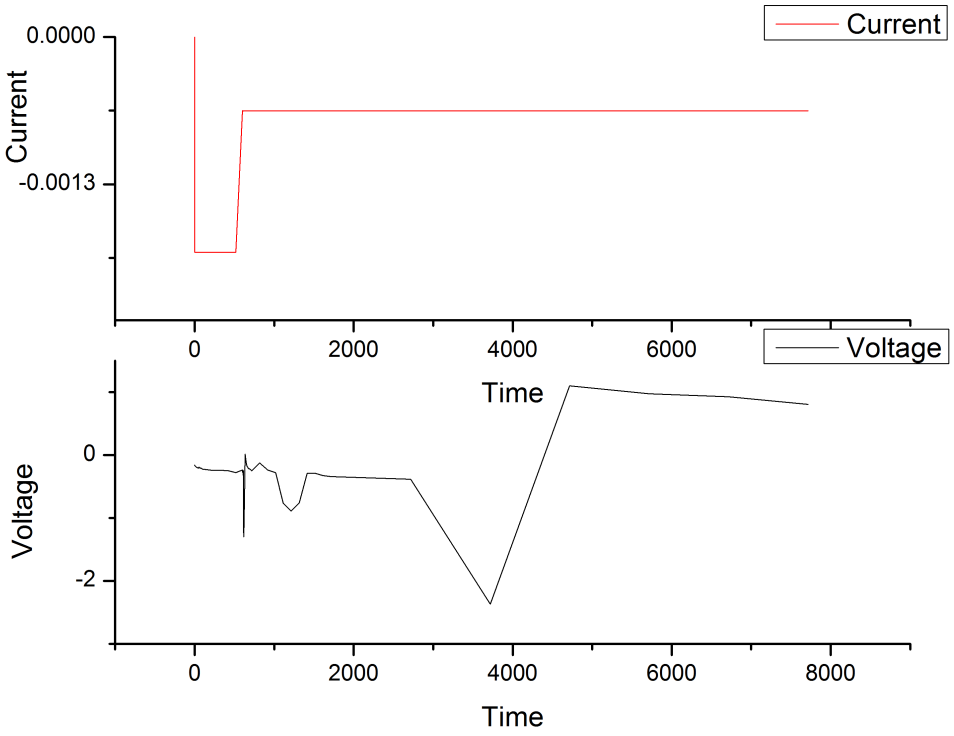

Figure 4.8: Chronopotentiogram 2.

In a linear sweep voltammagram shown in figure 4.9, the current-potential relationship is mostly linear as expected by Ohms Law. At approximately -2.7 V, a current peak occurs which again indicates the reduction potential of silicon tetrachloride in our deposition cell. In order to confirm that deposition occurred, a chronoamperometry scan was performed on the same cell. The results of this scan are shown in the chronoamperogram in figure 4.10. Voltage is stepped from approximately -1.0 V to -2.7 V. In the current versus time plot, a distinct downward spike is seen at the moment that the voltage steps to -2.7 V before stabilizing at a lower current. This current peak further enforces the argument that a reductive reaction occurs at this voltage.

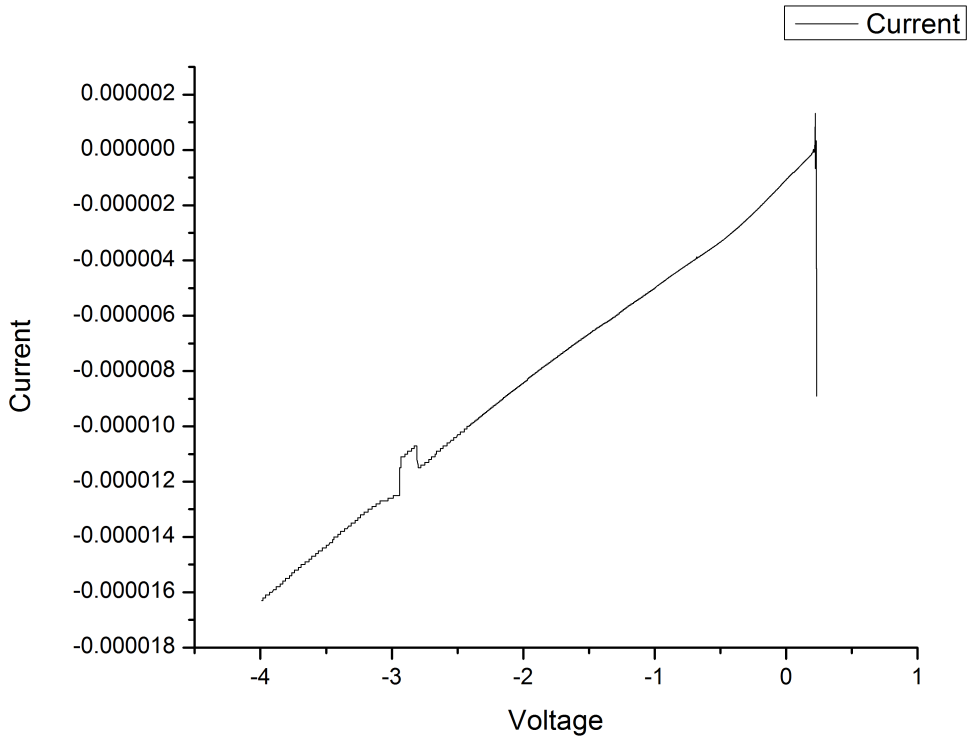

Figure 4.9: Linear Sweep Voltammagram

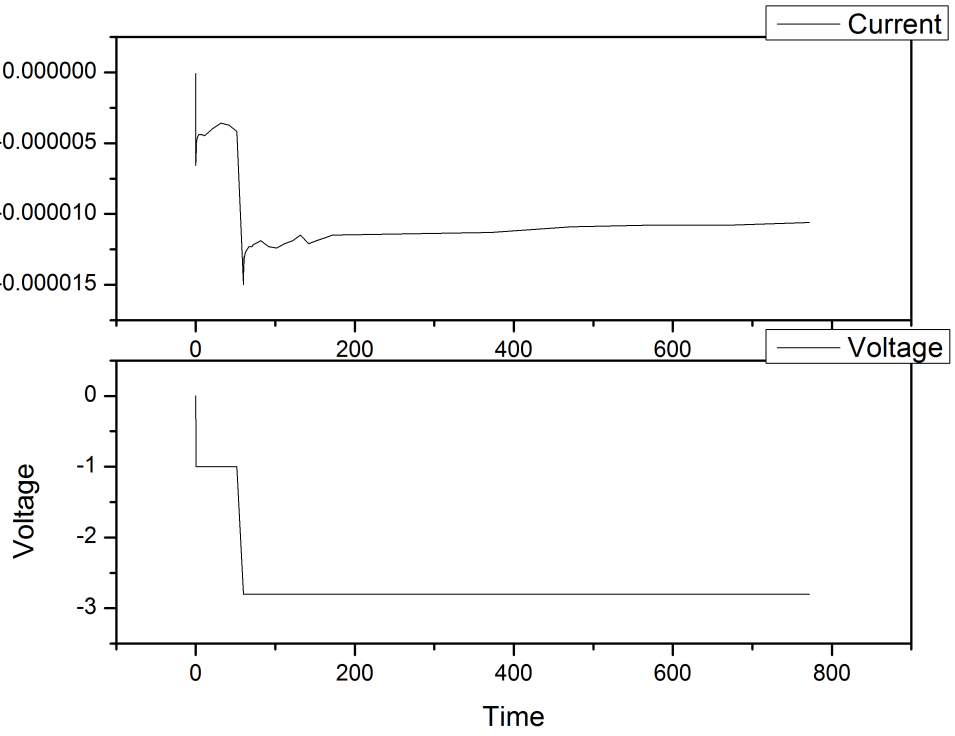

Figure 4.10: Chronoamperogram.

4.5 Cycling Data

Once the cells are tested for at least 60 cycles, the data can be recovered from the testing station. The raw data is contained in two excel sheets: one with data collected every 30 seconds during cycling, and the other with overall data corresponding to each total lithiation/delithiation cycle. From these data sets, we are able to develop graphs of voltage versus step time and charge capacity versus cycle in order to judge the electrochemical performance of each cell.

The first sheet contains data on the time during the test and current cycle at which the information was collected, as well as the current, voltage, and lithiation/delithiation capacities at these times. Using the step time and the voltage columns, a graph of the voltage versus the step time within each cycle can be gen-

erated. This graph shows how long each charge and discharge cycle took, which can reveal important information about how much of the electrode material was involved in cycling. For example, when comparing the initial discharge curves of a graphitic battery to that of a graphene-silicon one, the composites discharge would be seen to take a longer time than those of the pure graphene one due to the additional capacity of the silicon taking longer to discharge. Upon further inspection of the graphene-silicon graph, it may be seen that the subsequent discharge curves take significantly less time than the initial discharge, indicating a loss of capacity due to some of the electrode material separating from the current collector. Alternatively, if subsequent discharge curves occur on similar timescales, it could be concluded that the irreversible capacity loss of that electrode is low.

The second excel sheet contains data on the total time each lithiation/delithiation cycle took, as well as overall values for charge and discharge capacities. By graphing the cycle index versus the charge capacities, the cells overall performance can be described. Using the initial charge capacity and dividing by the electrodes active material mass, the cells initial specific charge capacity is calculated. As the capacity drops off with increasing cycle index, it is clear whether the cell has a long or short cycle life. The cycle at which the specific charge capacity drops to 80% of the initial value defines the cells cycle life and is then used to compare it to other types of cells.

Chapter 5

Results and Discussion

In order to prove that the electrochemical deposition process improves the cycle life of a graphene-silicon composite electrode, we must show that such an electrode can undergo more lithiation/delithiation cycles than a similar cell created through a mechanical mixing process. Additionally, to demonstrate that our results are significant, we will also need to prove that our cells are comparable to and better than traditional graphitic cells. By comparing a graphene-only cell to a mechanically mixed graphene-silicon (MMG-Si) cell, and then the MMG-Si cell to the electrochemical deposited silicon (Edep-Si) cell, we can make a comparison between the Edep-Si cell and the graphene-only cell.

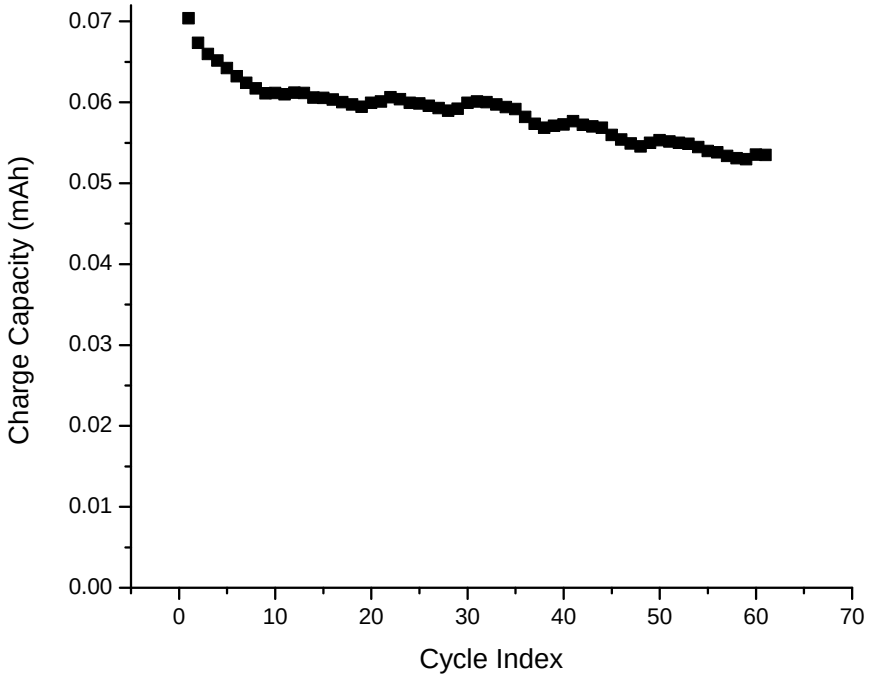

Figure 5.1: MMG capacity plot. Initial specific capacity of 175 mAh/g degrades to 140 mAh/g over 50 cycles.

Figure 5.1 shows the capacity plot for a mechanically mixed graphene electrode cell. Using its measured mass of 0.4 mg and the charge capacity of 0.07 mAh, a specific capacity of 175 mAh/g was calculated. This is comparable to current graphitic cell electrodes. We will consider the cells cycle life to be defined as the cycle number when the charge capacity reaches 80% of the initial capacity. By this definition, the MMG cells cycle life is 50 cycles, at which point the capacity drops below 140 mAh/g.

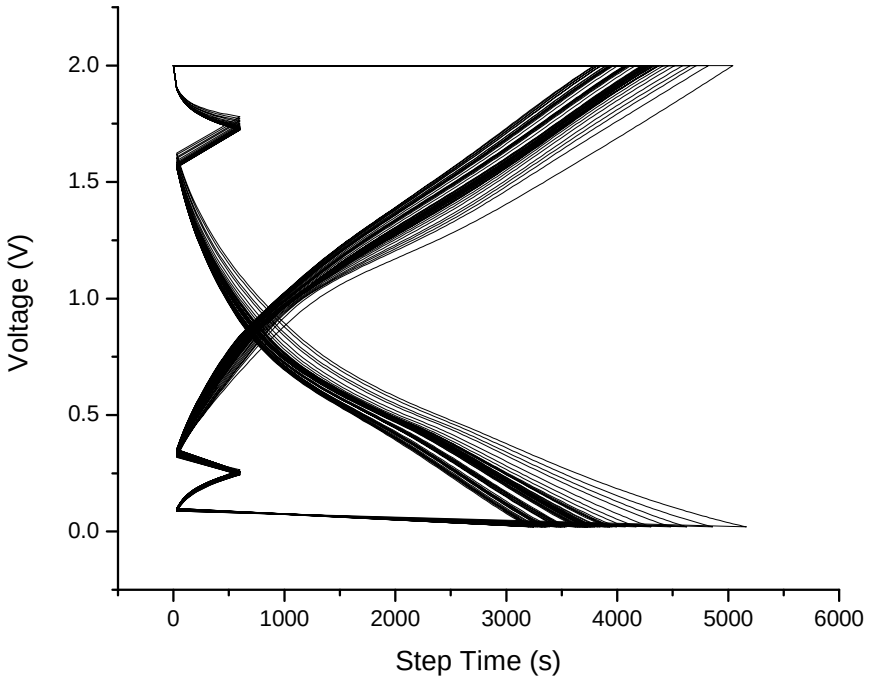

Figure 5.2: MMG cycling plot. Charge and discharge steps are shown to take about 4000 seconds on average.

The voltage versus step time plot (Figure 5.2) shows an average time of about 4000 seconds for both the charging and discharging steps of the cycling process that slowly decreases with cycling. This is consistent with normal graphitic electrode cell operation as the graphene doesnt degrade very quickly (as shown by the cycle life calculated above.)

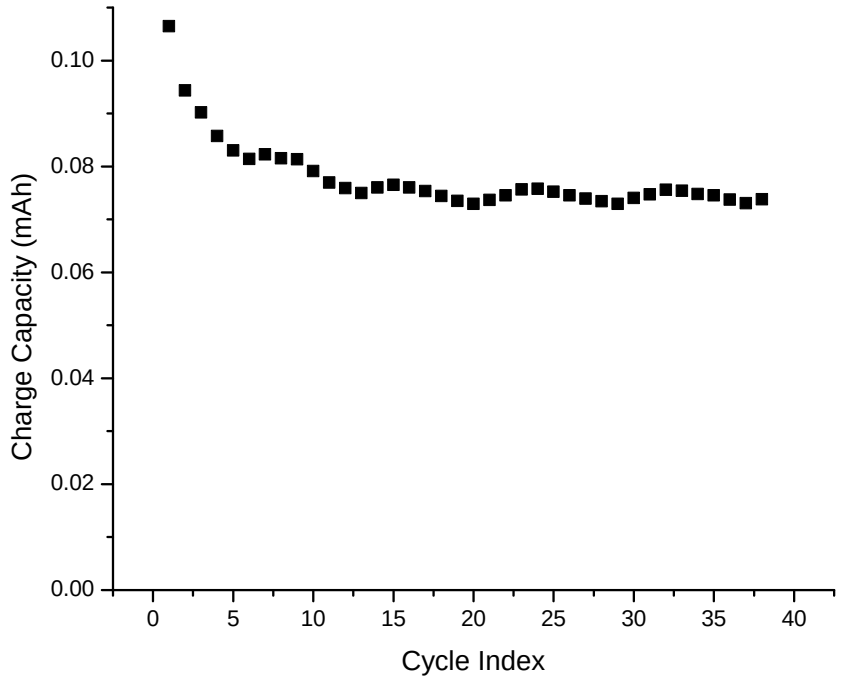

Figure 5.3: MMG-Si capacity plot. The initial specific capacity of 500 mAh/g drops by 80% after only 10 cycles.

Figure 5.3 shows the capacity plot for mechanically mixed graphene-silicon electrode cell. With a mass of 0.2 mg and an initial charge capacity of 0.1 mAh, it displays a specific capacity of 500mAh/g, similar to current research into silicon-graphene composites. This battery has a cycle life of 10 cycles, shorter than our MMG cell due to the agglomeration of silicon particles within the electrode. When several of the silicon nanoparticles are not separated by graphene during charging, they are free to expand against each other and cause pulverization of the silicon, decreasing its cycle life.

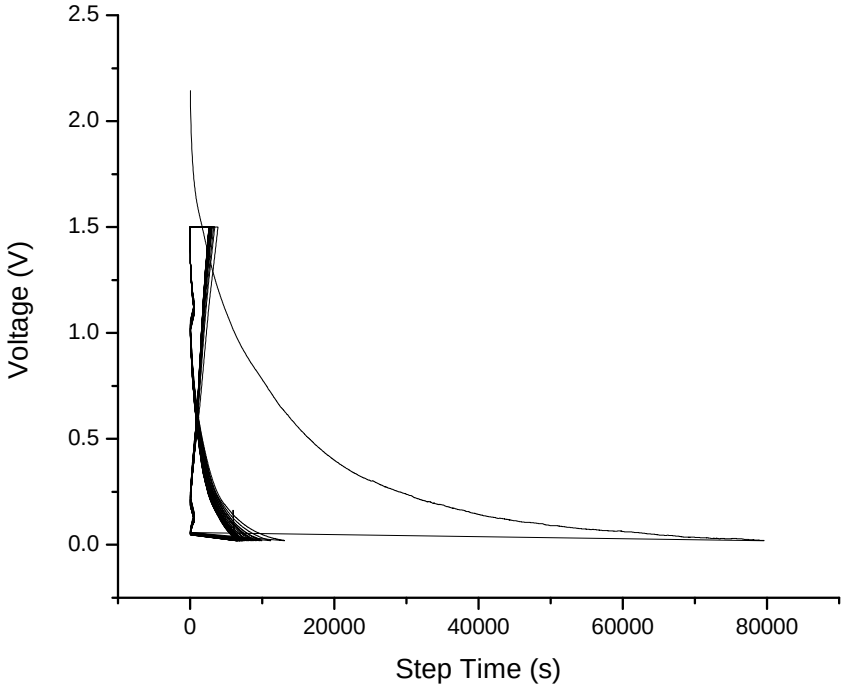

Figure 5.4: MMG-Si cycling plot. Note the much longer first discharge curve indicative of silicon participating in the discharge process.

The voltage versus step time plot for the MMG-Si electrode cell (Figure 5.4) shows a much longer time for the first charge step due to the presence of silicon within the electrode. Since it has a much larger capacity than graphene, it will take a longer time to charge and discharge at the same current. We will use this fact in subsequent analyses to prove the presence of silicon in our experimental batteries. Subsequent charge and discharge cycles dont take as long due to some irreversible capacity loss.

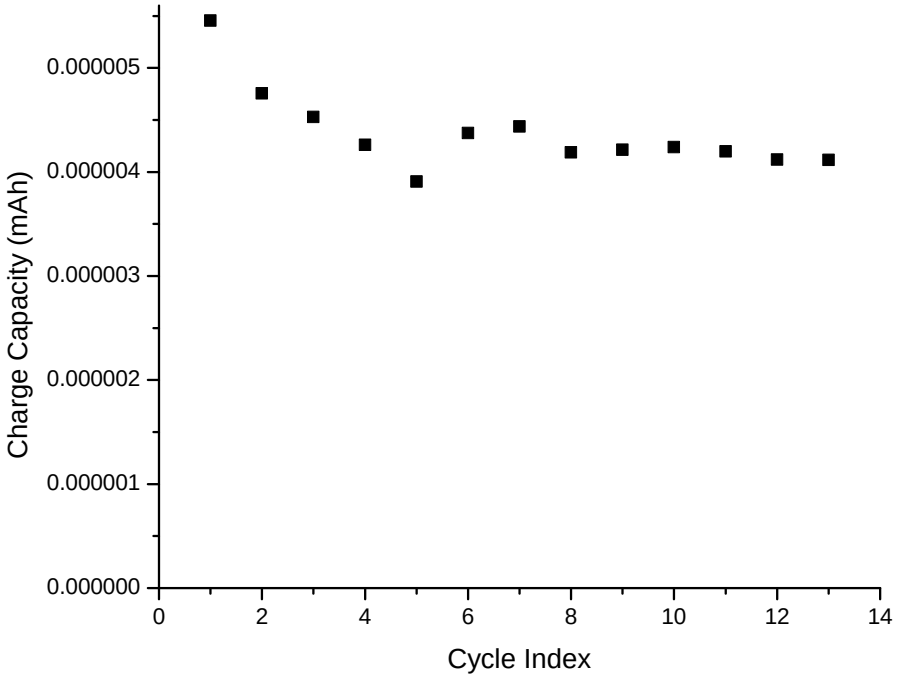

Figure 5.5: CVD-Edep-Si capacity plot. The capacities for this electrode type are very small due to their very small mass. One electrode is made up of a single graphene sheet with deposited silicon nanoparticles.

Figure 5.5 shows the capacity plot for CVD-Edep silicon electrode cell. A CVD-Edep silicon electrode is composed of a single layer of graphene with silicon nanoparticles deposited on top. As can be expected from such a geometry, the cells cycle life is very short (5 cycles). Since the silicon is not encapsulated by any graphene sheets, it tends to quickly disconnect from the current collector and cease to participate in cycling.

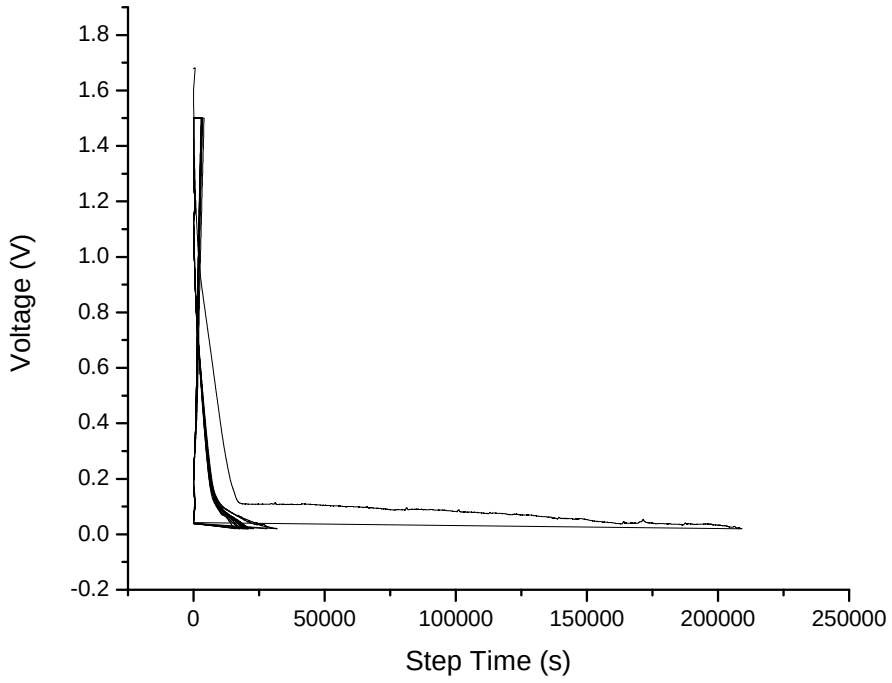

Figure 5.6: CVD-Edep-Si cycling plot. This plot again displays a long initial silicon discharge curve that drops away very quickly with subsequent cycles due to the silicon not being encapsulated at all.

However, the voltage versus step time plot for the CVD-Edep silicon electrode cell (Figure 5.6) can be used to prove that silicon was deposited using our electrochemical deposition process. As can be seen, the initial discharge step takes much longer than any subsequent charge or discharge steps. This shows that the layer of silicon nanoparticles participated in only one cycle before disconnecting. Subsequent, short charge and discharges display short step times, due to the graphene layer being the only one participating in cycling.

The experimental graphene with electrochemically deposited silicon material did not demonstrate any capacity when cycled, indicating that this material had lost all contact with the current collector. This contact loss can be attributed to the mechanical and electrochemical degradation of the anode material during the deposition

process. A combination of the mechanical stress on the material when twisting the cap and reduction of the solvent onto the copper substrate contributed to irreparably damaging the material itself. 5.7 summarizes the capacity over time graphs of the graphitic and graphene-silicon materials. The silicons quick capacity degradation can be seen in the steep drop of the composites capacity relative to the more stable graphites capacity.

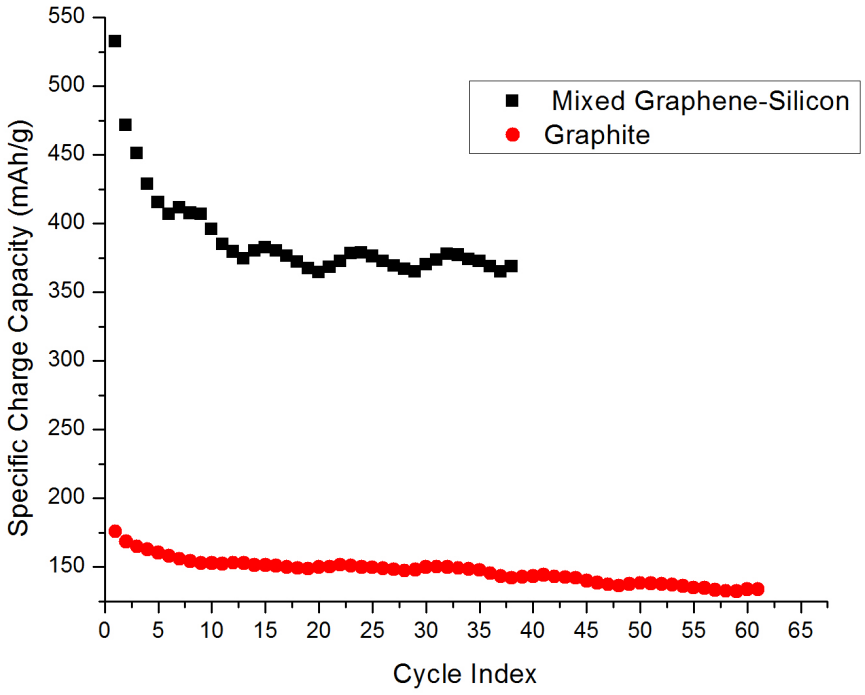

Figure 5.7: Summary capacity plot. This plot illustrates the difference in charge capacity over time between the graphitic and the mixed graphene-silicon materials. As can be seen, the graphene-silicon anode demonstrates a higher capacity that degrades much more quickly than the graphitic material.

Chapter 6

Conclusion

One of the large hurdles blocking the integration of graphene-silicon composite batteries with commercial applications is their short lifespans. Many different methods have been tried to combine silicon and graphene, and have resulted in varying levels of silicon aggregation within the electrode, which harms the cycle life of the cell. We began our research with the aim of specifically targeting this issue and developing a method of preventing this from happening.

Though we were able to successfully reduce silicon from silicon tetrachloride onto a graphene substrate, we were not able to demonstrate that such electrodes have higher cycle lives than the control group. This is due to the degradation caused by the electrochemical deposition method itself.

The difficulties with our MMG-Edep-Si cell show that improving the homogeneity of the graphene-silicon composite through an electrochemical deposition process is infeasible. In order to develop these improved batteries, other methods must be developed for efficiently synthesizing of a more homogeneous graphene-silicon composite electrode. The breakdown of the electrodes structure at high voltages during electrochemical deposition lead to bad performance of our MMG-Edep-Si cell. A method that ensures stable contact between the graphene-silicon composite and the copper

substrate is crucial to the improved performance of the cell. By having a more stable contact between the graphene-silicon composite and copper, the electrochemical deposition method can be adjusted to ensure silicon homogeneity while maintaining the integrity of the electrode. Such methods, if feasible, would prove whether or not a more homogeneous graphene-silicon composite would improve cycle life.

In the future, methods ensure stable contact between the graphene-silicon composite and the copper substrate will allow for the mass production of rechargeable lithium-ion batteries with much significantly higher capacities than currently available graphite-based cells. These batteries, critical to technologies such as transportation and power grid management, will enable the extensive proliferation of cleaner and more efficient publicly available energy usage.

Appendix A

Methodology

A.1 Electrochemical Deposition

The following is a step-by-step instructional guide on how to properly set up and run a cyclic voltammogram in order to electrochemically deposit silicon onto a graphene-copper electrode disk.

A.1.1 Confirm the Presence of All Materials

Here is a checklist of the materials you will need:

1. A copper sheet coated with Mechanically Mixed Graphene (MMG) the deposition will occur on a disk from this sheet.
2. A $\frac{1}{2}$ inch circular cutter will be used to cut out the button-cell from the sheet.
3. A 20 mL plastic or glass vial this will be used to transfer the electrode disk into the glove box.
4. The stock solution of tetrabutylammonium chloride, silicon tetrachloride, and propylene carbonate.

5. Two small, rectangular pieces of platinum foil
6. Sandpaper
7. A sawn-off glass bottle
8. A $\frac{3}{4}$ inch stainless steel disk
9. A silicone washer
10. Circular electrode piece
11. Two pairs of tweezers
12. The Gamry Machine this machine will run the software that performs the cyclic voltammetry. It is a computer, connected to a machine labeled GAMRY. It is mounted onto a black cart.
13. Confirm the presence of a red, green, and white alligator clip connected to the Gamry Machine. These will connect to the working, counter, and reference electrodes of the deposition cell.

See Appendix for Proper Procedure for Putting Items in Glove Box.

A.1.2 Prepare the Experiment

Make the electrode disk:

1. Place the graphene-coated copper sheet on the cutting board in front of the glove box.
   (a) Place the graphene (black) side face up
2. Place the $\frac{1}{2}$ inch circular cutter and hold it firmly on the sheet.
3. Press the cutter firmly down, ensuring that the edges cut through the sheet

(a) DO NOT hammer the cutter. This will cause the graphene layer to separate from the copper sheet.

4. Snip the points where it is still attached.

   (a) The disk should already be mostly cut out

   (b) Do not use tweezers to snip out the entire circular disk.

   (c) Do not disturb the graphene.

   (d) Use the tweezers to snip any uncut portions. This means that if the circular disk does not easily remove from the sheet, use the tweezers to Transport the disk using ONLY the tweezers. Do not touch the graphene surface with your fingers.

5. Measure the weight of the disk.

   (a) Place a weigh paper on the scale and tare the scale.

   (b) Place the electrode on the weigh paper using the tweezers.

   (c) Record this weight in your notes.

   (d) Place the electrode into the 20 mL plastic or glass vial using tweezers.

6. See below for Proper Procedure for Putting Items in Glove Box.

A.1.3 Set Up the Deposition Cell

Before beginning, use the checklist above to confirm all materials are where they should be. This guide will assume that the deposition solution has already been made.

1. Put both hands inside the glove box. This will be difficult the first few times

   (a) Place your left arm into the left glove first.

(b) Use your right hand to help get the fingers in.

(c) As you push your arm into the glove box, press the left side of the foot pedal under the glove box. This will reduce pressure in the glove box.

2. Bring the plastic container in the front left corner towards the center of the glove box directly in front of you.

3. Remove the black cap from the sawn-off glass bottle.

4. Take the stainless steel disk and place it at the bottom of the cap. The cap has a hole where the electrode will touch the stainless steel disk to provide current.

   (a) Ensure that it is tight against the inner surface of the cap to prevent leakage of the solution that will soon go inside the bottle.

5. MAKE SURE THE OUTSIDE DOOR TO THE GLOVE BOX IS CLOSED BEFORE CONTINUING.

6. Open the inside door to the glove box and take out the 20 mL vial that contains the button-cell electrode.

7. Open the vial and remove the disk using the tweezers inside the plastic container.

8. Place the disk carefully inside the cap on top of the stainless steel disk.

9. Place the silicone washer inside the cap.

   (a) Press down on the edges of the washer such that it produces a tight seal is made.

   (b) Ensure that the stainless steel disk is not visible in the center hole of the washer.

10. Screw this cap back onto the sawn-off bottle.

(a) Do not allow the stainless steel disk to be visible in the center hole of the washer.

(b) If the electrode disk moves during this step, use tweezers to push disk back into place.

11. Clip an edge of the sawn-off bottle to the edge of the circular plastic container.

    (a) This will make the following steps easier if the bottle is stable and unmoving.

12. Take the sandpaper.

    (a) Sand both sides of both pieces of platinum foil. This should only take about 15-20 seconds per foil.

    (b) Fold the sandpaper around the piece of foil, pinching it with the pointer and thumb.

    (c) Rub with the pointer and thumb.

    (d) Sand the surface of the circular electrode that is inside the plastic container.

13. Hold the sawn-off bottle in place with the alligator clip connecting it to the plastic container.

14. Open the alligator clip without letting the sawn-off bottle fall.

15. Place one of the platinum foils in the alligator clip and close the clip so that the platinum foil, the sawn-off bottle, and the plastic container are clipped together.

    (a) The sawn-off bottle should not slide out from the clip.

    (b) The sawn-off bottle should be stable and should not require you to hold it up.

16. Take the other alligator clip and remaining platinum foil.

(a) Clip it to the opposite edge of the first platinum foil in a similar manner. Note: Each alligator clip is connected to a wire that leads to the circuit system at the left end of the glove box. The color wire you use to connect the alligator clips to the platinum foil is arbitrary on the inside. However, it will be important to take the color of the wires in account later on. These inner wires will be connected to wires from Gamry on the outside of the glove box. There are three wires:

i. Alligator clip 1 brown wire

ii. Alligator clip 2 green/yellow wire

iii. Circular electrode blue wire

17. Take the vial containing the solution and pour the solution into the sawn- off bottle.

(a) DO NOT let the liquid contact the metal of the alligator clips.

(b) Only use enough to mostly submerge the platinum foil pieces.

18. Return the plastic container to the left corner of the glove box.

(a) Ensure that all pieces are attached as written in this guide.

A.1.4 Perform Electrochemical Deposition

The following portion of the instructional guide involves use of the Gamry machine. This guide will not go into details of the machine or its software component nor will this guide assist in the analysis of data.

This guide will give the step-by-step instructions to run a cyclic voltammetry on the cell made in the previous section.

Other electrochemical techniques are possible with the Gamry but the details of those techniques will not be discussed.

1. Move the Gamry Machine towards the left end of the glove box.
    (a) Check to see if the Gamry is being used for any other experiment.
    (b) Do not disrupt any wires when moving the cart.
2. Connect the white alligator clip (reference) to the wire tubing that corresponds to the yellow/green wire.
3. Connect the red alligator clip (counter) to the wire tubing that corresponds to the brown wire.
4. Connect the green alligator clip (working) to the wire tubing that corresponds to the blue wire.
5. Open software on desktop titled GAMRY
6. Go to the run menu.
7. Click on the electrochemical techniques option.
8. Click on cyclic voltammetry.
9. Scroll down to the scan rate box and type in your desired scan rate.
10. Scroll down to the max voltage box and type in your desired max voltage.
11. Repeat step 7 for min voltage.
12. Click run at the top left corner.
13. Allow the experiment to run to completion.

A.1.5 Proper Procedure for Putting Items in the Glove Box

The glove box is extremely sensitive to contact with the outside atmosphere. Great care must be taken to avoid contaminating the inside atmosphere of the glove box. Be sure to ask permission before putting in large objects or chemicals inside the glove box.

CAUTION: DO NOT OPEN BOTH DOORS AT THE SAME TIME. This will open the inner atmosphere to the outside atmosphere. If this happens close the doors and seek assistance.

Never allow the oxygen ppm reading (digitally located on the top right) to go over 10.

1. Set the black valve to Off.
2. Ensure that the inside door is closed before continuing.
3. Open the outside door.
4. Place objects inside the cylinder. Vials or containers should be left open to allow air to evacuate.
5. Close outside door.
6. Turn valve to the right to Evacuation until completely evacuated. Pressure will return to 0 on the dial.
7. Turn valve to the left to Refill. Pressure will return to -30 psi.
8. Enter the glove box.
9. Open the inside door.
10. Carefully remove the objects.

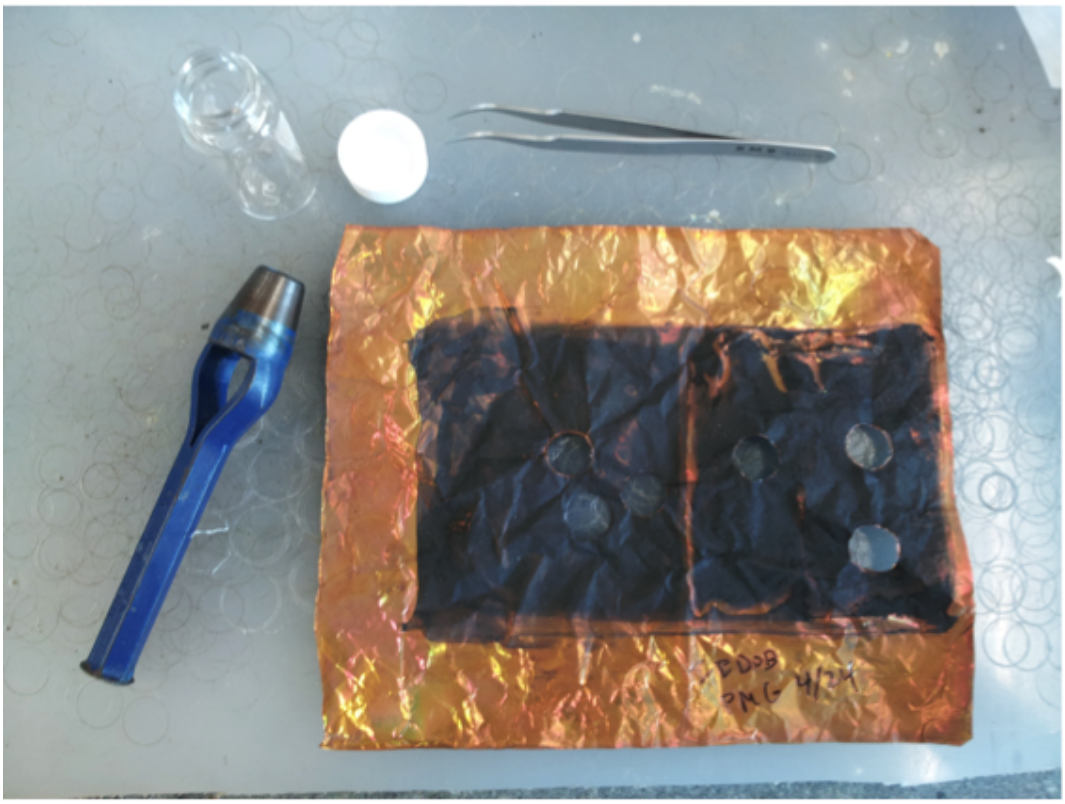

Figure A.1: Tweezers, glass vial, circular cutter, and graphene-copper sheet.

Figure A.2: Copper should not be visible after cutting disk from sheet

Figure A.3: Copper should not be visible after cutting disk from sheet

Figure A.4: Sawn-off half bottle can be seen here with electrode fit snugly into cap

Figure A.5: Stainless steel disk, then disk, then silicon washer, should be placed onto cap (before being screwed on)

Figure A.6: External wiring that connects deposition cell to Gamry Reference 3000

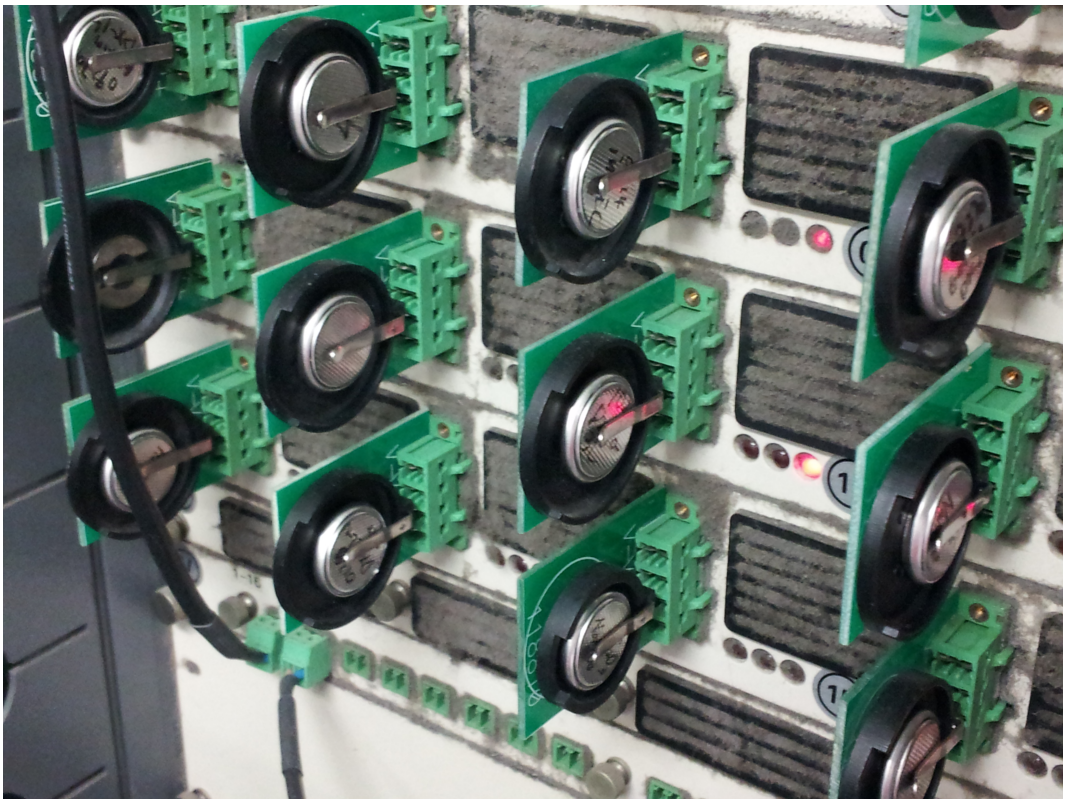

Figure A.7: Coin cells being cycled using the Arbin BT-2000 Battery Testing Station

Appendix B

Gamry

Chapter 5 -- Cell Connections

Cell Cable Overview

The Cell Connectors are two 15-pin D-connectors on the front of the Reference 3000.

The upper (female) connector is labeled Counter/Working. It carries the cell current between the Counter electrode wire and the Working electrode wires and the instrument

The lower male connector is labeled Sense Inputs. It contains only high impedance inputs used to sense potentials in the cell.

Gamry's standard cell cables always come in pairs. Each cable has a D-connector on one end and a number of leads to connect to electrodes in an electrochemical cell. The D-connector end of the cable is connected to the appropriate D-Connector on the front of the Reference 3000. The male and female cables cannot be interchanged.

Every Reference 3000 is shipped with a pair of standard shielded cell cables. The Gamry part numbers for these cables are 985-85 and 985-90. They are both 60 cm complex cables, with D-connectors on one end a color coded banana plugs and/or pin sockets on the other end.

In some cases, your system may also include special purpose cell cables. The special purpose cell cables will include documentation describing their use.

You should always screw both cell cables into place since cables can fall off the unit. This can be disastrous if it occurs during an experiment.

Ancillary Apparatus

Do not use the Reference 3000 with ancillary apparatus connected directly to any of the cell leads. Examples of ancillary apparatus include DVMs, oscilloscopes, chart records, and data loggers. Ammeters and voltmeters, regardless of their specifications, almost always create problems when connected to the Reference 3000 cell leads. Ancillary measurement devices can be connected to monitor points on the rear panel of the Reference 3000.

AE Connections

The AE (Auxiliary Electrometers) is an option for the Reference 3000. Its inputs often connect to an electrochemical device, such as a battery or fuel cell stack. The inputs can also connect to external measurement devices, such as a pressure sensor.

AE connections are not described here. See Chapter 7 for AE connection information.

Fuses in the Cell Cable

The Reference 3000 could be damaged if currents much larger than 3 amps were to flow into or out of the Counter electrode or Working electrode leads. Improper connection to a battery, fuel cell, or super capacitor could cause this type of damaging current to flow. All Reference 3000 Counter/Working cell cables contain fuses in the cable that will protect the instrument if it is misconnected. A later section of this manual discusses the fuses and their replacement.

Normal Cell Connections

This section assumes that you are using standard, shielded cell cables. This information does not depend of the length of the cables.

The cell end of the standard cell cables terminates in a number of banana plugs and two pin jacks. Each termination comes with a removable alligator clip. Table 5-1 identifies the terminals of the cables.

Table 5-1
Cell Cable Terminations - Potentiostat and Galvanostat Modes

Color	Type	Name	Normal Connection
Blue	Banana Plug	Working Sense	Connect to working electrode
Green	Banana Plug	Working Electrode	Connect to working electrode
White	Pin Jack	Reference	Connect to reference electrode
Red	Banana Plug	Counter Electrode	Connect to counter electrode
Orange	Banana Plug	Counter Sense	Used in ZRA mode - connect to counter electrode
Black	Pin Jack	Floating Ground	Leave open or connect to a Faraday shield

Connect both the blue and green cell leads to the working electrode. The working electrode is the electrode being tested. The blue pin jack connection senses the voltage of the working electrode. The green working electrode connection carries the cell current. The working electrode may be as much as 250 mV above the circuitry ground (floating ground).

Connect the white pin jack to the cell's reference electrode, such as an SCE or Ag/AgCl reference electrode. The measured cell potential is the potential difference between the blue and white cell connectors.

If the instrument is connected in stack mode and the reference input is not used, it should be connected to the floating ground wire. A pin plug shorting bar is provided for this purpose.

You may need to connect the Reference 3000 to a two terminal device (such as a commercial battery). In this case, you connect both the white cell and red cell leads to one side of the device and the blue and green cell leads to the other side. Try to connect the white and blue leads as close to the device as possible.

Connect the red banana plug to the counter or auxiliary electrode. The counter electrode is usually a large inert metal or graphite electrode. The counter electrode terminal is the output of the Reference 3000's power amplifier.

The orange lead is only used in ZRA mode and Stack Mode where it senses the counter electrode potential (see following section). Automatic switching to ZRA mode is possible if this lead is connected to the counter electrode. If you will not be using ZRA or Stack mode, this lead can be left open or connected to the Counter electrode.

The black pin jack is connected on the Reference 3000 end to Floating Ground. This is the circuitry ground for the analog circuits in the Reference 3000. In most cases, this terminal should be left disconnected at the cell end. When you do so, take care that its metal contact does not touch any of the other cell connections.

If your cell is a typical glass laboratory cell, all of the electrodes are isolated from earth ground. In this case, you may be able to lower noise in your data by connecting the Reference 3000's Floating Ground to an earth ground.

CAUTION
If any electrode in your cell is at earth ground, you must not connect the Reference 3000 chassis to earth ground. Autoclaves, stress apparatus, and field measurements may involve earth grounded electrodes.

A binding post on the rear panel of the Reference 3000 is provided for this purpose. A water pipe can be suitable sources of earth ground.

WARNING

Make sure that your earth ground connection is made to a legitimate source of earth ground. Consult a qualified electrician if you are uncertain how to obtain an earth ground. Connecting the Reference 3000 to an incorrect and unsafe voltage can create a safety hazard (see Chapter 1 for details).

If you are measuring very small currents, you may find that a metal enclosure completely surrounding your cell (a Faraday shield) significantly lowers measured current noise. This Faraday shield should usually be connected to both earth ground and Floating Ground. The Floating ground on the black cell lead is a convenient source of ground.

If any electrode in your cell is connected to earth ground, you should only connect your Faraday shield to the black cell lead (Floating Ground).

The alligator clip on any cell connection can be removed to access the underlying banana plug or pin jack. If you need to permanently change the terminations on your cell cable, feel free to remove the banana plugs and replace them with your new termination. Gamry Instruments can also provide additional standard or special cell cables.

ZRA Mode Cell Connections

The Reference 3000 can function as a precision Zero Resistance Ammeter (ZRA). It maintains two metal samples at the same potential and measures the current flow between the samples. It can also measure the potential of the samples versus a reference electrode.

The cell cable connections for ZRA mode are shown in Table 5-2. Note that the connections are very similar to those for the potentiostat and galvanostat modes. A second working electrode is substituted for the counter electrode and the Orange Counter Sense lead must be connected.

Table 5-2
Cell Cable Connections for ZRA Mode

Color	Type	Name	Normal Connection
Blue	Banana Plug	Working Sense	Connect to metal sample #1
Green	Banana Plug	Working Electrode	Connect to metal sample #1
White	Pin Jack	Reference	Connect to a reference electrode
Red	Banana Plug	Counter Electrode	Connect to metal sample #2
Orange	Banana Plug	Counter Sense	Connect to metal sample #2
Black	Pin Jack	Floating Ground	Leave open or connect to a Faraday shield

The counter sense and the working sense lead are each connected to different metal samples. In the ZRA mode the Reference 3000 is normally programmed to maintain zero volts between these leads. It therefore maintains the two metal samples at the same voltage.

The white pin jack on the cell cable is normally connected to a reference electrode. The potential between this lead and the working sense lead is reported as the cell potential.

If the instrument is connected in stack mode and the reference input is not used, it should be connected to the floating ground wire. A pin plug shorting bar is provided for this purpose.

If you don't have a reference electrode in your cell, we recommend that you connect the white reference lead to the working electrode. In theory, the measured potential will be exactly zero when this is done. In practice, A/D noise and offset will create a small potential signal with a value very close to zero.

Stack Mode Cell Connections

Batteries, fuel cells, and super-capacitors are often connected with several individual cells connected in series to allow higher voltage operation. This type of connection will be referred to as a Stack connection . Special experiment scripts allow the Reference 3000 to control and measure stack voltages as large as its compliance voltage (±15 volts or ±30 volts). These scripts will refer to Stack Mode cell connections. The cell connections in Stack Mode differ from those in Potentiostatic and Galvanostatic modes.

Voltages in Stack mode are measured as the voltage difference between the Counter Sense input and the Working Sense Input. A special high-voltage electrometer allows the orange lead to operate at high voltage and still draw minimal current from the system under test.

Connections in Stack mode are very similar to ZRA mode. The cell cable connections for Stack mode are shown in Table 5-3.

Table 5-3
Cell Cable Connections for ZRA Mode

Color	Type	Name	Normal Connection
Blue	Banana Plug	Working Sense	Connect to first end of a stack.
Green	Banana Plug	Working Electrode	Connect to first end of a stack.
White	Pin Jack	Reference	Can be connected to a reference electrode
Red	Banana Plug	Counter Electrode	Connect to the second end of a stack
Orange	Banana Plug	Counter Sense	Connect to the second end of a stack
Black	Pin Jack	Floating Ground	Leave open or connect to a Faraday shield

The Counter Sense and the Counter leads are connected to one end of a stack. The Working and the Working Sense leads are connected to opposite ends of a Stack.

The white pin jack on the cell cable can be connected to a low voltage point in the stack. Some Gamry scripts allow the voltage difference between the white and blue leads to be read, even though the Reference 3000 is in Stack Mode.

If the instrument is connected in stack mode and the reference input is not used, it should be connected to the floating ground wire. A pin plug shorting bar is provided for this purpose.

If you don't have a reference electrode in your cell, we recommend that you connect the white reference lead to the working electrode. In theory, the measured potential will be exactly zero when this is done. In practice, A/D noise and offset will create a small potential signal with a value very close to zero.

Membrane Cell Connections

The Reference 3000 can be used with membrane cells. In this type of cell, a membrane separates two electrolyte solutions. Two reference electrodes are used - one in each electrolyte. Each electrolyte also

contains a counter electrode. The Reference 3000 controls the potential across the membrane. Table 5-4 shows the cell connections used with a membrane type cell.

Table 5-4
Cell Cable Connections for a Membrane Cell

Color	Type	Name	Normal Connection
Blue	Banana Plug	Working Sense	Connect to reference electrode #1
Green	Banana Plug	Working Electrode	Connect to counter electrode #1
White	Pin Jack	Reference	Connect to reference electrode #2
Red	Banana Plug	Counter Electrode	Connect to counter electrode #2
Orange	Banana Plug	Counter Sense	Leave open (only needed in ZRA mode)
Black	Pin Jack	Floating Ground	Leave open or connect to a Faraday shield

Note that reference electrode #1 and counter electrode #1 must be on one side of the membrane and reference electrode #2 and counter electrode #2 must be on the other side.

Fuses in the Cell Cable

All standard Reference 3000 Counter/Working cell cables include fuses in the current carrying leads. These fuses protect the instrument from the extremely large currents that can flow through an improperly connected electrochemical energy generation or storage device (including batteries, fuel cells, and capacitors). For convenience, the term battery will be used here to refer to all single-cell or stacked electrochemical devices that can source energy.

Grounding errors on a battery can be particularly dangerous, since they can result in the battery being shorted through the instrument. During the development of the Reference 3000 several prototype instruments, without fuses, were damaged when connected to a Li-Ion battery stack.

NOTE

The fuses in the Reference 3000 Counter/Working cell cable do not protect against a safety hazard. They are needed to prevent damage to the instrument if it is improperly connected.

Both the counter electrode lead and the working electrode lead must be fused. Two different cell cable fuse arrangement have been built or are planned.

In-line Fuse-Holders and Fuses

The In-line fuse design is provided with Counter/Working cable supplied with early Reference 3000 shipments. The fuses in the cable are located plastic and brass fuse-holders located in-line with the current carrying leads, as shown in Figure 5-1. The photograph in this Figure shows the Working and Counter electrode leads with in-line fuse-holders. The Counter electrode fuse-holder has been opened to show the fuse. The fuse-holder contains a hidden spring that keeps the fuse in contact with the cell lead.

NOTE

Always turn off the Reference 3000 and disconnect both ends of the Counter/Working cable before checking or replacing the fuses in the cable.

In this fuse arrangement, the fuse can be removed from the cable by unscrewing the brass knurled nut on the fuse holder, just below the banana plug. Once a fuse has been removed, it can be checked using an

ohmmeter, such as that found on modern digital voltmeters. Do not trust a visual inspection of the fuse. A blown (open) fuse should always have a resistance of greater than 100 Ohms. The resistance of a good fuse is very small.

Figure 5-1
Open Fuse-holder Showing Fuse

Four replacement fuses should accompany every cell cable shipped by Gamry Instruments. The Gamry Instruments Part Number for the in-line fuses is 630-00019. If you need to source replacement fuses locally, we currently only recommend Fast Acting (FF), 3.15 amp, 5x20mm cylindrical fuses from the Bussman Corporation. The Bussman Part Number is BK/GMA-3.15-R. Fuses with similar ratings from other manufacturers have not been tested, so we cannot recommend their use.

CAUTION

Always replace the fuses in a Reference 3000 cable with the recommended fuse. Use of improper fuse, especially a fuse with a higher current rating, could cause instrument failure if a battery cell is improperly connected. Use of a non-approved fuse will void Gamry's factory warranty.

Fuses Located in the Cable Hood

The in-line fuses in the Counter/Working are expensive and large enough to be awkward, especially when low impedances connections are required. Newer Counter/Working cables use a simple design with fuses located within the cable hood. This approach is less expensive and allows for lower inductance cell connections

NOTE

Always turn off the Reference 3000 and disconnect both ends of the Counter/Working cable before checking or replacing the fuses in the cable.

Access to the fuses requires removal of two screws located on opposite sides of the hood covering the D-connector end of the Counter/Working cable. A drawing of the D-connector end of a cable with the hood opened is seen in Figure 5-2. The small rectangular fuses snap into fuse-holders labeled **Work** and **Cntr**. To remove the fuse, either grip it with small pliers and gently lift the fuse out of the fuse-holder, or pry the fuse out of the fuse-holder using a small screwdriver or knife blade.

Once a fuse has been removed, it can be checked using an ohmmeter, such as that found on modern digital voltmeters. A blown (open) fuse should always have a resistance of greater than 100 Ohms. The resistance of a good fuse is very small.

Don't forget the jackscrews when you reassemble the hood.

Figure 5-2
Drawing of Fuse-holder in the D-Connector Hood

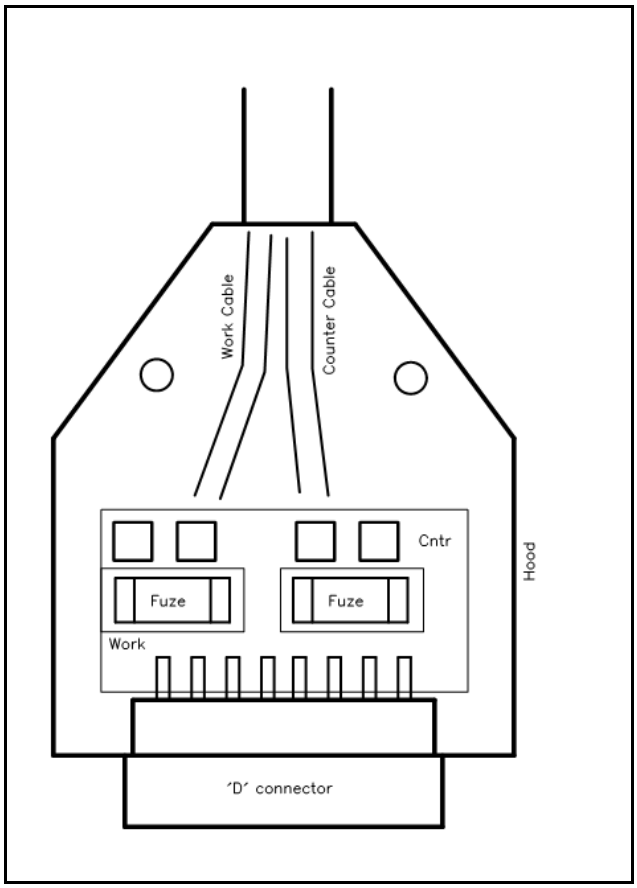

Four replacement fuses should accompany every Counter/Working cell cable shipped by Gamry Instruments. The Gamry Part Number for the small rectangular fuses is 630-00021. If you need to source replacement fuses locally, we currently only recommend Very Fast Acting, 3.15 amp, Nano Fuses from the Littelfuse corporation. The Littelfuse Part Number is 04513.15MRL. Fuses with similar ratings from other manufacturers have not been tested, so we cannot recommend their use.

CAUTION

Always replace the fuses in a Reference 3000 cable with the recommended fuse. Use of improper fuse, especially a fuse with a higher current rating, could cause instrument failure if a battery cell is improperly connected. Use of a non-approved fuse will void Gamry's factory warranty.

Testing For Open Fuses

A Gamry Framework test checks for blown fuses without having you remove the fuses. A simple Potentiostatic test is run on the Calibration Cell on the Gamry UDC4 Dummy Cell. The test is run using the "Set a Voltage.exp" script in the Framework's Utilities Package. Utility Package scripts do not require a Authorization Code, so every Framework installation can run this test.

Connect the cell leads to the Calibration side of the UDC4. You do not need to place the UDC4 within a Faraday cage. Select the command Experiment, Utilities, Set a Voltage on the Framework's menu bar. You will see a dialog box similar to this:

Figure 5-3
Setup Dialog Box for the "Set a Voltage" Script

Enter a **Voltage** of 1 volt as shown above, then press **Ok**. The Framework will open a Runner window and a graph of current versus time should appear.

Figure 5-4
Typical Runner Window with Good Fuses

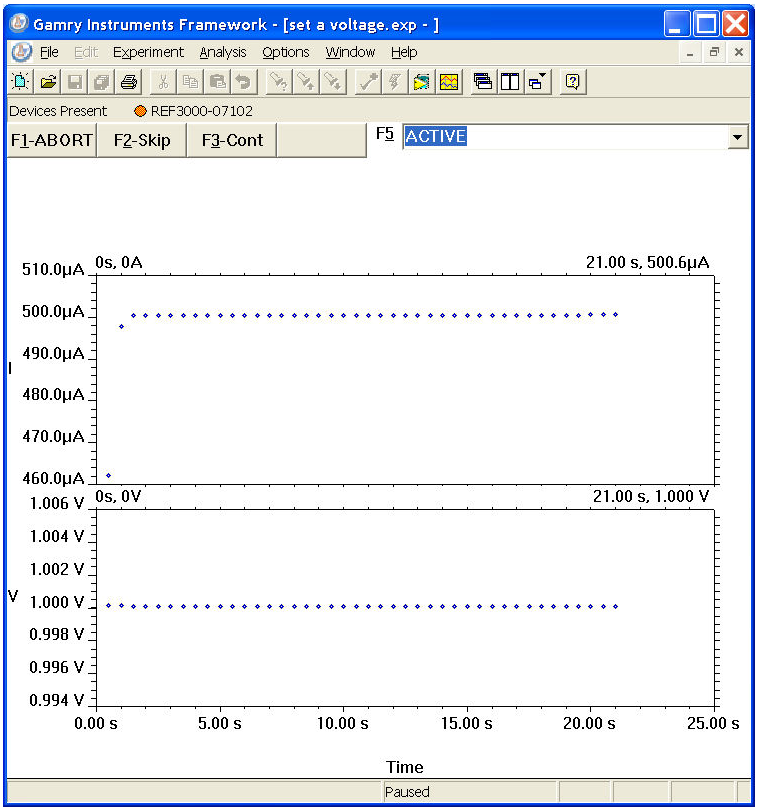

We expect you will see one of two very different results:

- If the instrument is working properly and the fuses in the cable are good, the measured current will be around 500 µA as seen above. No overloads are seen.
- If the one or both fuses are open, all the current readings will be near zero, and a red CA Overload indication may be seen at the bottom of the runner window.

If this test indicates an open fuse, use the procedures described above to check both fuses. This test cannot tell which fuse is blown. Both fuses can blow at the same time.

If the fuse test indicates an open fuse, and the fuses both check out a good with an ohmmeter, some other problem has occurred in the cables or the instrument. Contact Technical Support at Gamry Instruments at your earliest convenience.

Chapter 6 -- Panel Indicators and Connectors

Front Panel

The Reference 3000 front panel includes two connectors and four backlighted LED indicators. Each of these will be discussed in turn. A picture of the Reference 3000 front panel can be seen in Figure 4 - 1.

The cell connections are discussed at great length in Chapter 5. A pin-out of the two cell cable connectors can be found in Appendix B.

Counter/Working Connector

The **Counter/Working** connector is a 15-pin female D-type connector. It contains the high current connections between a Reference 3000 and an electrochemical test cell.

The **Counter/Working** connector is normally connected to a Gamry Instruments supplied cell cable. Gamry's **Counter/Working** cables always include fuses that prevent instrument failure when a battery of other energy source is improperly connected to the cable.

In addition to the pins used for cell connections, the Reference 3000 **Counter/Working** Connector also uses five pins to read a cell cable ID. Gamry's software can compensate for the cell cable characteristics for optimal system performance, especially in EIS (Electrochemical Impedance Spectroscopy).

Sense Inputs Connector

The **Sense Inputs** connector is a 15-pin male D-type connector. It contains high impedance voltage sense inputs. These inputs are used to measure voltages in the electrochemical test cell.

The **Sense Inputs** connector is normally connected to a Gamry Instruments supplied cell cable.

In addition to the pins used for cell connections, the Reference 3000 **Sense Inputs** connector also uses five pins to read a cell cable ID. Gamry's software can compensate for the cell cable characteristics for optimal system performance, especially in EIS (Electrochemical Impedance Spectroscopy).

The Power LED

The Power LED is located on the lower left of the Reference 3000 front panel. It normally glows a steady blue, when the Reference 3000 is turned on and has passed some simple self-tests.

When the Reference 3000 is first turned on, the Power LED will glow steadily for a second or two, blink three times, and then go to its normal steady blue output. Each blink in this sequence indicates successful completion of a portion of the Power PC's power-up self-test routine.

A Reference 3000's Power LED blinks when that instrument is selected in the Framework's Instrument Manager. This allows easy identification of a specific instrument in a MultEchem system without looking at the instrument Serial Label on the bottom of the instrument chassis.

When the Power LED is off, either:

- The rear panel power switch is off.
- There is no DC +24 volt supply connected to the rear panel DC Power In connector.
- The external DC power supply has no input power or is malfunctioning.
- One part of the Power PC's power-up self-test has failed.

CAUTION

The Power LED is used both to indicate power status and to indicate that power-up tests have passed. It therefore cannot be relied on as a true power status indicator. Always unplug the DC Power In connection if you suspect your Reference 3000 is malfunctioning.

The USB LED

The USB LED is located just above the Power LED. It is a tri-color LED, capable of glowing green, orange, or red.

The USB LED will be unlighted when:

- The Reference 3000 is not powered.
- The Reference 3000 does not have a USB cable plugged into its rear panel USB port.
- The computer end of the USB cable is not plugged into a USB port on a computer or hub.
- The USB cable is not supplying USB power to the Reference 3000.
- The computer has disabled the USB port going to the Reference 3000.

The USB LED will glow a steady green if a valid USB connection has been made and the Reference 3000's communication processor is receiving power down the USB cable.

The USB LED will flash orange whenever the Reference 3000 is receiving or transmitting valid USB messages to or from the host computer. It will not flash if there is USB traffic addressed to other devices on the USB bus, including messages aimed at a different Reference 3000.

The USB LED will indicate a solid RED in one special condition. It will be red when a firmware download is taking place. Interrupting a firmware download can cause a catastrophic failure of your system. Do not turn off the Reference 3000, do not unplug the USB cable, and do not stop the host computer operation when the USB LED is a steady red color.

CAUTION

Do not interrupt a firmware download while it is in progress. An incomplete download can render a Reference 3000 inoperable until it is returned to Gamry for reprogramming.

Cell LED

The Cell LED glows yellow whenever the Reference 3000 is actively applying voltage or current to the electrochemical cell attached to the Cell Cable. You should avoid touching the cell cable leads whenever the Cell LED is lighted, because the quality of the data being collected in your experiment may be compromised.

CAUTION

The Cell LED does not indicate a dangerous condition when it is lighted. The voltages output by the Reference 3000 are generally considered to be safe. Still, you should avoid touching the cell leads when the cell is on.

If you need to make changes to your cell leads, you normally do so between experiments, when the Cell LED is off and the potentiostat is inactive.

In a typical experimental sequence, the Cell LED will be off between experiments and during any open circuit potential measurements. It will glow yellow whenever the cell is polarized.

Overload LED

The Overload LED is normally unlighted. When it glows red, this indicates that some circuit in the Reference 3000 has exceeded its normal operating limit. Conditions that generate Overloads include:

- The absolute value of the differential electrometer output voltage (the difference in voltage between the Working and Reference leads) exceeds 10 volts. This condition is known as an E Overload.
- The control amplifier has lost control of the cell.

  Remember that the Reference 3000 can be operating with compliance limits of ± 1.5 Amps at ± 30 Volts or with compliance limits of ± 3.0 Amps at ± 15 Volts.

  The absolute value of the cell current may be trying to exceed the compliance current or the absolute value of the counter electrode voltage may be trying to exceed the compliance voltage setting. Either condition will be called a Control Overload.
- The absolute value of the cell current has exceeded full scale on the current range presently in use. This condition is known as an I Overload.

An Overload indication does not indicate an instrument failure or system malfunction. Many normal conditions can light the Overload indicator.

For example, transient (temporary) overloads <u>during</u> an experiment in which the cell voltage or current is being stepped or swept are often normal. Consider the case of an infinitely fast voltage step into a perfect capacitor. In theory, charging the capacitor requires an infinite current. The current spike seen at each step in a stepped voltage waveform can easily light the Overload LED. The current spike will normally decay to near zero before the actual current and voltage readings are taken.

Overload indications when the cell is being connected or disconnected are also common and usually do not indicate a problem. Overloads can also be seen when one of the cell leads is disconnected from the other cell leads, even though the cell is off. Again, this does not indicate a problem.

A steadily glowing Overload LED <u>during</u> an experiment most likely indicates a problem is occurring. Possible causes include:

- One of the cell leads is disconnected (this is the most common cause),
- a gas bubble in the cell is blocking one of the electrodes,
- the potentiostat could be oscillating (see the next chapter).

NOTE

As described above, a glowing red Overload LED does not necessarily indicate a system malfunction. The Overload LED can light when one or more cell leads are disconnected, without indicating a problem with the system. The Overload LED can often light momentarily during a swept or stepped experiment. The only Overload LED indication that definitely points towards a problem is a <u>continuously</u> glowing Overload LED during an experiment.

Rear Panel

The rear panel contains one switch and a large number of connectors. A picture of the Reference 3000 rear panel can be seen in Figure 4 - 2.

Power In Jack

The Reference 3000 derives all its power from a +24 volts DC supply connected to the Power In jack on the lower right side of the rear panel. The input current is less than 5 amps.

We recommend that you always use the power adapter (power brick) supplied with your Reference 3000 to power to the instrument.

Input power from the power adapter comes from your AC power main. The power adapter supply is rated for operation from 100 to 240 volts AC, at frequencies from 47 to 63 Hz. It should therefore be useable worldwide.

CAUTION

If your facility owns both Gamry Reference 600's and Reference 3000's, you must insure that the smaller power adapter from the Reference 600 is not used to power a Reference 3000. The Reference 3000 will not power up with the smaller adapter. Fortunately, neither the Reference 3000 nor the small power adapter will be damaged if connected in error.

The power adapter for the Reference 3000 is almost 22 cm long. The largest dimension on the Reference 600 power adapter is 11 cm.

While a Reference 3000 may work with other power sources, we cannot guarantee it will work to its full specifications. If you have to use the Reference 3000 with a different supply, make sure that the supply is regulated, has an output between 22 and 26 volts, and supplies at least 5 amps of load current. Inrush current drawn by the Reference 3000 at "power on" has been known to cause improper operation of an external power supply, even though the supply is rated for more than 5 amps of output current.

WARNING

Power input voltages less than 20 volts or greater than 32 volts can damage the Reference 3000's DC-DC power supply.

Power Switch

The Power switch is located just below the Power In jack. It switches the power from this jack to the input of the Reference 3000's DC-DC converter.

Normally, the DC Power is connected before the Power Switch is turned ON. However, no damage will occur if this switch is already in the ON position when the DC Power is connected, or when the AC power input is connected to the external power supply.

Chassis Ground

The rear panel Chassis Ground is intended for one use only. When the Reference 3000 is used with cells isolated from earth ground, connecting the chassis ground to earth ground may lower the noise measured in the system. Note that the chassis of the Reference 3000 is connected to Floating Ground. See Chapter 1, for safety information concerning this connection.

Either a banana plug or the stripped end of a wire can be connected to the Chassis Ground binding post. The other end of the wire is then connected to earth ground.

A black banana-plug to banana-plug lead has been provided with your Reference 3000. You may find it useful when making this earth ground connection.

USB Port

The USB port on the rear panel of the Reference 3000 is a Type B connector as defined in Revision 1.1 and 2.0 of the USB Specification. You use a standard, shielded, Type A/B cable to connect this port to a computer's USB port or a USB hub (preferably an externally powered hub). The two ends of a Type A/B cable are

different. The more-rectangular end plugs into the computer and the more-square end plugs into the Reference 3000.

A suitable USB cable was included with your Reference 3000 shipment. If this cable is lost, you can replace it with a cable from your local computer retailer.

The Reference 3000 is a High Speed USB 2.0 peripheral, capable of data transfer at 480 Mbits/second. If it is plugged into a computer port incapable of High Speed operation it will downgrade to USB 1.1 full speed operation (12 Mbits/second). Obviously data transfer speed will be slower if this occurs.

The Reference 3000 USB port is compatible with Revision 1.1 and 2.0 of the USB specification. It supports the Windows Plug-n-Play mechanism, including dynamic connect/reconnect.

The front panel USB LED should be green whenever a valid computer to Reference 3000 connection has been made and both the computer and Reference 3000 are fully powered.

Thermocouple Input

The Reference 3000 has an input jack for a K Type thermocouple. The ISO standard calls for color-coded mini-thermocouple connections. Yellow is the color assigned to K Type thermocouples. The mating connector on your thermocouple should therefore be yellow.

Possible uses for temperature measurement in an electrochemical test include:

- Looking for a temperature rise at end-of-charge on a battery.
- Measuring ambient temperature prior to a corrosion measurement.
- Measuring temperature in a cell before making a CV measurement that will be used to calculate reaction kinetics.

Gamry Instruments chose not to provide a thermocouple with the Reference 3000. There is simply too much variety in the mechanical design of thermocouple probes. Commercial thermocouples designed for measurement in air, on solid surfaces, and in immersion service are available from a variety of vendors. Make sure you get a K type thermocouple.

The Reference 3000 uses a temperature measurement IC to convert the thermocouple output to a useable voltage. It outputs a voltage that is nominally 10 mV per degree Celsius. The IC used, the Analog Device AD594A, is rated for an accuracy of 3°C. Even this accuracy is only achieved when the Reference 3000 is calibrated. The scaling at the A/D converter is ± 3 volts full scale, or ± 300°C full scale.

The Reference 3000 calibration script has an optional section for thermocouple calibration. An ice-water bath and a beaker of boiling water provide convenient standards for a two-point calibration.

CAUTION

One side of the thermocouple is connected to the Reference 3000's Floating Ground. An improper connection to the thermocouple input can compromise the Reference 3000's ability to float and invalidate data collected on earth grounded cells. A connection to an non-insulated thermocouple immersed in your electrochemical cell can also cause erroneous readings.

Misc I/O Connector

The Misc (Miscellaneous) I/O connector is a multipurpose connector. It contains both digital and analog signals used to interface external devices to the Reference 3000.

All of its signals are isolated from both earth ground and the Reference 3000's Floating Ground. The device connected to this connector establishes a ground reference. This isolation allows the Misc I/O connector to be connected to earth grounded apparatus, without compromising the Reference 3000's ground isolation.

A full description of this connector can be found in Appendix C of this manual. This appendix includes details such as connector pin-out, output and input voltage levels and full signal descriptions.

The following list is a short description of the signals in the Misc I/O Connector and their uses:

- Sync Out and Sync In signal allow two or more Reference 3000s to use one data acquisition clock.
- Four digital outputs can be used to turn on external devices under control of an Explain experimental control script.
- Some of Gamry applications assign three of the digital output to control stirring, flow of deaeration gas, and formation of mercury drops on a mercury drop electrode.
- Four digital inputs that can be read in an Explain experimental control script.
- A 12-bit D/A converter used to set "continuously variable" settings, such as electrode rotation rate on a rotating disk electrode.
- A 5 volt isolated power supply that can provide up to 50 mA of current for external circuitry.

Caution

Floating operation of Reference 3000 can be compromised by improper cabling to the User I/O Connector. We do not recommend use of standard 15-pin shielded cables with this connector. Custom cables with the shield connected to pin 6 of the D-connector are preferred.

I Monitor BNC

The I Monitor BNC connector represents the output of the Reference 3000's current measurement circuit. With the exception of the filtering described below, it is the raw signal. It will be high bandwidth on the less sensitive current ranges. The effective bandwidth of the current signal falls as you reach the nA and pA current ranges. IE Stability capacitors further slow the response.

The outer shell of this BNC connector is connected to the Reference 3000's floating ground.

CAUTION

The shell of the I Monitor BNC is connected to the Reference 3000's Floating Ground. Connection of this BNC to earth ground referenced equipment can compromise the Reference 3000's ability to float and invalidate data collected on earth grounded cells.

Scaling on this signal is ±3 volts for ± the nominal full scale current on the selected current range. Cathodic currents will cause a positive output voltage. If the software is auto-ranging the current-range selection, this signal will be discontinuous at each range change.

The I Monitor BNC connector is lightly filtered using an RLC circuit. It has a bandwidth of approximately 3 MHz when connected to a high impedance input. This bandwidth will be further reduced if a coaxial cable is connected to the BNC. Its output impedance is approximately 200 Ohms in parallel with 220 pF.

E Monitor BNC

The E Monitor BNC connector is the output of the Reference 3000's differential electrometer circuit. With the exception of the filtering described below, it is a buffered representation of the voltage difference between the white and blue cell cable leads. It has a high bandwidth.

The outer shell of the BNC connector is connected to the Reference 3000's floating ground.

CAUTION

The shell of the E Monitor BNC is connected to the Reference 3000's Floating Ground. Connection of this BNC to earth ground referenced equipment can compromise the Reference 3000's ability to float and invalidate data collected on earth grounded cells.

The E Monitor BNC connector is lightly filtered using an RLC circuit. It has a bandwidth of approximately 3 MHz when connected to a high impedance input. This bandwidth will be further reduced if a coaxial cable is connected to the BNC. Its output impedance is approximately 200 Ohms in parallel with 220 pF.

Ext. Sig. In BNC

The External Signal In BNC connector allows you to add a voltage to the Reverence 600's Signal Generator. This signal will be summed with the other signal generator sources including the IR DAC, the Scan DAC, and the DDS output.

The outer shell of the BNC is connected to the Reference 3000's floating ground.

CAUTION

The shell of the Ext Sig In BNC is connected to the Reference 3000's Floating Ground. Connection of this BNC to earth ground referenced equipment can compromise the Reference 3000's ability to float and invalidate data collected on earth grounded cells.

The signal generator output is usually directly connected to the potentiostat's input. When the cell is turned on in potentiostat mode, the feedback is such that a negative signal generator output creates a positive differential electrometer signal, which corresponds to a negative working electrode versus reference electrode voltage.

The polarity of the External Signal In signal is inverted at the signal generator's output. As described above, a negative input signal on this BNC will create a positive change in the working electrode versus reference electrode voltage. The input impedance of this signal is 3 kΩ in parallel with 15 pF.

Sig Gen Out BNC

The Sig Gen Out BNC connector allows you to monitor the "signal generator" signal being sent from the Reference 3000's controller board to the potentiostat board. This signal has a high bandwidth. The signal output range is –15 volts to +15 volts.

The outer shell of the BNC is connected to the Reference 3000's floating ground.

CAUTION

The shell of the Ext Sig In BNC is connected to the Reference 3000's Floating Ground. Connection of this BNC to earth ground referenced equipment can compromise the Reference 3000's ability to float and invalidate data collected on earth grounded cells.

The Sig Gen Out BNC connector is lightly filtered using an RLC circuit. It has a bandwidth of approximately 3 MHz when connected to a high impedance input. This bandwidth will be further reduced if a coaxial cable is connected to the BNC. Its output impedance is approximately 200 Ohms in parallel with 220 pF.

Aux In BNC

The Aux In BNC connector allows you to measure a voltage from outside the Reference 3000 using the Reference 3000's internal A/D. The scaling is: ±3 volts in equals ±30000 A/D counts. This is a resolution of 100 μV per bit. The results will be reported in volts. The input is differential (see Appendix D).

The allowed input voltage range is ±5 volts. Input voltages outside this range could result in damage the Reference 3000.

Consult Appendix D for additional information concerning this connector.

Expansion Interface

The expansion interface is a D-connector on the Reference 3000 reserved for use with the Gamry Reference 30k Booster to provide additional cell current up to 30Amps. A specially designed digital cable connects the Expansion Interface port to the booster. Consult the Reference 30k Booster manual for the details of setting up a booster.

Chapter 7 -- Auxiliary Electrometer Option

Overview

The AE is a factory-installed option for the Reference 3000. The AE acronym stands for **Auxiliary Electrometer**.

The AE allows eight independent, high voltage differential electrometer channels available to be read by the Reference 3000's A/D converter. Difference voltages (between the two inputs of each channel) of up to ± 5 V can be measured.

All AE inputs are rated to operate at all voltages available at the Reference 3000's Counter Electrode terminal. This allows operation between –18 volts and +18 volts in the 3 amp/15 volt compliance setting and between -36 volts and +36 volts in the 1.5 amp/30 volt compliance setting. These voltages are all versus the Reference 3000's Floating Ground.

The channels are all completely independent. One channel can measure the difference between -1 V and -2 V while a different channel measures the difference between 30V and 31V.

The primary function of the AE is simultaneous measurement of individual cells within a multi-cell battery, fuel cell, or super-capacitor stack. Both AC parameters and DC performance of the cells can be measured. The stack is often polarized using Galvanostatic control. Alternatively, you can use the Reference 3000 in Stack mode to control the voltage of the entire stack or of one cell in the stack.

Regardless of the control mode used, the same cell current flows though all the cells in the stack. As a result, we only need voltage measurements to measure the current and voltage of each cell in the stack. You can also use the AE to use to measure non-electrochemical signals. The voltage input to an AE channel can be the output from a temperature, pressure, or other transducer.

AC Performance and CMRR

Each AE channel has 2 differential inputs. The channel measures the difference voltage between these inputs, labeled as the **+ input** and the **- input**.

The AE inputs can operate with input voltages as high as 36 volts and can still maintain pA level input currents. They are also capable of high-speed measurements. The AE is specified to have less than 2° of phase shift for 100 kHz input signals applied to an input channel.

Another very important, although often disregarded, specification for differential inputs is common mode rejection (CMR). CMR is a measure of how well differential inputs reject a signal applied equally to both inputs (often called a common mode input). The ratio of output voltage to common mode voltage is called the common mode rejection ratio, CMRR. By convention, it has units of dB, a logarithmic scale where 20 dB represents a factor of 10. Assuming one volt of common mode voltage, 20 dB of CMRR corresponds to 100 mV of output voltage, 40 dB corresponds to 10 mV, 60 dB corresponds to 1 mV, etc.

CMR is generally dependent on frequency. As frequency increases, CMRR falls. Each AE channel is specified to have better than 94 dB CMRR at frequencies between DC and 5 kHz and better than 76 dB of CMRR between 5 kHz and 100 kHz.

NOTE

AC CMR is highly dependant on resistance in the measurement leads. The AE's CMR specifications only apply when the there is less than 10 Ω of resistance in the input leads. A typical aqueous reference electrode has 500 Ω of resistance. Gamry does not recommend use of reference electrodes in high frequency AE measurements.

Appendix C

Glossary

Aggregation A dense grouping in a mixture that is not homogeneously distributed.

American Recovery and Reinvestment Act A United States Act in 2009 that invested $2.4 billion in new advanced battery and electric drive projects.

Anneal To heat a material (traditionally, though not exclusively, metal or glass) and allow it to cool slowly, in order to remove internal stresses and toughen it.

aprotic solution Solutions that cannot break down and donate a hydrogen (proton). The electrochemical deposition setup utilized propylene carbonate (PC) as the solvent.

Arbin Equipment used for cycling batteries and recording battery performance. It can also be programmed to run electrochemical deposition experiments.

Ball Mill Equipment that is used to ensure homogeneous mixing. It is used for mixing graphene, graphene silicon mixtures, carbon black, and other slurries.

Capacity *See specific capacity, charge capacity.*

Charge capacity The amount about electrons that can be held in a battery.

Chronoamperometry A set current step used in electrochemical deposition.

Chronopotentiometry A set voltage step used in electrochemical deposition.

Coulombic efficiency The percentage of charge that is maintained between the charge and discharge cycles.

Current collector An integral element of the battery which makes electrical (and mechanical) contact with the material of the positive electrode in order to allow for electrical current generated by the chemical reactions in the positive electrode to flow to the outside of the battery and power the device in which the battery is installed.

Current The flow of electric charge through a circuit. A common unit is Ampere.

CVD Chemical Vapor Deposition.

Cycle life The number of lithiation/delithiation cycles a battery can endure before it loses 20% of its initial capacity.

Discharge Removing energy from a battery cell. The current moves from the negative electrode to the positive electrode as the battery discharges.

Electric Vehicles Automotive cars that rely on an electric charge instead of petroleum.

Electrochemical Deposition A process that uses electrical current to reduce dissolved metal cations to produce a coherent coating on an electrode.

Counter Electrode The metal that collects the electrons for electrochemical deposition

Reference Electrode Used to stabilize the voltage drop between the counter and working electrode

Working Electrode The metal that introduces electrons for electrochemical deposition

Electrolyte A material (usually liquid or gel) that contains ions and can be decomposed by electrolysis in order to facilitate the flow of ions through the battery.

Electrolytic Cell An electrochemical cell that undergoes a reduction-oxidation reaction when electrical energy is applied. The Gibbs free energy of the reaction is generally positive.

Galvanic Cell An electrochemical cell that produces electrical energy from a spontaneous reduction-oxidation reaction occurring within the cell. The Gibbs free energy of the reaction are generally negative.

Gamry Reference 3000 Equipment used to perform and conduct electrochemical analytical techniques, i.e. cyclic voltammetry, chronoamperometry, chronopotentiometry, etc.

Geothermal Technologies Harness the heat from the earth to create energy.

Graphene A single layer hexagonal carbon lattice structure.

Graphite-Oxide Graphite with oxygen that can be reduced to create graphene.

Graphite Carbon material that is a common negative electrode material for lithium-ion batteries. It is composed of many unordered layers of graphene.

Irreversible Capacity Permanently lost capacity in a rechargeable battery, i.e. due to lost structural integrity, chemical potential, etc. Often observed in the first few lithiation/delithiation cycles.

Lyophilization Freeze-drying.

Mechanically Mixed Homogeneous material that was made using a ball mill another apparatus to ensure uniform distribution.

Mechanically Mixed Graphene *See reduced-graphite oxide.*

Microwave Reduction Rapid heating and stirring of a mixture to aid in removing the oxygen content.

Moldatherm® A material engineered to be a heating element and insulation composite. Combines improved heat transfer and low thermal mass to give greater transfer efficiency.

Photovoltaic Technologies Harness light rays to produce energy

Power Density The amount of energy over time for a specific volume amount. Common units are W/m^3

Raman Spectroscopy A method to characterize the atomic makeup of a surface through the analysis of inelastic interactions between laser light and surface phonons

reduced-graphite oxide Multi-layered graphene. The oxygen has been removed from the structure. Also known as mechanically mixed graphene.

Reversible Capacity The average capacity that a battery can recharge over many cycles. Commonly established after the first irreversible cycle.

Secondary Batteries Rechargeable batteries.

SEM Scanning electron microscope.

Smart Grids A proposed electrical power grid of the future which relies on active sensing of the instantaneous demand for power and using localized energy generation and/or storage devices to meet the demand without creating excess

power. The Smart Grid concept is environmentally friendly because it eliminates wasted energy by dynamically adjusting the supply to the demand and because it integrates various localized renewable energy sources into a highly efficient distributed power generation system.

Solar Energy The use of the radiant light and heat evolved by the sun available to perform useful work.

Sonicator Equipment that mixes solutions through ultrasound. The sound energy can help homogenize a mixture on a nanoscale.

Specific Capacity The amount of energy per unit mass of the battery. Common units are mAh/g. The theoretical specific capacities for Li-ion with graphite and with silicon are 370mAh/g and 4200mAh/g respectively.

Specific Energy Density The power a battery can produce per unit mass of the battery.

Step-Time The duration of a particular cycle.

Substrate In electronics, the semiconductor base on which another material is deposited.

Tesla Roadster An all-electric-powered car manufactured by Tesla Motors.

TGA Thermogravimetric analysis.

Tube Furnace Equipment that heats material in a specific gas environment. Used for chemical vapor deposition of single layer graphene.

Voltage The electric potential difference between two points. Voltages are measured between the negative and positive electrode of a battery, and between the working and counter electrode in electrochemical deposition.

XRD X-ray diffraction.

Bibliography

[1] Roberts, B. *Power and Energy Magazine, IEEE* **2009**, *7*, 32–41.

[2] Energy, G. . What is your battery size? 2011.

[3] Etacheri, V.; Marom, R.; Elazari, R.; Salitra, G.; Aurbach, D. *Energy & Environmental Science* **2011**, *4*, 3243–3262.

[4] Xue, J.; Myrtle, K.; Dahn, J. *Journal of the Electrochemical Society* **1995**, *142*, 2927–2935.

[5] Wilson, A.; Dahn, J. *Journal of The Electrochemical Society* **1995**, *142*, 326–332.

[6] Zhou, X.; Yin, Y.-X.; Cao, A.-M.; Wan, L.-J.; Guo, Y.-G. *ACS Applied Materials & Interfaces* **2012**, *4*, 2824–2828.

[7] Luo, J.; Zhao, X.; Wu, J.; Jang, H. D.; Kung, H. H.; Huang, J. *The Journal of Physical Chemistry Letters* **2012**, *3*, 1824–1829.

[8] Yang, S.; Li, G.; Zhu, Q.; Pan, Q. *Journal of Materials Chemistry* **2012**, *22*, 3420–3425.

[9] Dimov, N.; Kugino, S.; Yoshio, M. *Electrochimica Acta* **2003**, *48*, 1579–1587.

[10] Chou, S.-L.; Wang, J.-Z.; Choucair, M.; Liu, H.-K.; Stride, J. A.; Dou, S.-X. *Electrochemistry Communications* **2010**, *12*, 303–306.

[11] Li, Z.; Zhang, D.; Yang, F. *Journal of materials science* **2009**, *44*, 2435–2443.

[12] DOE, Smart Grid. 2012; http://www.smartgrid.gov/the_smart_grid#smart_grid.

[13] Molderink, A.; Bosman, M. G.; Bakker, V.; Hurink, J. L.; Smit, G. J. Simulating the effect on the energy efficiency of smart grid technologies. 2009.

[14] Tesla, Tesla Roadster. 2011; http://www.teslamotors.com/roadster.

[15] Muthu, J.; Battaglini, J.; EE, M. *International Battery*

[16] Ellis, B. L.; Lee, K. T.; Nazar, L. F. *Chemistry of Materials* **2010**, *22*, 691–714.

[17] Hoffart, F. Proper Care extends Li-ion Battery Life. 2008; http://powerelectronics.com/portable_power_management/battery_charger_ics/proper_care_extends-li-ion-battery-0425/.

[18] Chan, C.; Peng, H.; Liu, G.; McIlwrath, K.; Zhang, X.; Huggins, R.; Cui, Y. *Nature nanotechnology* **2007**, *3*, 31–35.

[19] Yoon, T.; Cho, M.; Suh, Y.; Oh, E.; Lee, J. *Journal of Nanoscience and Nanotechnology* **2011**, *11*, 10193–10200.

[20] Furukawa, S.; Miyasato, T. *Jpn. J. Appl. Phys* **1988**, *27*, L2207.

[21] Ng, S.-H.; Wang, J.; Wexler, D.; Konstantinov, K.; Guo, Z.-P.; Liu, H.-K. *Angewandte Chemie International Edition* **2006**, *45*, 6896–6899.

[22] Walton, J.; Derhacobian, N.; Wong, Y.; Haller, E. *Applied physics letters* **1993**, *63*, 343–345.

[23] Wilson, A.; Zank, G.; Eguchi, K.; Xing, W.; Dahn, J. *Journal of Power Sources* **1997**, *68*, 195 – 200, ¡ce:title¿Proceedings of the Eighth International Meeting on Lithium Batteries¡/ce:title¿.

[24] Novoselov, K.; Geim, A.; Morozov, S.; Jiang, D.; Zhang, Y.; Dubonos, S.; Grigorieva, I.; Firsov, A. *Science* **2004**, *306*, 666–669.

[25] Geim, A.; Novoselov, K. *Nature materials* **2007**, *6*, 183–191.

[26] Kim, K.; Zhao, Y.; Jang, H.; Lee, S.; Kim, J.; Kim, K.; Ahn, J.; Kim, P.; Choi, J.; Hong, B. *Nature* **2009**, *457*, 706–710.

[27] others,, et al. *Science* **2009**, *324*.

[28] Saner, B.; Okyay, F.; Yürüm, Y. *Fuel* **2010**, *89*, 1903–1910.

[29] Wan, L.; Ren, Z.; Wang, H.; Wang, G.; Tong, X.; Gao, S.; Bai, J. *Diamond and Related Materials* **2011**, *20*, 756–761.

[30] Pu, N.-W.; Wang, C.-A.; Sung, Y.; Liu, Y.-M.; Ger, M.-D. *Materials Letters* **2009**, *63*, 1987–1989.

[31] Zhu, Y.; Murali, S.; Stoller, M.; Velamakanni, A.; Piner, R.; Ruoff, R. *Carbon* **2010**, *48*, 2118–2122.

[32] Chen, W.; Yan, L.; Bangal, P. R. *Carbon* **2010**, *48*, 1146–1152.

[33] others,, et al. COMPOSITE MATERIALS FOR BATTERY APPLICATIONS. 2012; WO Patent 2,012,151,094.

[34] Titelman, G.; Gelman, V.; Bron, S.; Khalfin, R.; Cohen, Y.; Bianco-Peled, H. *Carbon* **2005**, *43*, 641–649.

[35] Hummers Jr, W.; Offeman, R. *Journal of the American Chemical Society* **1958**, *80*, 1339–1339.

[36] Brodie, B. C. *Philosophical Transactions of the Royal Society of London* **1859**, *149*, 249–259.

[37] Staudenmaier, L. *Berichte der deutschen chemischen Gesellschaft* **2006**, *31*, 1481–1487.

[38] Agrawal, A.; Austin, A. *Journal of The Electrochemical Society* **1981**, *128*, 2292–2296.

[39] Munisamy, T.; Bard, A. J. *Electrochimica Acta* **2010**, *55*, 3797 – 3803.

[40] Schmuck, M.; Balducci, A.; Rupp, B.; Kern, W.; Passerini, S.; Winter, M. *Journal of Solid State Electrochemistry* **2010**, *14*, 2203–2207.

[41] Chen, X.; Gerasopoulos, K.; Guo, J.; Brown, A.; Wang, C.; Ghodssi, R.; Culver, J. *Advanced Functional Materials* **2011**, *21*, 380–387.

[42] WANG, L.; Yan-Na, J. *Acta Physico-Chimica Sinica* **2011**, *4*, 003.

[43] Momma, T.; Aoki, S.; Nara, H.; Yokoshima, T.; Osaka, T. *Electrochemistry Communications* **2011**, *13*, 969–972.

[44] others,, et al. *Physical Review Letters* **2006**, *97*.

[45] Gupta, A.; Chen, G.; Joshi, P.; Tadigadapa, S.; Eklund, P. *Nano letters* **2006**, *6*, 2667–2673.

[46] Subrahmanyam, K.; Vivekchand, S.; Govindaraj, A.; Rao, C. *J. Mater. Chem.* **2008**, *18*, 1517–1523.

[47] Zheng Yan, A. R. B. Characterization of Graphene by Raman Spectroscopy. 2010; `http://cnx.org/content/m34667/latest/`.

Acknowledgements

We appreciate the Gemstone program in the Honors College at the University of Maryland and the U.S. Department of Energy Materials Performance Division for supporting our research. We have immense gratitude to our mentor, Dr. Chunsheng Wang, our team librarian, Nevenka Zdravkovska, as well as Dr. Michael Fuhrer, and Dr. Ayyakkannu Manivannan for their continued guidance throughout the duration of this project. Finally, we wish to thank our discussants, Mr. Xinyi Chen, Mr. Alexander Kozen, Dr. Liangbing Hu, Dr. Yunhua Xu, and Dr. Ayyakkannu Manivannan for providing valuable critique of this thesis.